Techniques for determining bias and stability in satellite altimeters

Christopher Michael Murphy

Doctor of Philosophy

Aston University

December 1997

Aston University

Techniques for determining bias and stability in satellite altimeters

Christopher Michael Murphy

Doctor of Philosophy

December 1997

The case for monitoring large-scale sea level variability is established in the context of the estimation of the extent of anthropogenic climate change. Satellite altimeters are identi ed as having the potential to monitor this change with high resolution and accuracy. Possible sources of systematic errors and instabilities in these instruments which would be hurdles to the most accurate monitoring of such ocean signals are examined. Techniques for employing tide gauges to combat such inaccuracies are proposed and developed. The tide gauge at Newhaven in Sussex is used in conjunction with the nearby satellite laser ranger and high-resolution ocean models to estimate the absolute bias of the TOPEX, Poseidon, ERS 1 and ERS 2 altimeters. The theory which underlies the augmentation of altimeter measurements with tide gauge data is developed. In order to apply this, the tide gauges of the World Ocean Circulation Experiment are assessed and their suitability for altimeter calibration is determined. A reliable subset of these gauges is derived. A method of intra-altimeter calibration is developed using these tide gauges to remove the e ect of variability over long time scales. In this way the long-term instability in the TOPEX range measurement is inferred and the drift arising from the on-board ultra stable oscillator is thus detected. An extension to this work develops a method for inter-altimeter calibration, allowing the systematic di erences between unconnected altimeters to be measured. This is applied to the TOPEX and ERS 1 altimeters.

Keywords:

sea level change,

tide gauges,

altimeter range bias determination,

altimetric drift.

To Lisa — for making it all possible.

Acknowledgements

Contents

List of Figures

11

List of Tables

List of Abbreviations

A-S   Anti-Spoo ng.

ABS   Absolute Calibration.

C/A   Coarse/Acquisition.

CNES   Centre National d Etudes Spatiale.

CP   Calibration Point.

CSR   Center for Space Research.

DGM   Delft Gravity Model.

DORIS   Doppler Orbitography and Radiopositioning Integrated by Satellite.

DUT   Delft University of Technology.

DXO   Dual Satellite Crossover.

EMB   Electro-Magnetic Bias.

ERS   European Remote Sensing.

GDR   Geophysical Data Record.

GFO   Geosat Follow-On.

GPS   Global Positioning System.

IPCC   Intergovernmental Panel on Climate Change.

ITRF   International Terrestrial Reference Frame.

JGM   Joint Gravity Model.

LRR   Laser Retro-Re ector.

OPR   Ocean Product.

PCA	Point of Closest Approach.
PGR	Post-Glacial Rebound.
POL	Proudman Oceanographic Laboratory.
PRARE	Precise Range and Range Rate Equipment.
P	Precision.
QLOPR	Quick-Look Ocean Product.
RGO	Royal Greenwich Observatory.
RMS	Root Mean Square.
RP	Repeat Pass.
SA	Selective Availability.
SLR	Satellite Laser Ranger.
SPTR	Single Point Target Response.
SSB	Sea State Bias.
SWH	Signi cant Wave Height.
SXO	Single Satellite Crossover.
T/P	TOPEX/Poseidon.
TEC	Total Electron Count.
TG	Tide Gauge.
TOPEX	Topography Experiment.
USO	Ultra Stable Oscillator.
WCRP	World Climate Research Programme.
WOCE	World Ocean Circulation Experiment.

List of Symbols

A Area of sea surface illuminated by radar pulse.

B Number of TOPEX repeat pass locations.

C Number of ERS 1 repeat pass locations.

D Depth below water surface.

D_g Distance of the closest approach of the satellite to the gauge.

D_s Distance of the closest approach of the satellite to the laser ranger.

$D\ (t\quad t\ )$ Tide gauge-augmented dual satellite crossover between altimeter   at time t and altimeter   at time t .

E Noise in altimeter observation.

E^1_{tegi} Noise in the crossover observation $^1_{tegi}$.

E^2_{tegi} Noise in the crossover observation $^2_{tegi}$.

E^3_{tki} Noise in the repeat pass observation $^3_{tki}$.

E^4_{eki} Noise in the repeat pass observation $^4_{eki}$.

E_o Noise in observation by altimeter   .

E_T Total noise in a tide gauge-augmented satellite di erence.

E_g Amount by which the tide gauge is in error in estimating the variability measured by the altimeter.

G Number of tide gauges in calibration.

H Altitude of altimeter above the sea surface.

$H\ (t)$ Altimetric repeat pass height of altimeter   at time t.

L Radar pulse length.

N^1_{teg}	Number of crossover observations of type $^1_{tegi}$.
N^2_{teg}	Number of crossover observations of type $^2_{tegi}$.
N^3_{tk}	Number of repeat pass observations of type $^3_{tk}$.
N^4_{ek}	Number of repeat pass observations of type $^4_{ek}$.
P	Number of TOPEX cycles contributing to calibration.
Q	Number of steps in the ERS 1 altimetric drift function.
R	Range to satellite measured by tracker.
R	Tide gauge-augmented repeat pass difference.
S	Tide gauge-augmented single satellite crossover.
$S(t)$	Simulated ocean surface variability signal.
S_{POD}	Estimated position of the satellite derived from orbit determination.
S_{true}	True position of the satellite.
V	Inner radius of annulus of sea surface illuminated by radar pulse.
W^{e1}_{cor}	Corrected value of SWH for ERS 1.
W^{e1}_{opr}	Value of SWH for ERS 1 as it appears on the OPR.
$X_{p_1p_2}(c_1\ c_2)$	Single satellite crossover residual between pass p_1 of cycle c_1 and pass p_2 of cycle c_2 for a given satellite.
a_n	nth ascending pass number of a given satellite in a given repeat cycle.
$b\ (t)$	Altimetric range bias of altimeter at time t.
c	Speed of light in a vacuum.
c_n	nth repeat cycle number of a given satellite.
c_{geoid}	Ocean surface height change due to geoid structure between two locations.
c_{met}	Ocean surface height change due to meteorological effects between two locations.

c_{tide}	Ocean surface height change due to ocean tide between two locations.
$d_{t_0}(t)$	Altimetric drift function associated with altimeter with respect to the time t_0.
$d_{t_0}\ (t)$	Dual altimetric drift function associated with altimeter and with respect to altimeter at the time t_0.
d_n	nth descending pass number of a given satellite in a given repeat cycle.
g	Acceleration due to gravity.
$g(t)$	Tide gauge reading at time t.
g_c	Constant datum o set observed by a tide gauge in a tide gauge-augmented repeat pass height.
$g_v(t)$	Sea surface signal observed by a tide gauge in a tide gauge-augmented repeat pass height.
$h(t)$	Sea surface height measured by an altimeter at time t.
$h_{alt}(t)$	Altimetric sea surface height measured by altimeter at time t.
h_i	Common o set in ith set of single satellite crossover residuals which share a common satellite pass.
h_{alt}	Altimetric sea surface height.
h_{bias}	Altimeter range bias.
h_{gauge}	Sea surface height measured by a tide gauge.
h_{range}	Corrected altimeter range.
h_{sat}	Height of satellite above a reference ellipsoid.
h_{true}	True sea surface height.
n	Refractive index.
p	Water pressure measured by tide gauge.
p_0	Atmospheric pressure at ocean surface.
p_n	Pass number of a given satellite in a given repeat cycle.

r	Distance from the Geocentre to satellite.
r_e	Distance from the Geocentre to tracking station.
r_i	Time of start of step $i + 1$ in the altimetric drift function $d_{t_0}^T(t)$.
r_n	Reference satellite repeat cycle number.
$s(t)$	True sea surface height at time t.
s_c	Constant datum o set observed by an altimeter in a tide gauge-augmented repeat pass height.
s_i	Time of start of step $i + 1$ in the altimetric drift function $d_{t_0}^{E\,T}(t)$.
$s_v(t)$	Sea surface signal observed by an altimeter in a tide gauge-augmented repeat pass height.
$t_{p_1 p_2}(c_1\;\;c_2)$	Time during pass p_1 of cycle c_1 that the satellite ground-track reaches the point of intersection of that pass with the ground-track of pass p_2 of cycle c_2 in a single satellite crossover.
v	Radius of the circle of sea surface illuminated by radar pulse.
w_D	Weight assigned to dual satellite crossover observations.
w_E	Weight assigned to ERS 1 repeat pass observations.
w_T	Weight assigned to TOPEX repeat pass observations.
x	Distance between the sea surface and the pulse leading edge at nadir.
E	Radial orbit error remaining after orbit correction.
R	Residual in satellite tracker range.
a	Orbit error in the along-track direction.
c	Orbit error in the cross-track direction.
r	Orbit error in the radial direction.
	Geographically-correlated orbit error.

	Geocentric angle between the sub-satellite point and the point of closest approach.
f	Geographically-correlated orbit error averaged over ascending and descending satellite passes at a given location.
v	Portion of the geographically-correlated orbit error which varies between ascending and descending satellite passes at a given location.
n	nth harmonic parameter describing the resonant orbit error in TOPEX orbits.
$^1_{tegi}$	ith tide gauge-augmented dual satellite crossover between TOPEX and ERS 1 at tide gauge g where TOPEX contributes an ascending pass within the scope of drift parameter d_t^T and ERS 1 contributes a descending pass within the scope of drift parameter d_e^E.
$^2_{tegi}$	ith tide gauge-augmented dual satellite crossover between TOPEX and ERS 1 at tide gauge g where TOPEX contributes a descending pass within the scope of drift parameter d_t^T and ERS 1 contributes an ascending pass within the scope of drift parameter d_e^E.
$^3_{tki}$	ith tide gauge-augmented TOPEX repeat pass height at the kth repeat pass location at tide gauge g where the TOPEX pass is within the scope of drift parameter d_t^T.
$^4_{eki}$	ith tide gauge-augmented ERS 1 repeat pass height at the kth repeat pass location at tide gauge g where the ERS 1 pass is within the scope of drift parameter d_e^E.
	Slope in time series of difference between sea surface heights as measured by the altimeter and the tide gauge.
(t)	Random noise signal.
	Noise and correlated error in altimeter observation.
	Constant offset observed in a tide gauge-augmented repeat pass series.
	Geocentric angle between the tracking station and the point of closest approach.

Water density.

RMS difference between altimeter and tide gauge time series.

Chapter 1

Introduction and motivation

Earth observation has entered a new era with the onset of satellite altimetry. The oceanographer s long dreamt-of goal, to be able to measure the topography of the sea surface in a geocentric reference frame, has at last been realised. Climate science is one eld of interest to bene t from this new development, since estimates of the rates of long-term changes in the global sea levels can be exploited in the construction of global climate models. This thesis describes methods which may be applied to altimetric data in order to enhance the ability to resolve sea level change, and to detect inaccuracies which hinder the execution of this task.

Sea level change is an important issue. Various predictions have been made of climatic response to increased atmospheric concentrations of the so-called greenhouse gases associated with the burning of fossil fuels. Current theories suggest that one possible scenario is a signi cant rise in sea levels. The serious implications associated with this change drive the search for more evidence to validate the theories further.

Since 1975 a variety of satellite altimeters have operated, taking routine measurements of the sea surface height. Each has been unique and the satellite platforms upon which they have been mounted have orbited in several con gurations. Consequently each measures the sea surface with slightly di erent characteristics. This is a hurdle to the full utilisation of the combined altimetric dataset. The possibility of unifying the data gathered by these is attractive as it will yield a long time series of large-scale sea surface variability. However the problem of how to combine altimetry from these multiple sensors is a serious one. If not addressed, erroneous conclusions regarding sea level change may easily be reached. This drives the search for sources of inconsistency between the altimeters, and motivates the measures taken to overcome their e ects.

In addition to di erent characteristics in the way that the sensors measure the sea surface, the characteristics of an altimeter considered in isolation tend to change over time. This too stands in the way of accurate resolution of sea level

change.

The work presented in this thesis seeks to identify methods which will allow the blending of altimetry into a consistent format, suitable for the construction and validation of climate models. In particular, the techniques involved will be suitable for removing the e ects of the changing characteristics within a single altimeter mission. These will also account for the inherent di erences between the various altimeters allowing full exploitation of the whole dataset.

This thesis is split into several sections. Initially Chapter 2 provides a study of long-term sea level change within the context of other phenomena which cause periodic and transient uctuations in the sea surface. A review of possible future scenarios arising from climate change is carried out here. In Chapter 3 a study of the various techniques available for measuring or inferring sea level variation is provided, with particular emphasis on satellite altimetry. Possible sources of error which restrict the utility of altimetric datasets for sea level studies are summarised. Chapter 4 describes an altimeter calibration technique which uses a tide gauge and a satellite tracker to infer the absolute biases of the TOPEX, Poseidon, ERS 1 and ERS 2 altimeters. In Chapter 5 a scheme for modelling drift in altimeter range characteristics is presented. A theory of augmenting altimeter measurements with tide gauge data is then developed with a view to inferring such drift. In order to carry out a successful altimetric drift calibration, a set of reliable tide gauges is required. Such a set is derived in Chapter 6. This set is then employed in Chapter 7 to recover the drift in the TOPEX and Poseidon altimeters. Finally, in Chapter 8, a general method for the simultaneous calibration of multiple altimeters is developed and applied to TOPEX and ERS 1.

Chapter 2

The components of sea level

It is often stated that one scientist s noise is another scientist s signal. This is indeed an appropriate aphorism for physical oceanographers since the instantaneous height of the ocean at a given location is a snapshot of a superposition of many signals from a wide variety of sources with amplitudes from the sub-millimetre level to several metres. The height of the surface is constantly changing by virtue of many in uences acting over di erent spatial and temporal scales. In this chapter the various components of the sea level signal are examined along with their causes. Particular emphasis is placed on the long-term sea level change. The bene ts of being able to measure this phenomenon to a higher precision are assessed.

2.1   Tides and periodic components of sea level

2.1.1   Astronomical tides

The astronomical tides are a well-known cause of variations in the ocean surface. They arise principally from the orbit of the Earth/moon system around its combined centre of mass. Each particle comprising the Earth is in a constant state of acceleration towards the moon. Since gravitational attraction and distance are related by an inverse square law, this force is not the same on every particle in the Earth. Lisitzin (1974) explains how particles with the moon at zenith experience a stronger gravitational force than those with the moon at nadir. In fact if a sphere of water or some other   uid were performing this type of motion it would become elongated as shown in Figure 2.1. Of course the true composite Earth is more complex. Since the solid Earth is not free to deform to the extent of the ocean it cannot elongate by the same amount and the oceans tend to bulge. As the Earth rotates on its axis, this bulge moves round, resulting in the dominant semi-diurnal tides.
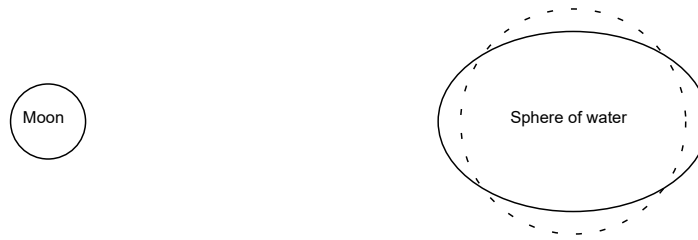
Figure 2.1: Orbit system of the moon and a hypothetical fluid planet (solid circle) with the reference spherical Earth (dashed circle).

The sun is also responsible for tides. Although it is nearly 2.8 10^7 more massive than the moon, it causes less of a tide-forming force since its distance results in a smaller gravitational potential gradient across the diameter of the Earth. The planets are also responsible for astronomical tides, although with a much smaller effect.

Other characteristics of motion within the solar system are responsible for long-periodic tides. Lisitzin (1974) isolates these tides as being the superposition of five angles, such as the longitude of perigee of the moons orbit around the Earth. These give rise to astronomical tides with a wide variety of wavelengths, some many years in length, although with amplitudes much smaller than those of their diurnal and semi-diurnal counterparts. Precision tide models may well include several dozen constituent harmonics which will account for very close to 100% of the tidal signal.

2.1.2   The loading tide

The mass of water comprising the oceans has to be borne by the lithosphere. This will deform the ocean floor away from the shape it would take if the ocean were not present. If the water of the oceans were static the ocean floor profile would be in equilibrium. However this is not the case since the waters are constantly shifting with the ocean tides. As the load on the sea floor changes, so does its shape and this will be reflected in the ocean surface. This ocean loading tide can be calculated along with the tide models since it is a direct result of the ocean tides themselves.

2.1.3   Earth body tides

Just as the oceans are subject to the tidal gravitation of the celestial bodies, so too is the solid Earth. The different response to these forces by the Earth is a result of its elasticity. Since it may be deformed, it can respond to the various forces. Since no flow is involved, there will be more geographical coherence and

25

the resulting signal will have a signi cantly longer spatial wavelength than the ocean tide.

It is not just the Earth s crust on land which is subject to these body tides. The sea oor also experiences the forces and the resulting movement will be transmitted through the column of water which it supports. This will cause a tidal e ect in the sea surface. If the sea surface is measured with a land- xed device such as a tide gauge, the body tide will not appear in the readings from that instrument since the ground upon which it sits will be raised and lowered along with the ocean surface.

2.1.4   Pole tides

The axis of the Earth s rotation is not xed. In fact the point where the axis intersects the Earth s surface will describe circles with periods of approximately 12 and 14 months. This is known as the Chandler e ect (Lisitzin, 1974) and arises from the orbit of the Earth-moon system inducing a centrifugal force on the Earth.

The solid Earth and the oceans respond independently to this forcing and the di erence can be seen in tide gauge time series. The sea surface is raised by the sum of these two e ects and is termed the geocentric pole tide. This is the signal which will be observed in a geocentric reference frame, as in the case of a satellite altimeter. Like Earth body tides, this quantity must be handled carefully depending on the frame of reference. Fortunately the magnitude of the e ect, and in particular the di erence in response between the ocean and the solid Earth is generally small (Trupin and Wahr, 1990).

2.2   Meteorological components of sea level signal

The atmosphere and ocean surface interact at their common interface which leads to usually short-term uctuations in the sea level. The critical properties of the atmosphere in this respect are the pressure and movement.

2.2.1   The inverse barometer e ect

Atmospheric pressure acts to depress the surface of the ocean. Since weather systems change atmospheric pressure, the component of sea surface height due to the pressure will not be constant. In fact a crude model of this phenomenon suggests that an increase in atmospheric pressure of 1 millibar depresses the sea

surface by approximately 1 cm (Mathers, 1996). This is referred to as the inverse barometer effect.

2.2.2 Storm surge

Winds cause the air and ocean at their common interface to have different velocities. Associated with this is a shearing force which causes movement in the upper layers of the ocean. This is a natural part of the global circulation system. However it is when this movement occurs as the result of extreme weather events, such as storms, in coastal regions that the effects are noticed. If the movement of this water is obstructed by land then the water will pile up against the coast. This can have catastrophic consequences as demonstrated in 1953 in the Netherlands, England and Belgium (Lisitzin, 1974).

Observations of the sea surface in coastal regions will contain a contribution from the storm surge effect during storms and other severe weather events.

2.3 The mean sea surface

All these signals cause the sea surface to deviate from some mean level. This mean may change gradually over time as a result of sea level rise, but it is useful to consider the mean level from which the tidal and meteorological phenomena deviate the sea surface. This mean sea level is itself a combination of various sources from the rotation and structure of the Earth to oceanographic phenomena.

The principal contribution to the mean sea level is the equipotential surface called the marine geoid. This is the shape that the ocean surface would form if it was under the influence of the Earth's gravity and rotation alone. The closest approximation to this is not the surface of a sphere — the best fitting sphere would be in error by over 10 km at the equator and the poles. The simple geometric shape which most accurately approximates the Earth is in fact the ellipsoid. A popular ellipsoid for the Earth is that of the World Geodetic System. This WGS 84 ellipsoid has a semi-major axis of 6378.137 km and a flattening coefficient of 3.35281×10^{-3}. The mean sea surface may still deviate from the ideal ellipsoid by up to 100 m through a combination of geological and oceanographic influences.

The movement of water in the world circulation system plays an important role in the climate of the Earth. It also contributes to the mean sea surface. The circulation is driven principally by the uneven heating of the fluids covering the Earth's surface. The density changes induce movement and set the oceans and atmosphere in motion. It is the Coriolis effect which dictates that these systems of transport adopt circular rather than linear movement (Houghton, 1977).
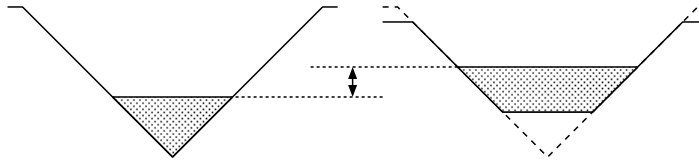
Figure 2.2: Sea level change due to a change in the shape of the Earth s crust.

Consequently, rather than a highly transient system, some approximation to equilibrium in the circulation system may be reached. Many medium- and long-term phenomena of ocean dynamics are in geostrophic balance, the pressure forces which cause the movement being balanced with the Coriolis e ect (Robinson, 1985). Changes in pressure in a moving body of water will cause a deviation from the geoid in the sea surface topography at the surface corresponding to that current. For instance Morner (1987) shows how the presence of the Gulf Stream in the Atlantic Ocean causes the mean sea level to deviate from the marine geoid. The extent of this is quite pronounced with the mean sea surface as low as 2 m below the geoid and up to 4 m above. The permanent components of circulation will therefore contribute to the mean sea surface.

2.4 Eustasy

Since it was rst used by E. Suess in 1888 Eustasy has come to have many di erent meanings (Morner, 1987). Essentially, eustasy refers to changes in sea level with a global e ect. This is of particular interest with the emergence of the greenhouse e ect as a potentially catastrophic climate-modi er. The subset of eustasy causing a net change in the global sea level is studied here. In particular changes arising from variations in the period or axis of the Earth s rotation, or changes in the structure of the geoid are excluded. Apart from these, Morner (1987) identi es two broad categories of eustasy.

First, sea level is a function of the degree to which the solid Earth surface is irregularly shaped. This can be visualised by supposing that the mountains in the Himalayas were removed above a certain height and dumped in the ocean. The mean height of the Earth s surface would go down and the mean sea level would go up. Changes of this nature are referred to as basin eustasy. Sedimento-eustasy can have this e ect where the erosion by tides, waves and rivers remove material from the crust and deposit it as sediment on the ocean oor. Another form of this levelling out is tectno-eustasy where tectonic processes modify the shape of the ocean basins. The e ect of these processes on sea level is illustrated in Figure 2.2.

The next broad category of global eustasy is that involving a change in the volume of water in the oceans. Since the last ice age, this has been a major contribution to sea level change as the extent of glaciation has reduced dramatically. It is the melting of land ice which is significant here since if volume changes are ignored, a glacier floating in the ocean only displaces its own weight so will not affect sea level in melting. The main candidates for providing more mass of water are the Greenland and Antarctic ice sheets along with glaciers and small ice caps (Warrick and Oerlemans, 1990). There is a huge mass of ice involved. For instance in the hypothetical scenario where the ice sheets of Antarctica melt, a rise in sea level of about 65 m would result. For the Greenland ice the estimated contribution is 7 m while glaciers and small ice caps would contribute approximately 35 cm. The complicated responses of each of these ice reserves to climatic change mean that building quantitative models for their dynamics is difficult. This fact, along with the uncertainty over whether equilibrium with the natural climate change since the last ice age has been reached, means that projections about future sea level changes arising from changes in the ice mass balance are difficult and imprecise.

Changes in sea water density which arise from temperature fluctuations will modify the volume of the oceans and also contribute to sea level change. This is termed steric change. The density of water is a maximum at about 4 C, a fact to which the existence of life on Earth is owed. If it were the case that ice were denser than water then the oceans would gradually freeze solid from the floor up, with the result that they could no longer circulate heat. This unusual density behaviour is due to the molecular structure of the substance. Whereas in warmer water molecules pair up by forming hydrogen bonds, at lower temperatures it prepares to freeze and the molecules form into groups of four, again linked by hydrogen bonds. One group of four molecules requires more space than two groups of two and thus the density decreases. Observational studies of actual steric change are sparse and limited in coverage. Attempts have been made to model the steric response of the ocean to climatic change, despite the complexity involved.

2.5 Sea level and climate change

It is now widely accepted that sea level has been rising over the last century. Douglas (1995) reviews the various methods for estimating the global rate of sea level change and summarises the various estimates available. By comparing analyses of relatively recent tide gauge time series with various archaeological studies, he concludes that the sea level rate has increased significantly from its

mean rate of the preceding two millennia to its current rate of approximately 1.9 mm/yr. This is also the consensus of the climate experts who comprise the Intergovernmental Panel on Climate Change (IPCC). They conclude that it is highly likely that sea levels have risen on a global scale over the last century (Warrick and Oerlemans, 1990). Their best estimate of the extent of the rise is that it is of the order of 1 2 mm/yr. The IPCC report goes on to present various models for future rise. If no steps are taken to combat the causes of climate change (the *business as usual* scenario), it is predicted that sea levels will have risen from the 1990 level by 18 cm in 2030 and 44 cm in 2070. In the ve years following their rst Scienti c Assessment, climate models and observational data were improved allowing for a re nement of the *business as usual* scenario. The best estimate in the updated assessment presented by Houghton *et al.* (1996) predicts a rise 25% less than that in the rst Scienti c Assessment. As they stand, these projections have obvious and serious implications for many countries with low-lying regions, while the economic repercussions of this degree of climate change will a ect all countries.

These estimates and projections raise various questions. First, it is important to establish the cause of the current sea level rise and determine what has triggered the accelerated rate of the last few centuries. In particular the implications will be far-reaching if the rise is anthropogenic in origin. The second question regards the future rate of sea level rise. The predictions mentioned above are subject to uncertainty. It is important to learn whether the rise is likely to continue and whether further acceleration in the rate should be expected. Attempts are being made, some of them successful, to stabilise emission of the greenhouse gases which are implicated in climate change. While uncertainties exist in the climate models used to make the predictions, the best response to the threat remains elusive. As long as the credibility of the Scienti c Assessment is doubted, and it is doubted vigorously by some, the policy-maker s task is an unenviable one.

2.5.1 The threat of the rising seas

The main negative e ects of sea level rise is that land which was not previously in contact with the ocean either becomes restricted in its usefulness owing to inundation by water, or is damaged through salination. The threat of land loss due to inundation varies from location to location since the land topography many kilometres from the coast can in uence the extent of encroachment. Large expanses of land just above sea level are most at threat, such as parts of Bangladesh, East Anglia or the Netherlands. A rise in sea level can also exacerbate erosion and weaken the coast. Expensive coastal defences are then required to avert loss of land to the sea.

The encroachment of the sea may have secondary e ects such as interference with the water table. If aquifers become polluted by salt water they are lost as a fresh-water resource unless expensive desalination is carried out. Agricultural land is vary hard to cultivate if it is salinated by a periodical deluge with sea water.

2.6   Monitoring sea level

Changes in the volume of sea water are the focus of climate scientists concerned with sea level rise. The global climate is modelled as the actions and interactions of the oceans, atmosphere and cryosphere. The responses of the various sources of ice to global warming are still the subject of debate, and the role of atmospheric moisture and precipitation is controversial. The continued monitoring of sea level change with as high a resolution and accuracy as possible not only allows any acceleration to be detected, it also has an important part to play in enabling the ne-tuning of climate models.

Before the dawn of satellite altimetry, sea level changes could only be measured or inferred at particular isolated locations and no overall global picture could be assembled. In fact, what was measured was the di erence in the sea level rate and vertical motion of the crust. The measuring has been carried out with tide gauges, while records going back more than about two hundred years must be inferred using clues found in geological formations.

With satellite altimetry the potential to measure sea level and its changes in a geocentric reference frame, with more precision and spatial resolution than ever before, has been realised. These instruments have the potential to join the established methods of sea level monitoring and so contribute to modern climate models. The result will be more accurate predictions about the future of the climate. However there are various hurdles to the optimum exploitation of altimetry. The principal limitation is the relatively short mission length. With few missions being operational in excess of ve years, data from multiple sensors at di erent times must be blended. For the most accurate climate models to be constructed, observations of sea level over several decades at least must be available so that periodic phenomena with a wavelength of several years are not aliased. There are hurdles to this merging of altimetry which must be addressed if the combination is to be successful.

There is a danger that altimeters may become regarded as a panacea for the problems of sea level scientists. This is harmful if it means that altimeters are expected to exceed their capabilities. When sea level is monitored with tide gauges, one places con dence in many independent sensors. With altimetry one

is forced to rely on half a dozen. If no independent monitoring of their results is made and they are not subject to quality control then there is a real risk of false conclusions being drawn.

It is intended to develop techniques to allow the accurate monitoring of sea level and its trends using altimeters. In particular the pitfalls inherent in merging data from multiple altimeters are to be avoided, and quality control is to be applied to the individual altimeters. If this is achieved then the full multi-altimeter dataset may be exploited as one.

Chapter 3

Satellite altimetry and the measurement of variability

Altimetry is the modern way to measure sea level. With this advancement has come the power to resolve variability with a large spatial coverage. However the sea level variations before the age of altimetry are not an unknown and have been measured or inferred by other more established methods. In this chapter the various methods for measuring the sea surface are reviewed with particular application to monitoring sea level change. The principle of sea level measurement using satellite altimetry is examined in detail, along with the various associated errors and corrections. Historical and operational altimeters are reviewed and planned missions are described. Finally, the hurdles which stand in the way of the optimal measurement of variability with altimeters are discussed and the possible solutions summarised.

3.1 Non-altimetric methods of variability measurement

3.1.1 Geological records

Past changes in sea level can be inferred by interpreting clues laid down in geological structures. For instance sedimentation rates can be related to water depth. Determining the age of progressive layers of sediment will therefore yield the historical depth pro le. This principle has been applied in various situations. For instance Shennan (1987) applies this to the North Sea. Ireland (1987) measures sedimentation around Rio de Janeiro and links this to sea level change. Radiocarbon dating of corals (Colonna *et al.*, 1996) and the ocean oor (Haggart, 1987) along with knowledge of the rate at which the material is deposited will yield the sea level rate of change. The sensitivity of these techniques and the errors

involved mean that any peculiarities of the last century or so certainly cannot be resolved.

Apart from the rare historical records of observations of usually dramatic and sudden changes, this technique of geological inference is the only method available to look at how sea level has changed before the age of tide gauges. The drawbacks come in resolution and accuracy. Only relatively large changes can be resolved and come nowhere near the millimetre per year accuracies of the modern techniques. Apart from the extensive sea level rise since the end of the last ice age, the application of this technique is mainly restricted to inferring geological activity which has caused substantial uplifting or descent of coastal regions, rather than changes in sea level. Certainly, this technique cannot be applied to high-resolution applications such as the measurement of eustatic changes which have occured since the onset of the industrial era.

3.1.2 Tide gauges

Whereas estimates of sea level change inferred from geological records are available over thousands of years, similar estimates from tide gauges only extend back for a couple of centuries at most. In this relatively short time however the accuracy and resolution of the tide gauge far exceeds that of the geological record. For instance, gauge measurements at Brest in Finistere on the western tip of France span 190 years, with only brief outages (Spencer and Woodworth, 1991). Tide gauges typically work by sampling the sea surface height relative to a fixed reference at a regular interval. In addition to long-term sea level change, the resulting time series will observe tidal harmonics and seasonal variability along with oceanographic, meteorological and atmospheric effects. These all add noise which must be accounted for when measuring longer variability.

Types of tide gauge

A highly desirable characteristic of any tide gauge is that it should filter out the signal due to high-frequency ocean waves. However this should not be at the expense of the sensitivity to detect variations with frequencies of ocean tides and below. This is usually achieved in one of two ways, namely bottom pressure or stilling well gauges. The first of these involves measuring the water pressure some distance below the water surface or at the sea floor. The measurement technique employs the hydrostatic relationship (Neumann and Pierson, 1966)

$$p = p_0 + \rho g D$$

where p is the measured pressure, p_0 is atmospheric pressure at the surface, ρ is the density of the water, g is the acceleration due to gravity and D is the depth

of the measurement below the water surface. The e ect of high frequency density

 uctuations with wave origin decreases as depth increases thus these uctuations
are excluded from the time series. Two types of bottom pressure gauges are the
bubbler gauge and the gas-purging gauge. In the former the pressure is actually
measured by slowly releasing compressed gas. The pressure of the gas just before
it is released is equal the water pressure and can be measured with a manometer
(Pugh, 1987). Two immediate problems with this technique are that variations
in atmospheric pressure and water density must be measured or modelled. This
can be a particular problem in the case of salinity changes arising from local
freshwater in ow. This can very well have a seasonal variability which if ignored
will corrupt the tide gauge readings.

Stilling well gauges di er from bottom pressure gauges in that the sea surface
is measured directly. This is usually achieved with a oat, the height of which
can be mechanically or electronically determined. To smooth the short period
ocean waves, the oat sits in a cylinder and is isolated from the ocean apart from
at the base of the cylinder, usually at the sea oor, where water is allowed to
travel between the cylinder and the ocean via small holes. Although this type
of gauge measures the ocean height directly, obviating the need for pressure and
salinity values, the main drawback is that the holes can become blocked by sea
life. In cold weather the static water in the stilling well is liable to freeze before
the surrounding ocean unless kerosene is used to lower the freezing point and
yield a maximal time series.

Other gauges employ an acoustic pulse. The time for the round trip of the
pulse to sea surface and back to a sensor is measured (Mitchum, 1994). This is
subject to similar restrictions as the bubbler gauge in that the speed of sound in
the water is dependent upon density which must somehow be found.

3.2   Satellite altimetry

The era of satellite altimetry started over two decades ago with the launch of
GEOS 3. The high spatial coverage, coupled with the accuracy of the modern
instruments means that there are new possibilities for the measurement of the
sea level. Each successful altimeter mission has been unique in design or purpose.
The instruments which are chosen to support the altimeter, along with the design
of the orbit and the height above the Earth all have an impact on the strengths
of that particular altimeter. These issues are considered here.

Satellite altimetry involves measuring the distance from an altimeter mounted
on an orbiting platform, to the sea surface at the sub-satellite point. If the height
of the satellite above some reference surface is known then the height of the ocean
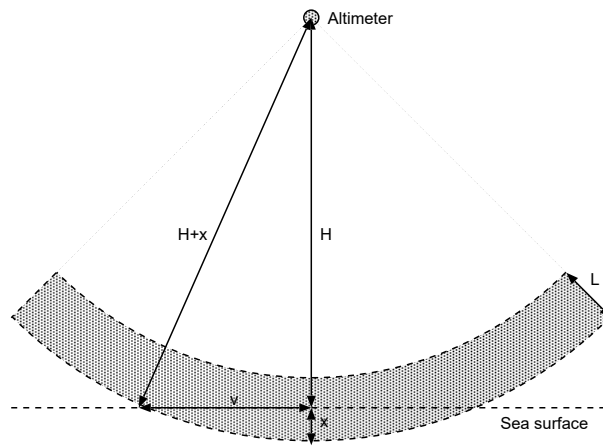
Figure 3.1: The altimetric radar pulse before the trailing edge reaches the sea surface.

above that same surface at the time of the measurement can be derived by simple differencing.

3.2.1 Measurements with satellite altimeters

In order to understand the application of satellite altimetry to the study of sea level change, the way that the instrument functions must be studied carefully. The raw altimeter height measurement is performed with a radar pulse which is transmitted in the nadir direction and then received on return after reflection at the sea surface. The time for the round trip can be multiplied by the speed of light and halved to yield the initial estimate of the range.

Physics of the waveform

For the best accuracy in the range estimate the signal to noise ratio of the returned pulse must be large enough for the sensor to detect the time of return. This is best achieved by concentrating the transmitted power into as short a pulse as possible. However with a larger peak output power comes a requirement for a larger altimeter, which is at odds with the design constraints of the satellite. This problem is overcome with the *pulse compression* technique. This consists of spreading the power of the transmitted pulse over a longer time but increasing the frequency of the pulse linearly with time. When the reflection of this *chirped* pulse is received it is fed through a selective circuit which delays signals as a function of frequency in such a way that the longer chirped pulse is compressed into a shorter pulse with a larger mean power. This pulse has a higher signal to noise ratio and can then be analysed more accurately.

An altimeter which could transmit a radar pulse with a planar wavefront would be impractically large for mounting on a satellite. Indeed the typical altimeter
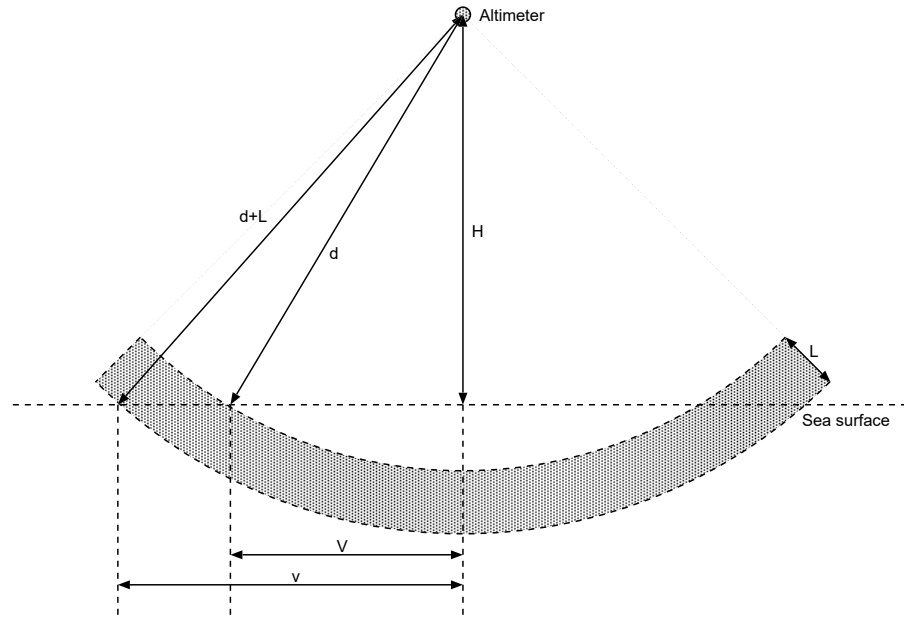
Figure 3.2: The altimetric radar pulse after the trailing edge reaches the sea surface.

beam spreads out to illuminate several square kilometres of ocean. The way that this wavefront interacts with the sea surface means that the shape of the returned pulse is not a simple repeat of the transmitted pulse, or even a noisier version of it. If a rectangular transmitted waveform and a perfectly at sea forming a plain normal to the direction of the pulse are assumed then there are two distinct phases of the interaction between the pulse and the sea surface. The rst phase starts when the leading edge of the centre of the beam reaches the sea surface. At rst glance it seems intuitive that the returned power increases linearly until the trailing edge reaches the sea surface. To establish the true nature the geometry of the pulse and sea surface as given in Figure 3.1 must be considered. The re ected power will be proportional to A, the area of sea surface illuminated by the pulse. A and its rate of change are given by

$$A = \quad v^2$$
$$\frac{dA}{dt} = 2 \quad v \frac{dv}{dt} \qquad (3.1)$$

where v is the radius of the circle of illuminated sea surface. This length and its rate of change can be expressed in terms of H, the altitude of the altimeter above the sea surface, and x, the distance between the sea surface and the pulse leading edge at nadir

$$v = \quad \overline{x(x+2H)}$$
$$\frac{dv}{dt} = \frac{x+H}{x(x+2H)} \frac{dx}{dt}$$

37

The term $\frac{dx}{dt}$ is equivalent to the speed of the pulse and is thus a constant. This constant is denoted c. The rate of A in Equation 3.1 becomes

$$\frac{dA}{dt} = 2\pi c(x + H)$$

Since H is very much larger than x it dominates the term and although x increases linearly, the rate of A approximates very well to the constant $2\pi cH$. This demonstrates that in this ideal case, the first phase of pulse reflection results in a linearly increasing power received at the altimeter. Now, the second phase of the reflection starts when the trailing edge meets the sea surface. From this point on, an annulus of sea surface will be illuminated resulting in nearly constant power in the return signal until the whole pulse cone has reached the sea surface. Figure 3.2 illustrates the pulse at this phase. In the Figure, v and V are the outer and inner radii of the annulus respectively and L is the pulse length. In this case the sea area illuminated by the radar as a function of V is

$$A = \pi(v^2 - V^2)$$
$$= \pi L(L + 2\sqrt{H^2 + V^2})$$

As V increases it is seen that in fact the area gets larger suggesting an increase in returned power as time goes on. However since H is much larger than V (by about three orders of magnitude), the increase in illuminated area is negligible and is dominated by the decrease in power at the fringes of the pulse away from the nadir. After the plateau stage the signal therefore starts to trail off and gradually drops back to zero.

From the above ideal case, the power received back at the altimeter will have two distinct phases. The first phase will involve the power rising linearly from zero. The second phase starts when the power levels off instantaneously at the start of the plateau phase. As the illuminated area of ocean moves further away from the nadir point, the power will gradually fall back to zero. Since the edge of the pulse is not well-defined, but is characterised by a gradual drop in intensity, there is no distinct boundary between the plateau and the fall in power.

Sea surface roughness

The above discussion on the returned waveform assumes that the sea surface is perfectly flat. This of course is not the case and ocean waves will cause significant deviation from this crude assumption. Ideally the presence of ocean waves should not change the range estimate, so the altimeter should measure the range as if the deviations at the surface were flattened out. Waves can be regarded as an error to be corrected for, and also an observable to be measured. Ocean waves can be split into two categories. Any wind at the sea surface will force the water

at the surface causing the familiar irregular roughness, referred to as wind waves. Although storms can cause wind waves which are powerful enough to endanger shipping, the predominant e ect in the absence of extreme meteorological conditions is the second category of waves, namely swell. These are the rhythmic motions of the upper regions of the water which can transfer energy over large expanses of ocean. This phenomenon typically originates in a region of the ocean experiencing a typhoon or other extreme weather condition. The strong wind sets up large amplitude wind waves which are e ectively an incoherent set of harmonic oscillations with di erent energies and hence wavelengths. Since the waves with longer wavelengths travel faster than those with shorter wavelengths the irregular collection of wavelengths soon separates into distinct wavelengths. Irvine (1985) describes this mechanism and draws the analogy between the storm and a stone thrown into a pond. This swell resulting from the storm will radiate away from the source of agitation and may well travel thousands of kilometres from the source. These waves can have very large amplitudes of up to 10 m or more from trough to crest.

The amplitude of waves is important when considering the e ect on the re ected altimeter pulse. It is easy to specify the amplitude of the wave when only one pure wavelength is present   the peak to trough distance can be used. In practice however there is usually a collection of di erent wavelengths and amplitudes present. The *signi cant wave height* is used to indicate the e ective height of the waves at a given location and refers to the average peak to trough height of the largest third of waves. This de nition is used in altimetry when determining the e ect of waves on the altimeter range measurement.

Wind waves and swell both a ect the shape of the waveform received at the altimeter. The peaks of the waves are convex in relation to the radar wavefront. This will increase the di usivity of the re ection and less of the energy at this stage will be returned to the altimeter. As the wavefront reaches the wave troughs, the concavity approximates a crude corner re ector and more of the energy from here will be sent back in the direction of the altimeter. The e ect of this phenomenon is that waves cause the ocean to appear lower to an altimeter (Rodrigues and Martin, 1994). This is referred to as electro-magnetic bias (EMB) (Yaplee *et al.*, 1971).

Another e ect of waves is that as wave height increases, the time between the leading edge of the radar pulse reaching the tops of the waves and the trailing edge reaching the troughs will increase. This will spread out the leading edge of the returned waveform, giving it a shallower gradient.

There is another e ect of surface roughness, particularly the small irregular agitations caused by wind. For a perfect re ector, the incident and re ected

beam are coplanar, and the angle that each beam makes with the normal to the reflecting surface is equal. Surface roughness causes deviation from this ideal. Indeed altimeters operate by virtue of the ocean being a non-perfect reflector. If it were perfect, the sensor would only receive the small amount of energy reflected from the sub-satellite point, not enough to detect above the noise level. However higher levels of roughness increase the tendency of the radar pulse to be reflected away from the direction of the satellite thus reducing the power received at the sensor. The apparent radar cross-section of the sea surface as measured by the altimeter can therefore be related to the wind speed, allowing the latter to be inferred from the returned power.

The tracker

The tracker is the part of the altimeter responsible for deciding when the return pulse has been received. The job of the tracker involves analysis of the signal from the receiver around the time that the radar pulse is expected to return from the sea surface. It works by anticipating the return pulse and looking for this signal arriving at the receiver. It must estimate the mean height of the reflecting facets so that the initial range estimate may be derived; the slope of the leading edge for calculation of the significant wave height; and the level of power returned which is used in calculation of wind speed. Design constraints mean that rather than measure the mean sea surface height from the returned pulse, it actually measures the median (Carnochan, 1996). If the median does not on average represent the mean then a bias will be introduced. This is called the skewness bias. As mentioned above, larger waves spread out the returned pulse and the altimeter must estimate the time at which half of the leading edge has been received. If it does this with a systematic error which is dependent upon the slope then a similar error will appear in the ranges it makes. This bias is termed the tracker bias (Gaspar *et al.*, 1994). The effects of the skewness and tracker biases are combined with the EMB (described above) and the sum total is termed the sea state bias (SSB). This bias is related to the significant wave height (to account for swell) and wind speed (to account for wind waves).

3.2.2 Media Delays

Once the tracker has measured the time taken for the reflected pulse to arrive at the receiver, the initial estimate of the altimeter range can be calculated using the speed of light in a vacuum. This initial approximation will not suffice as a final range estimate since the pulse will be delayed by the atmosphere, leading to an apparent ocean surface several metres too low (Klokocnk *et al.*, 1994). This error is a result of the refractive index of the atmosphere being greater than that

of a vacuum. Since the altimeter is nadir-pointing, the angle of incidence of the beam to the atmospheric boundaries will be very close to zero and there will be negligible refraction. However the speed of light through a material is equal to c n where c is the speed of light in a vacuum and n is the refractive index of the material. This will slow the radar beam and cause an error in the calculated range. Correction for this delay requires knowledge of the amount of gas making up the atmosphere below the satellite when a particular range estimate is made. While the relative composition of the atmosphere from the common gases such as nitrogen, oxygen and carbon dioxide will not deviate significantly from their nominal values, the water vapour content of the atmosphere is subject to huge relative variations. To account for this the tropospheric delay is split into a contribution arising from the dry mass of the atmosphere and a contribution from the water vapour content.

The diurnal bulge and variations in atmospheric density arising from weather systems affect the dry mass of the atmosphere. The dry mass cannot be measured or inferred from an altimeter range and so must be independently derived. It can be shown that the delay to the radar is related to the total atmospheric pressure at nadir. Modern meteorology provides operational measurement and modelling of weather systems and data derived for the purpose of weather forecasting can be further exploited by altimetry. For instance, the European Centre for Medium-Range Weather Forecasting provides the values of atmospheric pressure required to correct European Remote Sensing (ERS) altimetry for the dry tropospheric delay.

Whereas the dry mass of the atmosphere cannot be measured from an altimetric satellite, the water vapour content can be deduced by an orbiting platform. This is done by measuring the amount of microwave radiation emitted by the water vapour present in the column of atmosphere between the satellite and the sea surface. This function is typically performed by a radiometer. For instance T/P is equipped with a multi-channel radiometer which measures the microwave brightness primarily at the 21 GHz frequency.

The contributions of the sun and cosmic rays mean that much ionising radiation is incident on the Earth. The result is the ionosphere, which consists of the particles which have become charged through absorption of this type of energy. This comprises various discrete layers at altitudes between 50 and 1000 km above the surface of the Earth (Hofmann-Wellenhof *et al.*, 1994). A charged medium such as the ionosphere is transparent to microwave radiation but the velocity of the wave will be modified. This effect applies to the altimeter pulse and must be corrected for. The magnitude of the effect on the calculated altimeter range can be shown to be proportional to the number of free electrons in the column

at the nadir point of the altimeter (Robinson, 1985). The delay to a wave can be calculated if this total electron count (TEC) can be calculated or measured.

The delay of an electro-magnetic pulse by the ionosphere is a function of wavelength. Altimeters can be designed to exploit this fact and measure the TEC. If microwave signals at more than one frequency are transmitted and used in the range calculations then two expressions involving the unknowns of range and TEC can be derived. The range can then be uniquely calculated. Altimeters which do not have the dual frequency facility must rely on tracking systems which operate at more than one frequency, such as the DORIS system (see below), or on ionospheric models such as the Bent model to estimate the TEC.

3.2.3 Satellite altitude

By correcting for the potential sources of error discussed above, modern altimeters have very high accuracies. These accuracies are wasted unless the other critical component of the range is treated with a similar precision. This component is the altitude of the satellite. The complexity of the system, with the many sources of acceleration other than the Earth s geopotential, mean that the orbit cannot be approximated by Keplar s ideal case. Unfortunately orbit generation for altimetric satellites is not as simple as nding the six orbital elements. Estimates of the path of the satellite in an Earth-centred reference frame, which are known as orbit ephemerides, are calculated for these satellites by modelling the accelerations which the vehicles experience and applying Newton s laws of motion. Satellite tracking plays an important part in estimating the various unknowns in the orbit computations.

Force modelling

The forces experienced by an Earth satellite arise from various sources, some of which are gravitational. The Earth s geopotential is the dominant source of force on the satellite. Ephemerides which are accurate enough for altimetry applications require that the Earth be considered as more complex than a point mass. A higher order geopotential model is required to take account of the variations in density within the Earth. Tidal deformation of the oceans and the solid Earth make the geopotential a dynamic quantity and these variations must be considered in the production of orbit ephemerides.

Third body attraction constitutes another important source of gravitational force to be included in the force model. Third body attraction is more complicated than the geopotential case in that the force a ects the whole system of Earth and satellite. It is the di erence in attraction between the Earth and the satellite which is critical since only such a di erence will deviate the satellite from its

geopotential-determined path. This is the same principle which produces the accelerations which lead to ocean tides. Therefore the perturbing acceleration on the satellite s orbit depends not only upon the distance of the third body and its mass, but also on the orbital position of the satellite with respect to the body being orbited. Despite its low mass, the proximity of the moon means that it is the main source of this type of perturbation for an Earth satellite. The sun is also a major in uence in this respect, with the greater distance overcome by the increase in mass. Where accuracy is critical other planets in the solar system must be considered. It is not the closest planets which are most important. After the sun and moon, Jupiter and Venus are the celestial bodies which have the greatest perturbing e ect on the Earth satellite after the moon, while our neighbour Mars, with its low mass, has less impact than the remote but more massive Saturn. Of course as the distances between the Earth and the third bodies vary, particularly in the case of the planets, the perturbing forces vary too. The positions must be modelled and considered in the construction of a force model for ephemeris generation.

Amongst the non-gravitational forces is the friction experienced by lower orbiting satellites as they move through the outer reaches of the Earth s atmosphere. The acceleration experienced by a body moving through a gas is proportional to the density and the square of the velocity, and is inversely proportional to the mass, amongst other factors (Zandbergen, 1991). The extent of this atmospheric drag is therefore dependent upon the altitude of the platform and the state of the atmosphere since this will determine the atmospheric density. This can be a ected by the solar cycle, with solar maxima coinciding with atmospheric drag which is more erratic. This is due to the more active sun imparting higher energy to air molecules and causing the limit of the atmosphere to extend further from the Earth s surface. The changes in the atmosphere leading to this e ect are hard to model accurately and the e ect of drag is often inferred empirically as part of the orbit generation process.

Another category of perturbation to be considered is the force arising from electro-magnetic radiation incident upon the spacecraft. The pressure from the charged particles comprising the solar wind and the radiation arriving directly from the sun, as they meet the skin of the satellite is signi cant and they should be included in any ephemeris generation. There are two possible courses for solar ultra-violet radiation which arrives at the Earth s surface. First it may be absorbed and contribute to raise the temperature of the Earth. Since the Earth must dissipate this heat, some is re-radiated. The Earth is not hot enough to radiate in the ultra-violet band so this heat is lost as infra-red energy. The second possible course for the incoming ultra-violet radiation is that it may be re ected

back into space as the Earth s albedo (Zandbergen, 1991). These forces from the Earth must also be considered in force models if the most accurate ephemerides are to be generated.

The nal type of force has a major impact on satellite orbits but is only active occasionally. This is the force originating from the satellite boosters. These are required periodically to maintain the orbit of the satellite and preserve the ground-track con guration. Without this orbit maintenance the ground-tracks of repeating cycles would gradually deviate from the analytical ground-track and it would cease to be a repeating ground-track. These maintenance operations are usually short lived but are of such a magnitude that they will have a signi cant impact on the ephemerides and thus cannot be ignored in orbit generation. Since the main e ect of such man uvres is to cause a kink or discontinuity in the satellite path, these events are usually excluded from orbit generation so that an ephemeris ends just prior to a man uvre and another starts immediately after the man uvre has ended.

A force model used in the orbit generation process must take the above forces into consideration. Any error in the model will lead to error in the generated ephemerides.

Satellite tracking

Tracking devices are designed to observe some part of the instantaneous state of a satellite s motion[1]. Satellites tted with a laser retro-re ector (LRR) can be tracked with a satellite laser ranger (SLR). An SLR measures the range between the optical centres of the ranger and the LRR by transmitting a pulse of laser light in the direction of the satellite and measuring the time for the return.

Another tracking system is the Doppler Orbitography and Radiopositioning Integrated by Satellite (DORIS) which requires an active receiving instrument to be installed on the satellite to be tracked. By measuring the doppler delay in the signals received from various ground-based transmitters, the rate of change of the range between the transmitter and receiver may be calculated. Measurement is made at two frequencies to allow correction for ionospheric delay. These range rate observations may be used for parameter estimation in ephemeris generation.

The ERS satellites are tted with Precise Range and Range Rate Equipment (PRARE) which, as the name suggests, tracks the satellite with the same observables as SLR and DORIS combined. Unfortunately this device on ERS 1 failed just after launch which left laser ranging as the main tracking system. This problem was overcome on its successor and this system is now used to track ERS 2.

---

[1] The tracker, which is part of the altimeter, is not to be mistaken for a satellite tracker, which is a separate instrument for monitoring the position of the satellite.

Despite being plagued by problems concerning the calibration of the equipment and the unreliability of the ground stations, the PRARE system now makes a significant contribution to orbit generation for ERS 2.

Ephemeris generation

Orbit ephemerides are generally calculated by applying the force model to an estimate of the initial state of the satellite at a given time where this initial state consists of the position and the velocity. The aim is to generate better estimates of the initial state and any coefficients of the force models, such as the atmospheric drag parameters, by comparing orbits generated using the rudimentary parameters to the observations by the tracking systems. Starting with the initial state and applying the components of the force model, the state of the satellite at subsequent regular time intervals can be calculated by numerical integration. Each time a tracking system makes an observation, the observed quantity can be compared to the value derived from the integration. Discrepancies, or residuals, between the observed quantity and the corresponding calculated value can be interpreted as arising from an error in the initial state or other coefficients. Partial derivatives of the tracking observation with respect to each of the various parameters can be calculated. The residuals of all tracking observations may then be minimised by adjustment of the initial state and model parameters using the least squares technique. Spurious observations may then be rejected and iteration can be used to refine the estimates of the parameters.

The ephemeris will not perfectly describe the true motion of the satellite owing to errors in the force model. Errors such as mis-modelling of atmospheric drag will in general contribute noise which although undesirable, is not as troublesome as systematic error. In particular, errors in the geopotential model will lead to errors which are correlated by geographical location. For instance Tapley *et al.* (1994) estimate T/P orbits generated with SLR and DORIS tracking to be accurate to 3.5 cm root mean square (RMS). While the noise component of this can be removed with long time series, the systematic component can be up to 2 cm. Such errors are of particular concern for geoid studies and when combining data from different altimetric satellites.

3.3   The Global Positioning System

Since the US Department of Defense set up the Global Positioning System (GPS), various techniques have been found to increase the accuracy and apply the technology in new areas. This has important implications for studies of altimetry and sea level change.

The primary purpose of GPS is to allow military personnel to locate their position accurately and in real time. This is achieved with satellites in high Earth orbit which transmit signals from which the time of transmission can be derived by a GPS receiver. The receiver can then determine its range from the GPS satellite by calculating the time lag from transmission by the satellite to reception at the receiver. Allowance is made for the receiver clock to be slightly incorrect leading to an error in the range, so this range is actually called a pseudorange, since it represents the true range plus an error. This error will be solved for later. Coupled with the pseudorange is the location of the satellite at the time of transmission, which is also transmitted by the GPS satellite. This information allows the receiver to restrict its location to some point on the surface of a sphere with the centre coinciding with the original location of the GPS satellite and the radius equal to the measured pseudorange. If the pseudorange to a second satellite is determined then the position can be determined to be lying somewhere on a circle. A third satellite restricts the uncertainty further to one of two unique points, one of which can usually be rejected as unreasonable. In practice this arrangement requires a very precise and expensive atomic clock as part of the receiver. To keep the receiver costs low, a cheaper and less precise clock can be used in the receiver and a fourth GPS satellite can be used to solve for the error in the receiver clock. The 24 GPS satellites are con gured in six orbital planes such that at any time and location on the Earth s surface at least four are visible at an elevation of at least 15 (Hofmann-Wellenhof *et al.*, 1994).

3.3.1   GPS codes and frequencies

All GPS satellites transmit at the two frequencies of 1575.42 MHz and 1227.60 MHz, called L1 and L2 respectively. The receiver derives pseudoranges from code sequences transmitted by each satellite. Each GPS satellite transmits two code sequences unique to that satellite. These are the Coarse/Acquisition code (C/A code) and the Precision code (P-code). In normal circumstances the P-code is encrypted to deny access to non-military users (see below). First the case where encryption is not enabled and the raw P-code is accessible to all is considered. Whereas the P-code is modulated onto both the L1 and L2 carriers, the C/A code is only modulated onto the L1 carrier. In principle, the P-code can be read from each carrier leading to two pseudoranges and the opportunity to measure the ionospheric delay.

3.3.2 Denial of accuracy

To reduce the bene t of GPS to potential adversaries of the US military, various precautionary measures are included in the GPS system to deny full accuracy to users other than the authorised military personnel. Selective Availability (SA) is one such measure whereby an error is introduced into the GPS clock or position as broadcast by the satellite. This introduces an error into positions derived using data from that satellite. Another precaution is Anti-Spoo ng (A-S). As mentioned above, the P-code can be modulated onto both carriers. However when A-S is in operation the P-code is encrypted with a secret W-code to yield the Y-code which is modulated onto the carriers. This cannot be read by a non-military receiver so recourse must be made to the C/A code. Since this is only modulated onto the L1 carrier, the ionospheric delay cannot be measured and the model values transmitted by the GPS satellite as part of the navigation message must be used. The primary role of the A-S mode is to prevent bogus GPS signals from being generated and confusing receivers, but the denial of accuracy is critical to non-military users who want optimal performance for altimetric applications.

3.3.3 Novel applications of GPS

Many novel applications have arisen from the GPS system in a variety of elds including sea level studies and altimetry. These are made possible by the ingenious techniques used to overcome the accuracy denial measures. As a result, the accuracy denial is most e ective only for instantaneous point positioning. Various civil authorities generate precise GPS satellite ephemerides with a time lag of a few days, so the ephemerides transmitted as part of the navigation message which may be corrupted by SA need not be used. There are numerous geodetic reference points around the world whose locations are known to high accuracy. Measuring the GPS-observed locations of these reference points can allow the clock o sets for each satellite to be determined. Results from such exercises are widely circulated within a similar time scale.

Although post-processing can remove the e ect of SA, A-S cannot be overcome easily without access to the W-code. This means that model values for the ionospheric delay must still relied upon. However for two receivers situated close to each other, the unknown ionospheric delay will be approximately constant. This fact may be used to derive the baseline between two GPS receivers to very high accuracy. This accuracy is better than can be achieved from traditional surveying techniques. In this way, an altimeter may be geodetically linked to ground-based instruments so that independent estimates of the sea surface can be made in a consistent reference frame.

Since there is no reason why the GPS receiver has to be on the ground, satellite tracking is one such novel applications of the GPS system, and TOPEX/Poseidon has such a receiver tted. This exploits the more accurate ephemerides of the higher orbiting GPS satellites, re-calculated to overcome SA, to x the path of the platform in a lower orbit. In this case the GPS position estimates augment the data from other satellite trackers in the orbit determination process.

The geological applications of GPS are useful in the area of sea level studies. The movement of a reference point in an Earth-centred reference frame can be monitored over time using GPS. A receiver can be installed permanently at the point of interest or regular short surveys may be carried out every few months. In this way the stability of the reference point may be determined, in particular the movement due to activity in the Earth s crust may be monitored. This is very useful for monitoring the vertical stability of tide gauges. Any vertical motion of the land on which the gauge is mounted will appear in the gauge readings. Independent measurement of the movement can be used to correct the readings or to eliminate unreliable gauges.

3.4   Altimetry past and present

After experiments were carried out on Skylab to test the altimeter concept, altimetry rst became operational when GEOS 3 was launched on 9 April 1975. Despite a mission length of over three and a half years, the limited on-board storage of data restricted the amount of altimetry that could be retrieved. Additionally the design requirements for accuracy were such that long-term sea level variability could not be resolved (Martin and Butler, 1977). The instrument was a success in that it was intended to be a proof-of-concept altimeter and its scienti c contribution was limited to the determination of a more accurate marine geoid than was available at that time.

NASA s Seasat, launched June 1978, held more potential with its more accurate altimeter which had an estimated noise level of less than 10 cm. In an orbit with an inclination of 108 Seasat initially described an orbit which caused the ground-track to repeat every 17 days. It subsequently entered a 3 day repeating con guration. Unfortunately, despite its potential it was the victim of a terminal failure after collecting data for only three months.

1985 saw the launch by the US Navy of Geosat into a similar orbit to Seasat. Geosat had two main phases, namely the Geodetic Mission and the Exact Repeat Mission. The former lasted for 18 months and was designed to sample the ocean surface with a very high spatial resolution, thus allowing a very accurate geoid to be calculated. This allowed inertial navigation systems, on missiles as well as

submarines, to determine location in an Earth-centred reference frame to higher accuracy. Additionally the US Navy obtained an accurate sea floor topography map, thus allowing submarines to avoid detection by staying much closer to the sea floor whilst avoiding features such as seamounts. Owing to the significant advantage this knowledge gave the US, the data from this phase were classified. However it was recently decided that the advantage of secrecy had become outweighed by the benefit of declassification of the data and the data from this phase were released in November 1995 (Yulsman, 1996). The second phase of Geosat was configured to follow the 17 day repeating ground-track of Seasat. For this reason it was named the Exact Repeat Mission. With its lower spatial sampling, the data from this phase were available from the outset.

Geosat continued operating nominally until late in 1989 when it started to suffer technical problems and eventually failed in January 1990.

ERS 1, which was launched in 1991, is a state-of-the-art remote sensing satellite. In addition to an altimeter of greater accuracy than had been achieved before, it is well-equipped with sophisticated peripheral devices, producing data with applications in many areas of remote sensing. The radar altimeter is supported by a radiometer which allows correction to be made for the water vapour content of the troposphere. The tracking system consists of a LRR for satellite laser ranging. As mentioned above, the compliment of sensors at launch included a receiver for PRARE system which unfortunately failed within hours of the launch. ERS 1 has flown in several orbit configurations. After two short phases with 3-day repeating ground-tracks, ERS 1 was manuvred into an orbit with a ground-track which repeated every 35 days. This is called the first multi-disciplinary phase since it provides a good compromise between spatial and temporal resolution for measuring the mean sea level and mesoscale variability respectively. The first multi-disciplinary phase was followed by another short 3-day repeating mission called the ice phase and then the geodetic mission. The latter was designed to sample the mean sea surface with very high resolution and to that end had a ground-track which repeated every 168 days. After nearly two cycles of the geodetic mission ERS 1 returned to the 35-day repeating configuration for the second multi-disciplinary phase which lasted until it was retired in 1996.

The joint efforts of the USA and France led to the launch of TOPEX/Poseidon (T/P) on 10 August 1992. Unlike the ERS satellites this is a dedicated altimeter mission with each of the two countries providing an altimeter instrument. T/P is the first satellite to carry two radar altimeters. NASA s altimeter TOPEX is the first dual frequency satellite altimeter and operates in the Ku-band at 13.6 GHz and the C-band at 5.3 GHz, allowing easy correction for ionospheric delay. France s contribution to the mission was provided by Centre

National d Etudes Spatiales (CNES) in the shape of the Poseidon altimeter. This is an experimental solid state instrument which operates at a single frequency of 13.65 GHz. The altimeters share an antenna and only one can operate at once. In practice, Poseidon has been in operation for about one tenth of the time that TOPEX has.

T/P orbits at a height of 1340 km. This is unusually high for a satellite altimeter where the orbits are usually kept low to minimise the power requirement of the altimeter and to allow other scientic instruments to operate. The higher orbit carries with it a number of advantages. First, atmospheric drag is not a consideration in the orbit computations, meaning that T/P ephemerides are subject to less noise. Secondly, geographically-correlated orbit errors arising from higher order errors in the geopotential model reduce as orbit height increases. Thirdly, at higher altitudes the satellite is visible to ground-based tracking stations for longer periods, allowing more tracking data to be collected. The higher orbit in conjunction with the impact of the DORIS tracking system lead to lower noise and systematic error in the calculated orbit heights. This results in more accurate sea level measurements.

The T/P platform carries several supplementary devices to support the two altimeters. The water vapour content of the atmosphere is measured with the TOPEX microwave radiometer for calculation of the associated path delay. Various tracking instruments are available. A LRR provides a reference point for SLR tracking. Other tracking is carried out with a DORIS tracking device and an experimental GPS receiver.

The latest satellite altimeter to be launched is ERS 2, which has been designed as the successor to ERS 1. ERS 2 started ranging in May 1995. The design is very similar to that of ERS 1 with the addition of a new sensor, the Global Ozone Monitoring Equipment. This is unrelated to the radar altimeter and the processing of altimetry from ERS 2 is very similar to that of ERS 1. An important dierence between ERS 1 and its successor is that the PRARE equipment has functioned nominally since launch, allowing for reduction in noise in the orbits. ERS 2 has only followed one ground-track pattern which is the same as the multi-disciplinary phases of ERS 1.

3.5   Altimetry for variability

Satellite altimetry has played an important part in measuring the various components of sea level and its variability. The high accuracy and resolution of modern geoid models is thanks to the excellent altimetric coverage of the last dozen years. In the case of ocean tides a similar situation prevails. The altimetric satellites

have provided a sampling rate high enough to allow enhanced models for the astronomical-tides. It is also true that satellite altimeters can be employed to answer questions concerning the extent of large-scale and long-term sea level change. For instance, the rate of global eustasy can be estimated by calculating the mean sea level with an altimeter throughout its life. These can be compared to determine a mean rate of change over that period. To have con dence in these rates, the stability of the altimeter is heavily relied upon. Any drift in the altimeter device or any systematic trend in the way sea surface is calculated will cause the calculated sea level change to be in error.

3.5.1 The absolute altimeter range bias

The absolute range bias of an altimeter is a phenomenon which causes it to measure too long or too short. It is essentially caused by the design of the tracker in the altimeter. If this measures the return with a constant error, this error will manifest itself in the range. This range bias is distinct from the tracker bias which is the component of the error related to wave height. This range bias is a systematic e ect which acts in addition to the noise associated with each individual range measurement. To determine the e ect of this phenomenon, consider the calculation of altimetric sea surface heights. The altimeter provides an initial estimate of the range which is corrected for the instrumental and geophysical e ects as described in the above sections to give h_{range}, the corrected altimeter range. This is used to derive an estimate of the sea surface height:

$$h_{alt} = h_{sat} \quad h_{range}$$

where h_{sat} is the height of satellite above a reference ellipsoid and h_{alt} is the associated estimate of the sea surface height above the same reference ellipsoid. Of course there will be noise in this estimate but the systematic range bias can be corrected for. By convention the range bias, h_{bias} is expressed such that

$$h_{true} = h_{alt} + h_{bias} + \qquad (3.2)$$

where h_{true} is the true sea surface height and   is the residual noise and any other correlated error in this observation. Thus a positive range bias implies that the altimeter is measuring too long and the measured altimetric sea surface is lower than the true surface. To correct the altimeter range for this e ect, the absolute range bias must be subtracted.

The term   in Equation 3.2 may be split into geographically-correlated error and noise. The former arises principally from radial orbit error induced by mis-modelling of the geopotential (see Section 3.2.3), although it may have a

component from media correction errors. The true sea surface height may thus be more precisely related to the altimetric sea surface height by the expression

$$h_{true} = h_{alt} + h_{bias} + \quad + E \quad\quad\quad (3.3)$$

where   is the geographically-correlated error and E is the noise in the observation.

When using a single altimeter to study an oceanographic phenomenon such as an ocean tide, it is not necessary to consider the absolute range bias. As long as the bias is constant over time, the sea surface height may be sampled as the ground-track allows and a time series of sea surface heights at a given location can be derived. The mean sea surface may then be removed from the series since it is only the relative o sets of the measurements from each other which matter. Similarly, to derive an estimate for the an equipotential surface with an altimeter in isolation, the range bias can be ignored since the geoid is expressed as o sets from some reference surface. Problems arise when data from more than one altimeter are to be included in the generation of these models. Here, assuming that the absolute biases do not coincide, the mean sea level will no longer absorb the whole bias and the altimeter measurements will be contaminated by the di erence between the biases of the two altimeters. This relative bias must be overcome if data from multiple altimeters are to be included in models.

To consider sea level change over long time scales, it is necessary to combine the data from several altimeters. To date, no altimeter has equalled T/P for length of reliable operation. This satellite is currently producing its sixth year of sea level data. The altimetry of T/P can be used to derive an estimate for sea level change. This will be subject to uncertainty arising from noise. The way the mission samples long term periodic variations in sea level, such as those associated with the solar cycle, may also lead to an unrepresentative estimate for true long-term eustasy. To reduce these sampling errors and reduce noise, data from more than one altimeter need to be combined. This sort of application also requires careful handling of the relative bias. Sea level rates may be derived with each altimeter, but they cannot be related to each other unless any relative bias between the altimeters is corrected for.

There has been continuous altimeter operation since ERS 1 was launched. This allows the systematic di erences between the various altimeters to be estimated by comparing common points on their ground-tracks. This may not be the case in the future. At least three altimeter missions are currently being planned. The Geosat Follow-On (GFO) is due to be launched in February 1998 and it is hoped that at least one of T/P or ERS 2 will be operational for a signi cant amount of time after this so that e ective inter-calibration may be carried out. This will provide continuity between the missions. Even assuming that GFO is

not delayed and does not fail in launch, there is no guarantee that any altimeter will be operational when the subsequent planned mission is launched. Jason-1, the follow-up to T/P, and ENVISAT, the next generation remote sensing satellite from the European Space Agency, are scheduled for launch around the turn of the century. Delays often occur and there is a chance that the continuity of altimeter mission coverage may be broken. If this happens, bridging the gap will not be trivial.

3.5.2 Bias instability

Even if the absolute range bias is ignored and a sea level rate is to be estimated using an altimeter in isolation, the stability of the range bias is an issue. If this quantity varies over time then sea level rates will be corrupted with this extra drift. Accurate eustasy estimates demand that this drift be accounted for.

3.5.3 Other sources of systematic bias and drift

Any phenomenon which causes systematic error in the altimeter range is indistinguishable from the range bias in the altimeter instrument if that altimeter is used to derive variability estimates. Sources of such errors include the various corrections applied to raw altimeter ranges. This may be inherent in the models employed to derive the corrections or the instruments used to measure them. Other sources of bias may be more obscure such as errors in the algorithms used to process the altimetry.

The systematic errors need not be spatially invariant. As mentioned in Section 3.2.3, errors in the geopotential model will give rise to geographically-correlated orbit errors. While this orbit error will average to zero globally, values for the range bias over limited geographical regions may well contain a component of this error.

Although the sources of range bias which have their origin in the tracker may not be separable from those other sources, it is still useful to measure this composite bias since a range corrected with it will be more accurate than one corrected just for the absolute bias induced by the tracker. These other sources of range bias are also prone to drift over time. Any method to measure drift in the bias should also resolve the whole drift from whatever cause.

3.5.4 Overcoming the range bias

In the following chapters the nature of the range bias in the satellite altimeter is studied and ways of measuring it and monitoring its stability are examined. More accurate knowledge of this major hurdle to the merging of data from distinct

altimeters will allow the unification of altimetry from two or more missions. The value of such a unified set would exceed the sum of the parts.

Chapter 4

Measuring the absolute altimeter bias using in situ instrumentation

The range bias in altimetric satellites is a hurdle to measuring and understanding sea level change. This characteristic of altimeters must be considered when combining data from multiple sensors if a spurious sea level change is to be avoided. Here, a technique proposed by Lam *et al.* (1993) is developed. The method aims to derive estimates for the range biases of ERS 1, TOPEX, Poseidon and ERS 2 by combining data from the tide gauge installed at Newhaven with local ocean models to obtain an in situ estimate of the sea surface height at points where altimeter ranges are made. Additionally, globally determined precise orbits are improved in the locality of the calibration area by employing the satellite laser ranger at Herstmonceux. The significant impact of the radial orbit error is thus dramatically reduced. The attraction of this approach is that it uses existing instrumentation and models and thus has few costs associated with it as compared with the dedicated campaigns of the space agencies. Preliminary results were encouraging and a study of the application to a large portion of the T/P and ERS 1 missions is presented. This is extended to the initial Calibration/Validation phase of ERS 2 where the newly-launched satellite shared the same ground-track as its predecessor, allowing the range biases of both instruments to be derived in a consistent way.

4.1   Absolute calibration

The absolute bias of an altimeter causes it to measure too long or too short. The apparent sea surface height will not therefore coincide with the true surface. One way to determine the absolute bias is to compare the sea surface height measured

using the altimeter with the height derived from an independent estimate. The method is based on Equation 3.2 which is rearranged to

$$h_{bias} = h_{true} - h_{alt} \qquad (4.1)$$

If the true sea surface height h_{true} can be computed independently of the altimeter, then it may be compared to the altimetric sea surface h_{alt} and the bias can be inferred. This is the principle underlying the work presented here.

A tide gauge can be employed to determine an initial estimate of h_{true}. Since tide gauges are only available at the coast, the altimeter ranges are not available at the point at which tide gauge estimates of sea surface height are taken. Even where ranges are available at the coast, they are unreliable due to corruption of the radar returns and radiometer readings by land. To overcome this a tide gauge reading at the time of an altimetric measurement, which is nearby but clear of the coast, may be corrected for the sea surface topography difference between the gauge and the sub-satellite point. There are several contributions to this difference. First, the mean sea surface will change between the gauge and the altimeter point. Similarly, the dynamic ocean topography, including the ocean tide and meteorological effects at the time of the range must be corrected for. The term h_{true} in Equation 4.1 can thus be estimated as

$$h_{true} = h_{gauge} + c_{geoid} + c_{tide} + c_{met} \qquad (4.2)$$

where h_{gauge} is the sea surface height measured by the tide gauge, c_{geoid} is a correction for the geoid, c_{tide} is a correction to allow for the ocean tide and c_{met} is a correction to allow for meteorological effects.

4.1.1   Precise orbit height

Accurate orbit heights are also critical in absolute calibration since any radial orbit error will translate directly into the h_{bias} in Equation 4.1. Although high quality satellite tracking systems along with good force modelling mean that global precise orbit ephemerides are now very accurate, geopotential mis-modelling still gives rise to significant orbit error which is a function of the orbit configuration and the geographical location. It is the correlation by geographical location which is a hurdle to this type of range bias determination. Although the effect of noise in the radial orbit height can be reduced with larger samples, the correlated error will be absorbed by the bias. The radial orbit accuracy of ERS 1 is typically quoted as 10 15 cm at best (Scharroo et al., 1994). (Moore et al., 1996b) predict the radial orbit errors of gravitational origin to be 5.5 cm in the region of the English Channel using the Joint Gravity Model 2 (JGM 2) covariance matrix. Further covariance studies of ephemerides revealed that this error
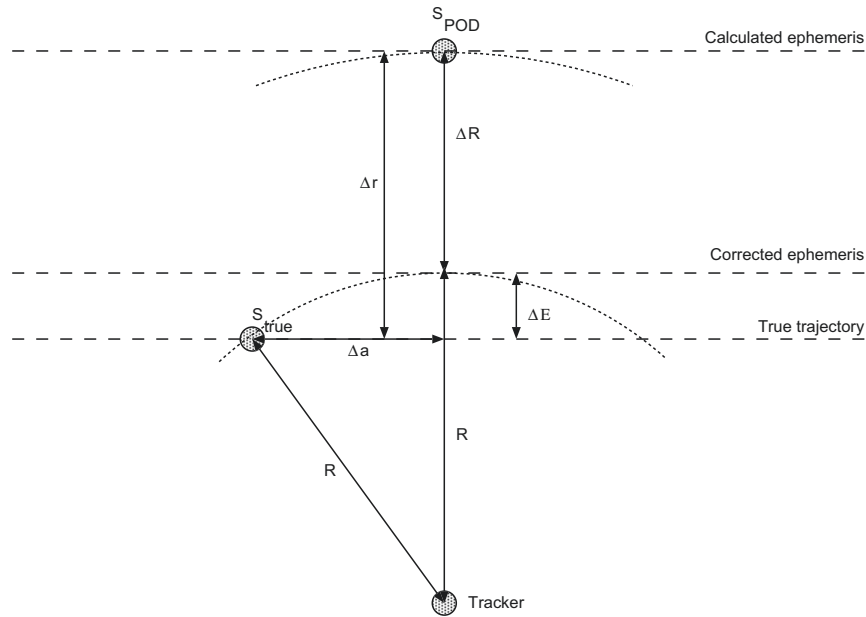
Figure 4.1: Mis-measurement of the radial orbit error as the satellite passes over the tracker.

was close to 4 cm in the same region. These values are purely of gravitational origin and assume that terms of period in excess of four days are absorbed within the initial state vector of the long arc orbit. Errors of this magnitude are clearly unacceptable for range bias calculations and must be addressed.

A satellite tracker used in the generation of precise ephemerides can be employed to estimate the radial orbit error of a satellite in the region of the tracker. First it is assumed that the satellite passes directly over a tracker. The orbit height generated from global orbit determination will in general disagree with the height predicted by the tracker. This disagreement will be expressed in the form of a residual between the measured range of the vehicle and the range calculated from the ephemeris at the time of a range measurement. This residual can be interpolated to the time of over-flight of the tracker by the satellite and be interpreted as radial orbit error. If the radial orbit error is assumed to be constant over distances of a few hundred kilometres then the residual can be removed from the global orbit in the region of the tracker making an accurate local solution comprising a short arc free from radial orbit error. This special case of an exact over-flight also assumes that there is no orbit error in the direction along the path of motion and that the tracker residual is thus interpolated to the exact moment of over-flight. This will not be true in general and there will be such an along-track component of the orbit error. This along track error will mean that the residual is not taken at the exact moment of over-flight and so the residual will not be measuring orbit error purely in the radial direction. The along-track orbit error will contribute to the tracker residual and an error in the

radial correction will result. Figure 4.1 illustrates this, showing the configuration at the time of overflight as estimated from the global orbit determination. The Figure shows the estimated position of the satellite derived from orbit determination (S_{POD}), the true position of the satellite (S_{true}), the radial orbit error (Δr), the along-track orbit error (Δa), the interpolated tracker range (R), the tracker residual (ΔR) and the radial error remaining in the orbit after correction with the residual (ΔE) in relation to the tracker. ΔR can be used as an approximation for Δr, the radial orbit error, and removed from the radial orbit heights. The effect of using this approximation for the time of overflight is to introduce the error ΔE into the radial correction and hence into the radial orbit height. However, the error ΔE is not likely to be significant as it depends on ΔR and Δa as follows

$$\Delta E = \Delta R - \sqrt{\Delta R^2 - \Delta a^2}$$

This can be rearranged to

$$\Delta a = \sqrt{2\Delta R \, \Delta E - \Delta E^2}$$

For ERS 1 the effect would be most pronounced since R is smaller, corresponding to a lower Earth orbit in addition to the lower precision of generated orbits for satellites in lower orbit. In this case R is about 720 km. An along-track error of approximately 38 m would be required for an error in the radial correction of 1 mm. An error of this magnitude is unlikely and its effect on the radial orbit is hardly significant. Although not illustrated in Figure 4.1, there may well be orbit error in the direction normal to both the vehicle path and the line connecting the Geocentre to the vehicle. This cross-track error will also contribute to an error in the radial correction although cross-track errors of similarly large magnitudes are required to induce radial errors at the millimetre level.

The assumption above is that the satellite passes directly over the tracker. Now, this is very unlikely, except in specific contrived cases and is certainly not a restriction that should be placed on a flexible absolute bias calibration method. Lam (1994) demonstrates how this restriction can be avoided and the method extended to the case where the satellite passes sufficiently close to, but not directly over the tracker. In this case the required radial correction can be approximated by the tracker residual at the time when the satellite is closest to the tracker. To demonstrate that this is the case, consider the general position of the satellite when it is being tracked. The associated tracker residual ΔR can be expressed as

$$\Delta R = \frac{r - r_e \cos\theta \cos\phi}{R}\, \Delta r + \frac{r_e \cos\theta \sin\phi}{R}\, \Delta a + \frac{r_e \sin\theta}{R}\, \Delta c \qquad (4.3)$$

where R is the laser range; r and r_e are the distances from the Geocentre to the satellite and tracking station respectively; θ is the geocentric angle between
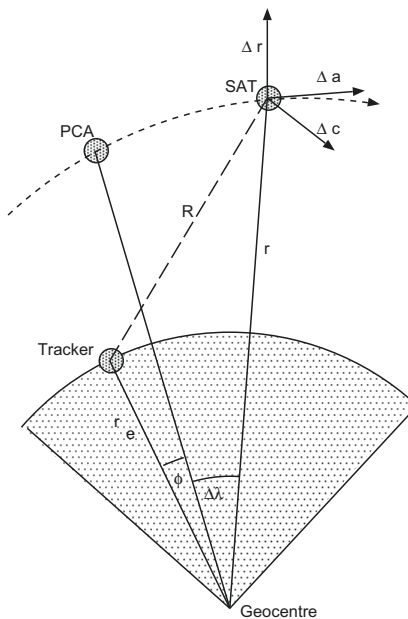
Figure 4.2: Mis-measurement of the radial orbit error by the tracker when the satellite does not pass directly overhead.

the tracking station and the point of closest approach (PCA) of the satellite to the tracker, $\Delta\lambda$ is the geocentric angle between the sub-satellite point and the PCA; and Δr, Δa, and Δc are the orbital error in the radial, along-track, and cross-track directions, respectively. In the special case of the PCA, $\Delta\lambda = 0$ and Equation 4.3 reduces to

$$\Delta R = \frac{r - r_e \cos\phi}{R}\Delta r + \frac{r_e \sin\phi}{R}\Delta c. \tag{4.4}$$

The parameters at the general position and at the PCA are shown in Figure 4.2. Equation 4.4 can be used to estimate the typical error in the correction for radial orbit error for given passes of various satellites.

4.2 Calibration in the UK

The UK is endowed with a selection of quality tide gauges. In addition to this, the Royal Greenwich Observatory (RGO) maintains a satellite laser ranger (SLR) at Herstmonceux. Figure 4.3 shows the locations of these along with the ground-track of T/P. From the previous section it has been shown that a successful absolute calibration requires a tide gauge situated as close as possible to the SLR for the purpose of reliable estimation of the sea surface height and radial orbit error. In this respect the gauge at Newhaven is the best choice as it is only 31 km to the south-west of the Herstmonceux. The gauges at Portsmouth, Dover and Sheerness are also close to the SLR but the complexity of the tides in the Solent, the Straights of Dover and the Thames estuary, added to their
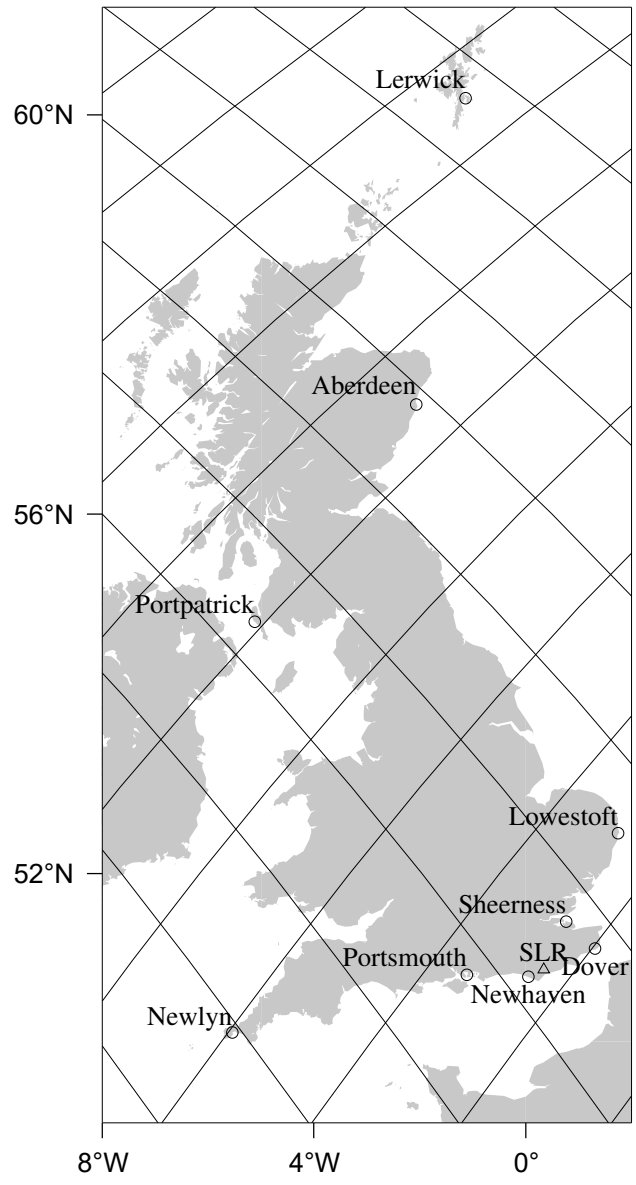
Figure 4.3: Locations of the UK tide gauges (circles) and the RGO SLR at Herstmonceux (triangle) with the T/P ground-track overlaid.
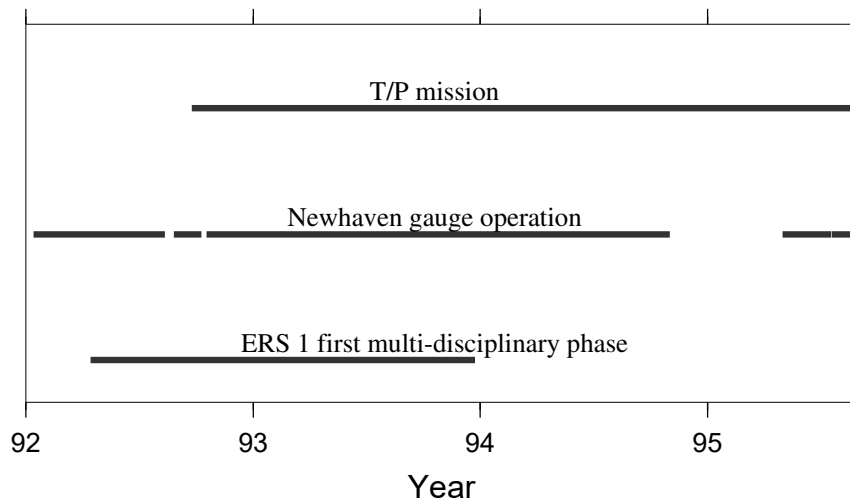
Figure 4.4: The time during which the Newhaven tide gauge is in operation as compared to the T/P mission and the rst multi-disciplinary phase of ERS 1.

further distances from the SLR, mean that these gauges are not as ideal as the Newhaven installation. Data from the UK tide gauges are available from the Proudman Oceanographic Laboratory (POL) in the form of unprocessed hourly readings.

Figure 4.4 shows the times at which the Newhaven tide gauge is operational in comparison to the rst multi-disciplinary phase of ERS 1 and the rst 35 months of the T/P mission. For ERS 1 the tide gauge coverage is excellent, with only two short periods of outage lasting for 14 days and eight days. For T/P there is a large amount of data missing which spans the start of 1995, corresponding to the period from cycle 77 to cycle 96. It was later determined that the gauge was fully operational during this period. The apparent long outage was caused by an out of date dataset at Aston University.

4.2.1 Tide gauge datum

Reliable estimation of the altimeter bias depends upon accurate positioning of the tide gauge datum in the geocentric reference frame. The GPS survey carried out at Nottingham University, the UK Ordnance Survey, and POL (Ashkenazi *et al.*, 1993) linked the GPS reference pillar at the Herstmonceux laser and the bench mark of the Newhaven tide gauge, with respect to the International Terrestrial Reference Frame (ITRF) of 1991. The results from this survey are employed in this work.

61

4.2.2 Ocean models

The sea surface height as measured by the tide gauge as the satellite passes over the Channel must be extrapolated to each sub satellite point at which an altimeter range is available. The independent estimate of the sea surface height at these calibration points (CPs) can then be compared to the altimeter-derived sea surface height. There are three important factors to consider here.

The rst component which contributes to a change in height between the gauge and the CP is the ocean tide. The tides in the seas surrounding the United Kingdom are extremely complex due to the sea being shallow and restriction by land masses. In particular, the width and depth of the Channel are such that global tidal models are not reliable in this area and so dedicated models are required. A 50-constituent numerical model was provided by POL (Flather *et al.*, 1991). Ocean tidal displacements in this model are estimated on a 1/9 latitude by 1/6 longitude grid (approximately 12 km by 12 km). This can be used to provide di erential correction to remove the e ect of the ocean tide between the gauge and the CP.

Geoidal corrections are also important. Although this is a static e ect, neglecting to correct for the geoid di erence would mean that the o set between the gauge and the CP would be present in each bias estimate. The precise local geoid computed by Featherstone (1992) was used in this work. This geoid utilises high-resolution gravity data and GPS data to compute a solution relative to the Ohio State University 91A (Rapp *et al.*, 1991) gravity eld on a grid of spacings 2 in latitude and 4 in longitude (i.e., 4 km by 5 km).

Outside of the summer months, the wind climate in the seas surrounding the British Isles can cause substantial forcing of the waters and signi cant gradients can result. There is a model for this storm surge e ect which is run operationally at the UK Meteorological O ce twice a day during the storm surge season, September to May (Smith, 1994). The surge model uses the same grid as the ocean tide model and determines surge motion from meteorological e ects (wind and atmospheric pressure) and produces forecasts up to 36 hours ahead for weather prediction with a hindcast of 12 hours using assimilated meteorological observations. Residual elevations at hourly intervals of the hindcast are archived at POL. This model is ideal for reducing the noise in the calibration and allows the work to be carried out for all satellite passes for which tracking data are available throughout the year.
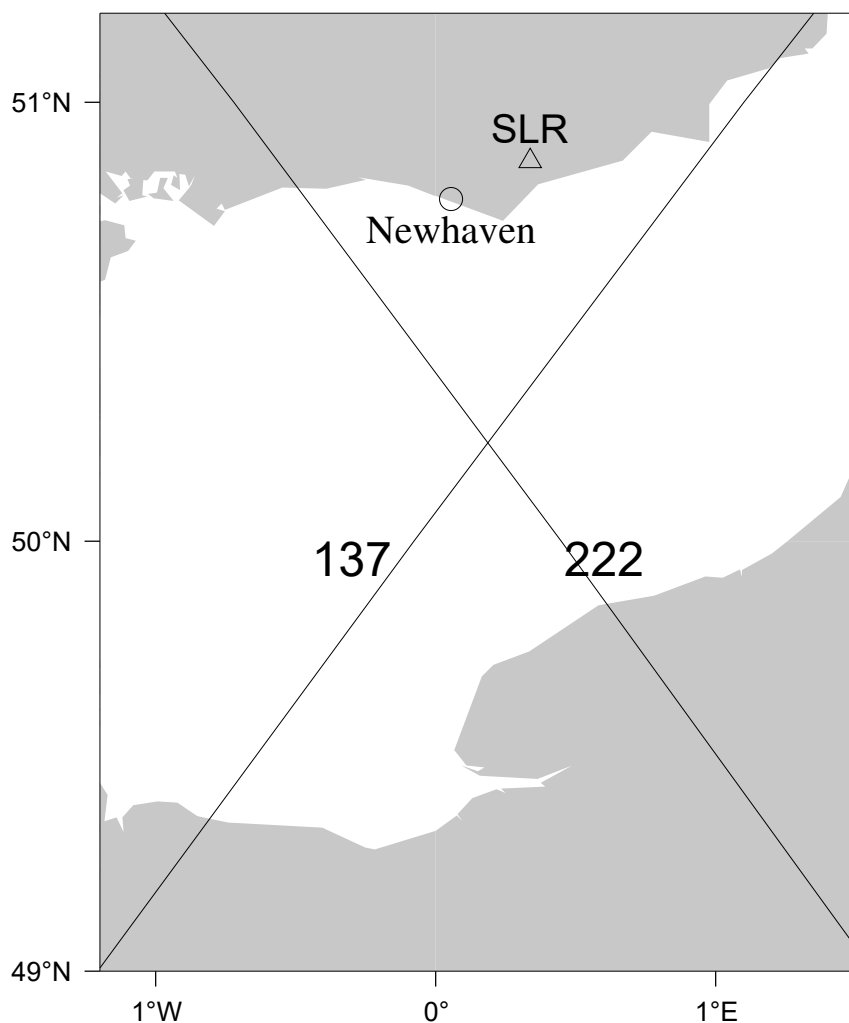
Figure 4.5: Passes 137 and 222 of T/P in the region of the Newhaven site.

Pass	D_g (km)	D_s (km)	( )	R (cm)
137	31	20	0.18	0.07
222	36	57	0.51	0.20

Table 4.1: Statistics for the two T/P passes in the range bias calibration. D_g is the distance of the closest approach to the gauge, D_s is the distance of the closest approach to the SLR,   is the geocentric angle of D_s and R is the anticipated error in the correction of the radial component of the orbit error.

4.3 Calibration of T/P

Figure 4.5 shows the two closest passes of T/P to the Newhaven tide gauge. These are ascending pass 137 and descending pass 222. Table 4.1 gives the distance of the closest approach of each pass to the Newhaven gauge and the SLR, along with the geocentric angle between the SLR and the PCA (in Figure 4.2 and also labelled in the Table). The satellite passes within 40 km of the gauge in both cases which is less than four grid elements in the tide model suggesting the suitability of the differential correction method. Similarly, both passes approach the SLR to within 60 km with pass 137 being much closer, leading to reliable radial correction of the computed ephemerides. The parameter estimates used to generate the expected error in these radial corrections (R in Equation 4.4) as given in the last column of Table 4.1 are $r_e = 6378$ km, $R = 1400$ km and $c = 5$ cm. A value of $c = 5$ cm is consistent with the expected accuracy of computed long arc T/P orbits over Europe. Table 4.1 gives the expected error in the radial correction arising as a consequence of ignoring the cross-track term.

4.3.1 Altimeter ranges

The first stage of the calibration involved the first 50 cycles. Passes 137 and 222 from each cycle in this range were considered and those where tracking data from the Herstmonceux SLR were not available were edited out. Of the 100 potential passes, 33 passes were found to meet this criterion, 16 for pass 137 and 17 for pass 222. Four of these passes comprised altimetry from the Poseidon altimeter. For each accepted pass, the altimetry for that segment of the pass over the Channel was extracted from the version 2 Geophysical Data Records (GDRs) (Archiving, Validation and Interpretation of Satellite Data in Oceanography (AVISO), 1992). The data were filtered for readings flagged as being over land along with readings with the rain/excess liquid flag set. The raw altimeter ranges were corrected for the media delays and the pole tide. The values for the wind speed and the significant wave height (SWH) were taken from the GDRs and used as input for a sea state bias (SSB) model. Rather than using the SSB values from the prelaunch algorithms as they appeared on the GDRs at that time, the newer postlaunch models for this quantity are investigated as described below. Since all other oceanographic effects are observed by the tide gauge, it was not necessary to correct the altimetry for them.

4.3.2 Precise radial orbit heights

Precise orbits were generated for the required passes. A step length of three seconds was used to ensure maximum accuracy in interpolation of the radial

orbit heights to the locations of the CPs. The resulting ephemerides expressed in cartesian coordinates were converted to geodetic coordinates with respect to the standard reference frame used throughout this work. This has a semi major axis of 6378.1363 km and the inverse of the coefficient of flattening is 298.257. The laser range residuals from the Herstmonceux SLR for each pass were analysed. A low order polynomial was fit to the residuals and this was evaluated at the time of the PCA of the satellite to the tracker. This ΔR was interpreted as the radial orbit error and was removed from the radial orbit heights. The radial orbit heights were then interpolated over the time variable to the locations of the altimeter observations.

4.3.3 The tide gauge datum

The tide gauge is used to provide an independent estimate of the sea surface height at the CP. The starting point for this calculation is the tide gauge datum, the location of which is known from the GPS survey of Ashkenazi *et al.* (1993). However consideration must be given to the reference frames used. Orbit heights are radially corrected with the SLR ranges and residuals, so the radial heights are expressed with respect to the reference frame in which the location of the SLR is specified. The station coordinates used for orbit computations are expressed in the ITRF 1992 reference frame. However the GPS survey which linked the gauge datum to the SLR reference solar pillar was carried out using the ITRF 1991 reference frame. A problem arises since in general the position of a reference station will vary between two reference frames. Such an offset in the calibration region, unless accounted for, will mean that the tide gauge datum will be offset from the reference of the orbit heights. This will in turn lead to a systematic error in the derived altimeter biases. Ideally, to overcome this a set of vector transformations are needed to convert coordinates in the ITRF 1991 reference frame to coordinates in the ITRF 1992. Such a transformation is not available but an approximation can be adopted using the fact that the SLR coordinates in both reference frames are available. The full set of transformations would consist of translations and rotations in three orthogonal axes, along with a scaling. Even though the coordinates of a fixed point (the SLR) in both reference frames are known, all seven transformation parameters cannot be uniquely solved for. However, the full transformation can be approximated by translations in three axes. This approximation will hold for points close together on the surface of the Earth, such as the SLR and the gauge which are separated by only 19 km. By differencing the coordinates of the SLR in both reference frames an approximate translation can be derived. This translation was used in this work to convert the coordinates of the tide gauge datum from the ITRF 1991 to the ITRF 1992

reference frame.

4.3.4 Independent sea surface height

The gauge reading at the time of each altimeter observation was determined by interpolation of the raw hourly data. The interpolating third-order polynomial for the four hourly readings closest to the required time was found and this function was used to interpolate the gauge readings. If any of the four hourly values were missing then the gauge reading was flagged as invalid. However the gauge was found to be operational for all passes in this case. The reading was added to the height of the tide gauge datum and corrected for reference frame offset to give an ocean elevation at the gauge.

Since the effect of the solid Earth tide will appear in the altimeter range but will not be observed by the tide gauge, a model value for this tide at the time of the observation was derived and added to the raw tide gauge reading. No account was made for a differential effect between the gauge and the CP. This approximation is acceptable, given the very long spatial wavelength of this phenomenon.

The geoid height at a given location was derived using bilinear interpolation of the four surrounding grid points in the model. Geoid heights were derived at the gauge and each CP so that the geoid gradient between the two could be applied.

A differential correction for the ocean tide between the gauge and each CP was derived using the tide model. Tidal elevations at an exact location were calculated using bilinear interpolation on the grid before the required time and then at the same location on the grid after the required time. Linear interpolation over time gave the elevation at the required location at the required time. The tidal offset at the gauge could then be subtracted from the gauge reading and the offset at the CP added so that the tidal gradient was then accounted for. For CPs which lay in the range of the storm surge season, a correction for this effect was derived in the same way as for the tide.

The independent estimate of the true sea surface height (h_{true} in Equation 4.2) was thus calculated as

$$h_{true} = h_{datum} + h_{reading} + h_{set} + h_{geoid}^{CP} \quad h_{geoid}^{TG} + h_{tide}^{CP} \quad h_{tide}^{TG} + h_{surge}^{CP} \quad h_{surge}^{TG}$$

$$(4.5)$$

where h_{datum} is the height of the tide gauge datum above the reference ellipsoid, $h_{reading}$ is the tide gauge reading and h_{set} is the model value for the solid Earth tide at the gauge. h_{geoid}^{CP} and h_{geoid}^{TG} are the model values for the geoid at the CP
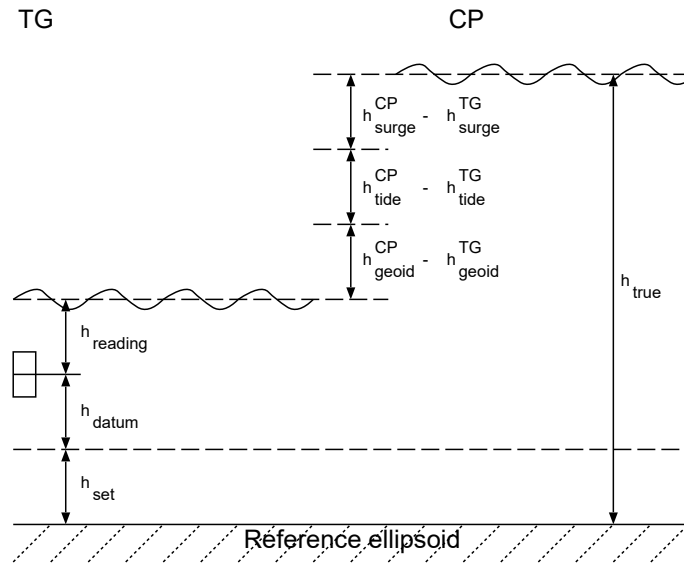
Figure 4.6: The calculated ocean elevation at the calibration point (CP) derived from the reading at the tide gauge (TG) as calculated using Equation 4.5.

and the gauge respectively, with analogous notation for the ocean tide and surge. This correction procedure is illustrated in Figure 4.6.

4.3.5 Derivation of bias estimates

In general each pass over the Channel yields several bias estimates while only one bias estimate for the pass is desired. All estimates in a pass must be considered for inclusion and then an averaging process must be applied. The locations of the CPs could range from close to Newhaven down towards the French coast. CP points taken on or near the coast will evidently not be reliable since corruption by land of the radar return and radiometer readings will occur. For typical conditions in the Channel, the diameter of the TOPEX altimeter footprint is of the order of 3 km. The radiometer footprint is at least an order of magnitude larger and will thus be the limiting factor in restricting measurements close to the coast. Each bias estimate in a pass was checked for deviations in the proximity of land. If land was causing corruption, it usually led to a jump in the measured bias of at least several centimetres, and could be rejected easily after a visual check. In order to be able to combine all accepted CPs in a given pass into a single bias estimate for that pass, a weight is derived for each CP by taking the inverse square of an estimate of its likely error. To derive this expected error, consider the likely accuracy of each bias estimate. As the distance between the gauge and the CP increases, the expected accuracy of the model values for the differential correction of static and dynamic topography between the two points decreases. In consequence, each CP is assigned an expected error proportional

67
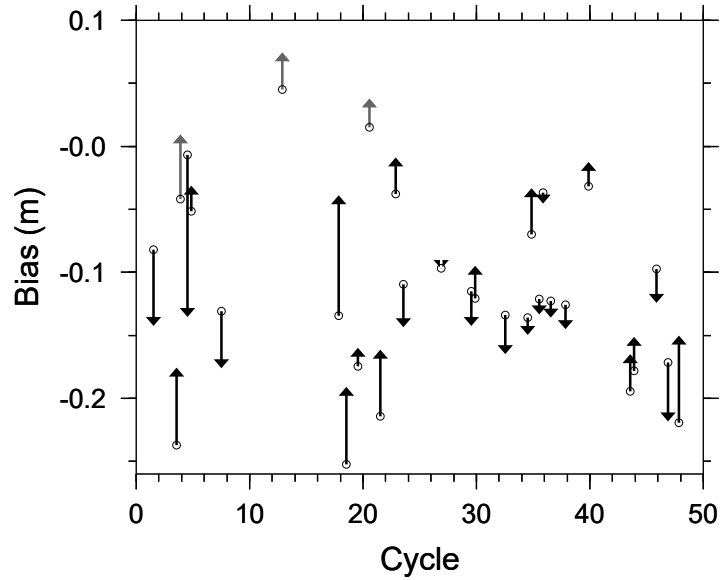
Figure 4.7: Bias estimates before (circles) and after (arrowheads) correction for radial orbit error for TOPEX passes (dark arrows) and Poseidon passes (light arrows).

to its distance from the gauge. This is satisfactory except for bias estimates at CPs which are close to the gauge. These will have an unduly high weight which is undesirable given that radiometer footprints at CPs close to the gauge are subject to corruption by land. To overcome this, bias estimates within 40 km of the gauge were assigned a constant expected error unrelated to the distance from the gauge. Since the expected error of any CP more than 80 km from the gauge was high and hence the weight very low, any such CP was rejected from the calibration.

Using the bias estimates at each CP in a pass and the associated weights, one bias estimate, h_i, for each pass, i, was estimated as follows

$$h_i = \frac{\sum_{j=1}^{n_i} w_{i\,j} h_{i\,j}}{\sum_{j=1}^{n_i} w_{i\,j}}$$

where $h_{i\,j}$ is the bias for the jth CP of the ith pass, $w_{i\,j}$ is the corresponding weight, and n_i is the number of calibration points in pass i. All h_i can then be averaged to give a nal bias estimate.

4.3.6 Comparison of corrected Aston orbits and NASA orbits

The 33 passes identi ed as having tracking data available were examined. Of these, passes where the minimum angle between the tracking observations and the zenith were larger than 25 were rejected. Passes where the derived bias

68
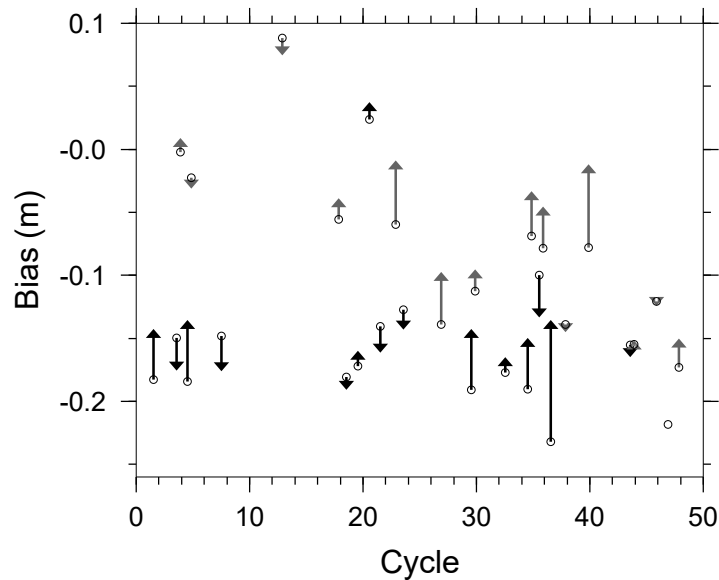
Figure 4.8: Biases derived from the NASA GDR orbits (circles) compared with the biases derived from the corrected Aston orbits (arrowheads) for pass 137 (dark arrows) and pass 222 (light arrows).

was found to be spurious in that it deviated excessively from the mean over all passes were rejected although the reason for the deviation was not apparent. Such problems were found with three of these passes. These passes were rejected, leaving 15 passes each for pass type 137 and pass type 222. The bias estimate for each of the 30 passes was derived as described above, using the precise orbits generated using Aston University software (Ehlers, 1993) which were corrected for radial orbit error. The process was repeated using the precise orbits generated by NASA as they appear on the GDRs. Since the tracking residuals were not available in the latter case, no radial correction was calculated or applied. This allowed both the overall e ect of correcting the orbits for radial orbit error, along with the extent of the radial orbit error present in the NASA precise orbits to be assessed. Figure 4.7 shows the bias estimates derived from the Aston orbits before and after correction for the radial orbit error. The arrows indicate the sense of the correction applied.

Figure 4.8 shows the biases derived using the corrected Aston orbits and the corresponding biases derived using the NASA GDR orbits. The o set between the corresponding biases is interpreted as arising from radial orbit error in the NASA orbits. Where the bias derived from the NASA orbits is more positive than the bias derived from Aston orbits, the NASA radial orbit is lower than the Aston radial orbit. The mean modulus of the bias di erence is 2.62 cm. Corrected Aston biases are, on average, more positive than the NASA biases by 1.45 cm. This value can be interpreted as the mean radial orbit error in the NASA orbits in the area of the calibration. If passes of type 137 or 222 alone are considered,

Altimeter	Author	Parameters	A	B	C	D
	Gaspar	4	0.0230	0.00360	-0.000166	-0.0025
TOPEX	Gaspar	3	0.0021	0.00430	-0.000210	
	Walsh	3	0.0029	0.00380	-0.000150	
	Gaspar	4	0.0470	0.00230	-0.000112	-0.0010
Poseidon	Gaspar	3	0.0390	0.00250	-0.000120	
	Shum	3	0.0259	0.00380	-0.000150	

Table 4.2: Parameters comprising the various models for sea state bias.

this value becomes 1.13 cm and 1.78 cm respectively. By assuming that these values account for the radial orbit error in the GDR orbits, the restriction on using passes where satellite tracking data are available is lifted and all passes with available altimetry can be considered. The standard NASA orbits can be used with the 1.13 cm or 1.78 cm o sets added to biases from pass type 137 and 222 respectively. Using all available passes rather than just those with laser tracking vastly increases the sample size and provides more certainty in the nal bias estimate, which is a traded o against a chance of corruption by radial orbit error. Note that mixing TOPEX and Poseidon passes above increases the sample size and does not a ect the calculation since the radial orbit height is independent of which altimeter is in operation.

4.3.7 Sea state bias

The accuracy of calculated bias is heavily dependent upon the quality of the algorithm used to generate the SSB correction. Models typically express the SSB in terms of SWH and wind speed. In addition to a simple parameterisation calculated before launch of the satellite, there are various models available which have been inferred from crossover data since the launch. Gaspar *et al.* (1994) has developed three- and four-parameter models for SSB for both TOPEX and Poseidon. Additionally, three-parameter models have been developed by C. K. Shum as presented in Christensen *et al.* (1994) and Walsh *et al.* (1991) for TOPEX and Poseidon respectively. These models take the general form of

$$S = \ W \ (A + B \ U + C \ U^2 + D \ W)$$

where S is the sea state bias correction which can be added to the altimeter range, U is the wind speed in metres per second, W is the signi cant wave height in metres and A, B, C and D are the model parameters. Table 4.2 shows the various parameterisations as given in Christensen *et al.* (1994).
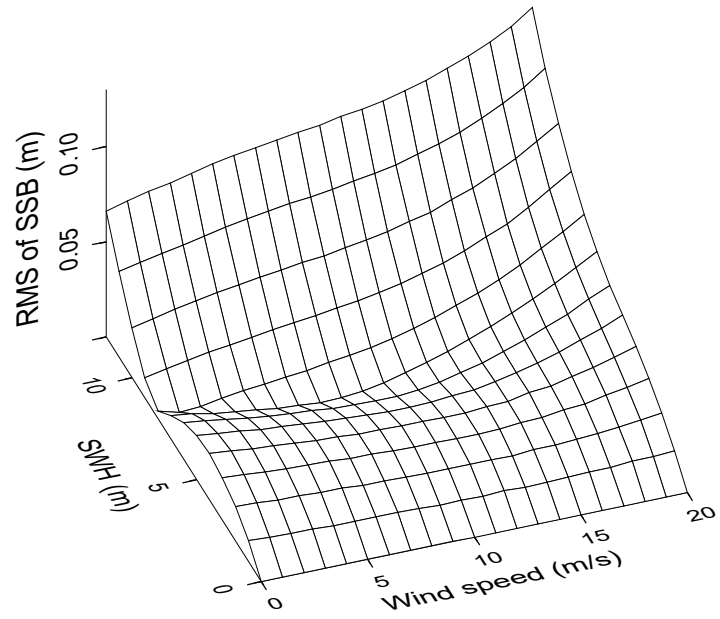
Figure 4.9: Range of sea state bias values for TOPEX.
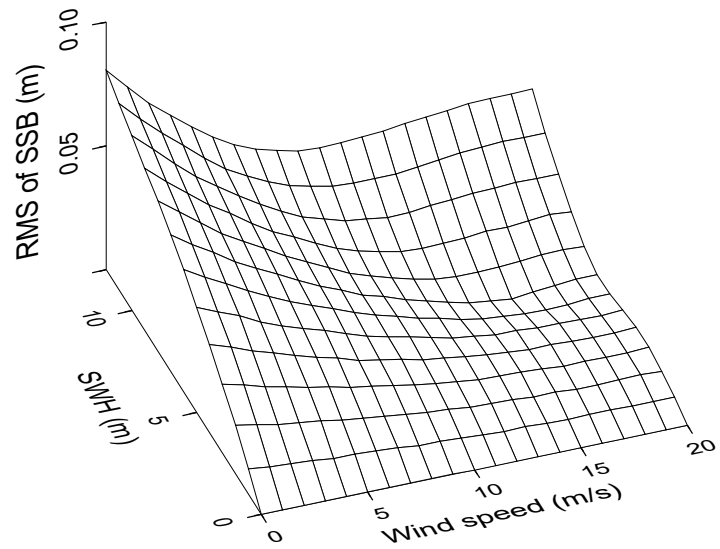
Figure 4.10: Range of sea state bias values for Poseidon.
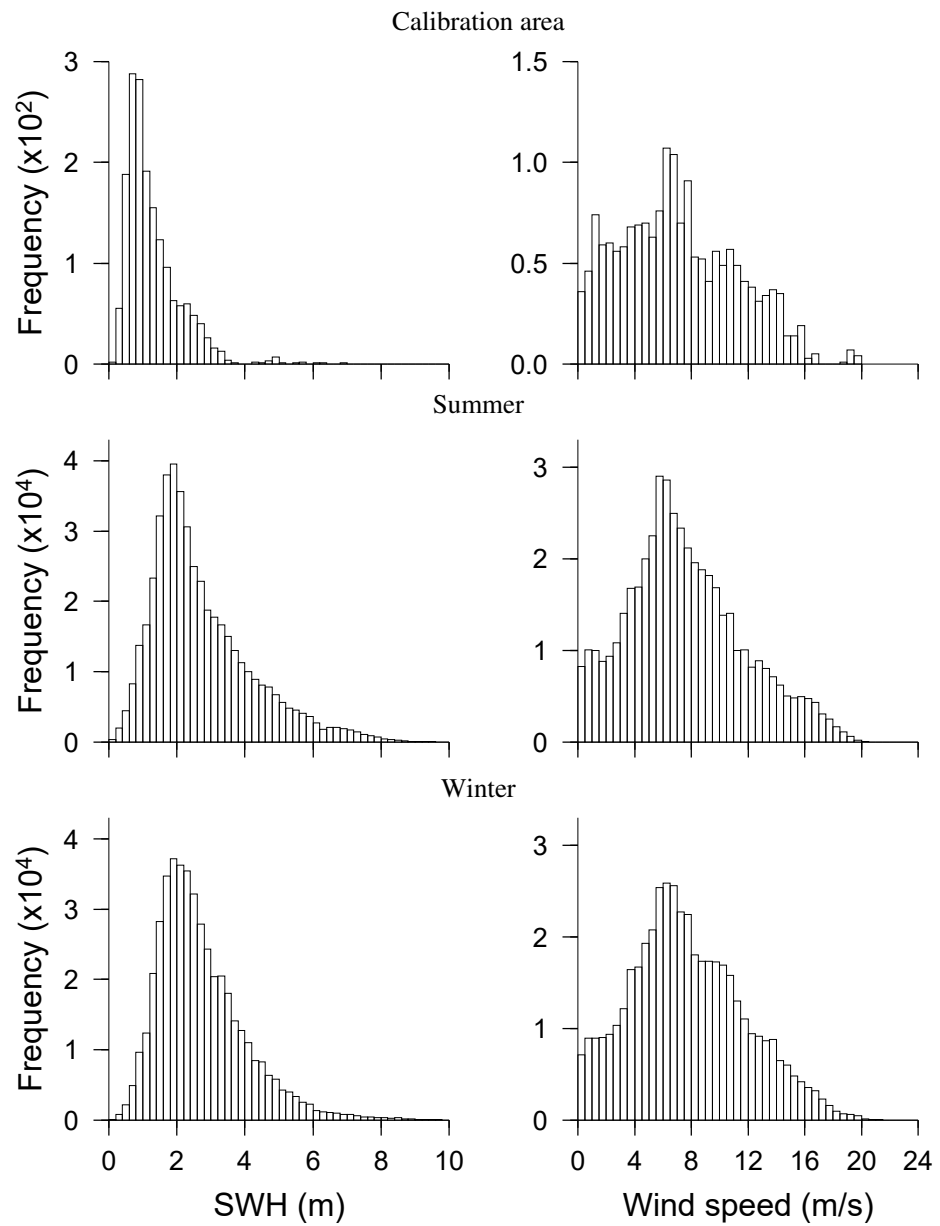
Figure 4.11: TOPEX wind and wave profile of the altimeter points comprising the absolute calibration compared with global profiles taken from the GDRs. Cycles 34 and 16 corresponding to northern hemisphere Summer and Winter respectively are used for the comparison.

Upon comparison of alternative algorithms, the range of values for SSB given by the different algorithms rose rapidly as the SWH increased. This is demonstrated for TOPEX in Figure 4.9 and for Poseidon in Figure 4.10. These graphs were constructed by evaluating the SSB with each available parameterisation. For each combination of values of U and W the three values of SSB were determined corresponding to the three parameterisations available for that altimeter, and the value plotted is the RMS about the mean of all three SSB values for those particular values of U and W. For values of W greater than about 10 m the disagreement between the models is striking. Waves of this magnitude are relatively rare, and where they do occur, may be due to corruption of the returned waveform by land or rain. Under these circumstances it is hard to fix model parameters to give sensible values in this area. Where values of W and U are low, there is still disagreement which can reach a few centimetres. Since these parameters will have values in this range for many observations in the Channel, the derived bias will in general vary when different models are used. In essence, bias in the SSB model will be absorbed into the range bias estimate. This side effect is not unwelcome since the resulting range bias accounts for more sources of inherent bias in the measurement system. However problems arise if the error in the SSB model is not constant but is rather a function of SWH or wind speed, as is suggested by Figures 4.9 and 4.10. If this condition is coupled with a wind and wave climate in the Channel which is not representative of the global climate, then the error in the derived range bias arising from SSB mis-modelling may not compensate exactly for the corresponding error in the range bias as it applies globally. For instance the comparatively short fetch available to generate swell in the Channel will result in a smaller average SWH than that in the global ocean. If a SSB model is used which is biased for lower values of SWH then an error will be introduced into any derived altimeter range bias. Figure 4.11 shows the wind and wave profile of observations in the calibration compared to the global profile from two complete cycles as taken from the GDRs. One of the cycles is from the Summer season of the northern hemisphere and corresponds to cycle 34 of August 1993. The other is from the Winter season corresponding to cycle 18 of February 1993. The wind speed profile in the Channel closely matches the global profiles of both seasons. The mean wind speed measured in the Channel is 6.8 m/s. The corresponding global means are 7.4 m/s and 7.5 m/s for the Summer and Winter seasons respectively. However the SWH profile in the Channel is significantly different from the global profiles. The mean SWH in the Channel of 1.3 m contrasts with 2.6 m for both global profiles presented here.

This demonstrates that the SWH profile of the observations used in the calibration is not representative of the global oceans. If there is a bias in the SSB

Pass	Four-parameter model		Three-parameter model		Walsh model	
137	-14.7	4.0	-12.9	3.9	-13.3	4.1
222	-12.2	7.3	-11.1	7.4	-11.4	7.6
Both	-13.6	5.8	-12.1	5.8	-12.4	6.0

Table 4.3: Derived range biases, in centimetres, and their standard deviations for TOPEX with respect to the two Gaspar models and the Walsh model.

Pass	Four-parameter model		Three-parameter model		Shum model	
137	2.3	2.2	2.8	2.3	3.5	2.4
222	4.9	6.2	5.3	6.5	6.2	6.1
Both	4.4	5.7	4.8	5.9	5.7	5.6

Table 4.4: Derived range biases, in centimetres, and their standard deviations for Poseidon with respect to the two Gaspar models and the Shum model.

model which is dependent upon SWH then any component of the derived range bias which accounts for error in the SSB model will be slightly in error when applied globally.

4.3.8 Bias estimates using the full dataset

With the restriction on tracking data lifted, all cycles were considered between cycle 1 and cycle 78, where the outage on the Newhaven gauge commenced. Processing on these was carried out as above but the standard NASA orbit as it appears on the GDRs was substituted for the Aston-derived orbits. Ten of the 156 possible passes were rejected, three owing to the non-operation of the tide gauge, six where altimetry was not available and one where all the altimetry was rejected as being too far from the gauge. Of those accepted passes, 75 were pass 137 and 71 were pass 222. Poseidon accounted for three and 12 of the pass 137 and pass 222 respectively, the rest being TOPEX passes.

All models for the SSB as mentioned above were considered. The bias for each pass was calculated relative to the SSB models appropriate to that altimeter. To account for the radial orbit error in the GDR orbits, the biases were increased by 1.13 cm or 1.78 cm in the case of pass 137 and pass 222 respectively. The values for each pass using a given SSB model could then be averaged together to yield an overall value for the bias with respect to that model. These values are given in Tables 4.3 and 4.4 for TOPEX and Poseidon respectively.

Component	Error contribution (cm)	
	Pass 137	Pass 222
Wet troposphere	1.2	
Dry troposphere	0.7	
Ionosphere	1.0	
Sea state bias	1.3	
Radial orbit height	1.5	
Radial height of TG	0.9	
Di erential models	1.5	4.0
Total	3.2	4.9

Table 4.5: Systematic error sources and estimated magnitudes in the TOPEX range bias calibration.

4.3.9 Error analysis for T/P bias estimates

If estimates of the systematic errors in the calibration system can be produced then a fuller picture of the overall con dence in the derived bias values will follow. Systematic errors will arise from all three components of the calibration, namely the altimeter range, the in situ sea surface height and the satellite height. A breakdown of the error estimates are presented in Table 4.5. As in the case of SSB, systematic errors in the media delays can usefully be absorbed into the range bias. It is only the extent to which the TEC of the ionosphere and the water content of the troposphere is unrepresentative of the global conditions, along with a bias in the system for measuring these quantities, which gives rise to error in the derived range bias. Estimation of the likely systematic bias is thus very di cult but the worse case can be assumed and estimates for the extent of the likely error taken from Archiving, Validation and Interpretation of Satellite Data in Oceanography (AVISO) (1992). Poseidon could be considered to exhibit a slightly larger systematic error owing to its single frequency design, and the ionospheric delay as a result being calculated from DORIS tracking or the Bent model. This is not expected to be substantial or to signi cantly raise the total error. An anticipated 1% error in the mean SWH can be used to estimate the error contribution of the SSB correction (Rodrigues and Martin, 1994). For the radial orbit height, the radial di erences between the Aston-derived orbits and the NASA orbits can be interpreted as the uncertainty in this quantity. The error in the in situ ocean elevation is dependent upon the uncertainties in the radial height of the tide gauge datum and the di erential topography models between the gauge and the average calibration point. The error in the former is
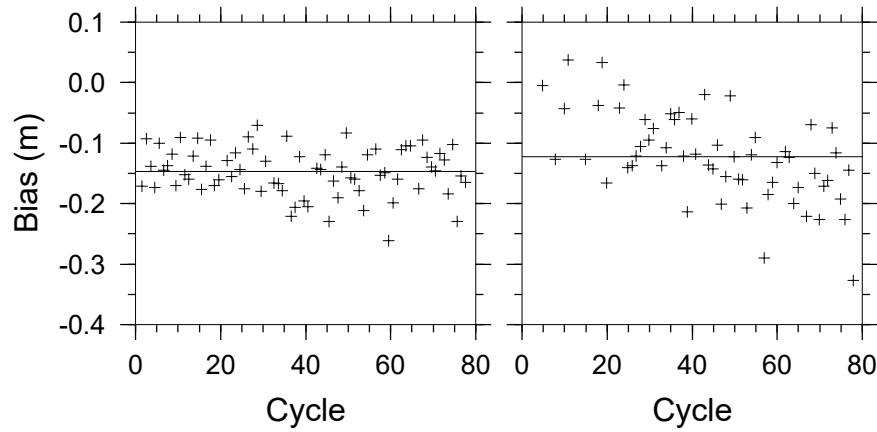
Figure 4.12: Range bias estimates for TOPEX using passes 137 (left) and 222 (right), with the averages indicated by horizontal lines.

derived from the GPS survey. In the case of the differential models, an estimate of the error is based on how bias estimates vary with latitude, averaged over all passes. The gradient of this accounts for error between the gauge and the typical calibration point. Such a mean gradient was calculated separately for pass 137 and pass 222 and was found to be 4.3 cm/degree and 11.2 cm/degree respectively. A typical point is about 40 km from the gauge which corresponds to approximately 0.36 in latitude. Over this distance the gradient suggests an error in the ocean models of 1.5 cm and 4.0 cm respectively. The gradient for pass 222 is nearly three times that for pass 137 suggesting that the models are less reliable in this area.

Since all error sources given in given in Table 4.5 are independent, the square root of the summation of the squares of the contributing error estimates will yield the total estimate for the systematic errors. As shown in the Table, this total systematic error estimate is 3.2 cm for the bias estimates involving pass 137 and 4.9 cm for those involving pass 222.

4.3.10 Bias estimate for TOPEX

Figure 4.12 shows the individual bias values from each pass for the TOPEX altimeter. The values shown are relative to the corresponding four-parameter SSB model of Gaspar *et al.* (1994) as described above. This SSB model is adopted and its careful parameterisation is relied on to reduce the risk of significant skewing of the bias with error in the SSB model. The mean bias estimate for all passes of type 137 is -14.7   4.0 cm where the uncertainty is one standard error. The corresponding value for passes of type 222 is -12.3   7.3 cm. While the bias appears stable when type 137 passes are considered, type 222 passes exhibit a significant drift over time. Linear regressions reveal that the apparent drift rates
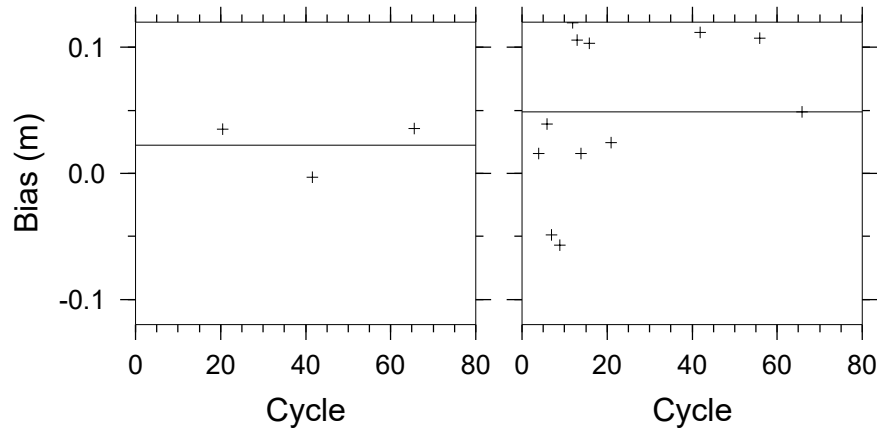
Figure 4.13: Range bias estimates for Poseidon using passes 137 (left) and 222 (right), with the averages indicated by horizontal lines.

are -0.9   0.8 cm/yr and -7.8   1.4 cm/yr for pass 137 and pass 222 respectively. The large noise and rate for the 222 passes is unrealistic and are probably partly due to the ocean tides in the western parts of the calibration region containing a multiplicity of strong, shallow water constituents which may not be well produced by, or even included in the Flather *et al.* (1991) tide model. Another factor which may be a cause of the discrepancy between pass 137 and pass 222 is that the latter is a descending pass. It will take the altimeter a finite time to regain lock on the ocean surface after leaving the south of England and until that point, altimeter ranges will be unreliable. If the tracker characteristics change over time then a variable bias near land could result. These factors lead to the exclusion of pass 222 from the bias determination and pass 137 alone is relied upon to provide the range bias estimate, which is -14.7 cm.

Although this work has concentrated on the four-parameter model of Gaspar for the SSB, the biases derived here using the other parameterisations can be similarly applied where that parameterisation is used for sea level work. However, the values derived from pass type 137 alone are recommended.

4.3.11   Bias estimate for Poseidon

Figure 4.13 shows the bias estimates for the Poseidon altimeter. Again the four-parameter SSB model of Gaspar *et al.* (1994) is used. Unfortunately the much lower availability of Poseidon data detracts from the reliability of the method. The mean bias is +2.3   2.2 cm and +4.9   6.2 cm for passes of type 137 and 222 respectively. Estimates from passes of type 222 have a much larger spread than those of type 137, as seen in the TOPEX case. Although there are only three passes of type 137, these must be relied on to provide the estimate for the bias. The estimate for the Poseidon bias is thus +2.3.
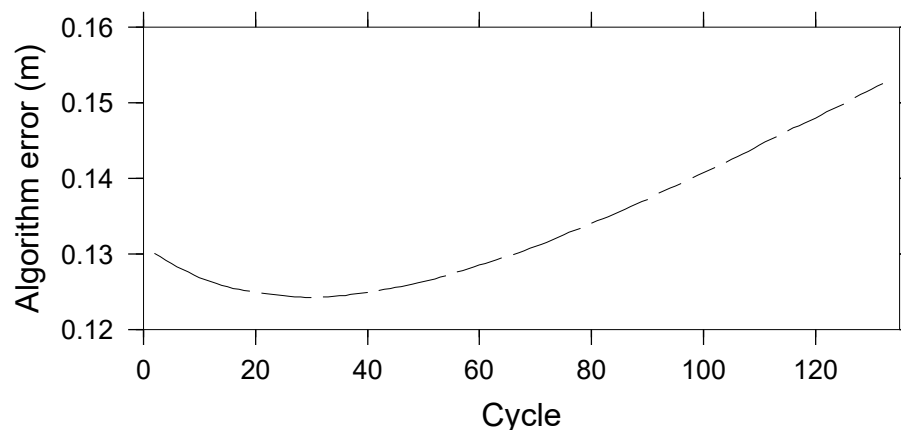
Figure 4.14: The additive correction to TOPEX ranges required to remove the
e ect of the oscillator algorithm error.

4.3.12 The oscillator algorithm error

It was announced in July 1996, after the results presented above were produced,
that the TOPEX altimetry was exhibiting a drift owing to the incorrect treatment
of the drift in the ultra stable oscillator (USO). This is the instrument which
coordinates the various phases of the ranging operation of the altimeter. Contrary
to the implication of the name, these instruments are known to drift slightly and
are monitored so that the e ect of this drift may be corrected for in the altimetry.
The error had arisen when an algorithm to take account of drift in the USO
was speci ed incorrectly, a ratio being mistakenly inverted. The e ects of this
error are twofold. First it causes the bias in the TOPEX instrument which is
signi cantly negative (Christensen *et al.*, 1994; Menard *et al.*, 1994). Secondly,
rather than counteracting the e ect of drift in the USO, using the corrections
suggested by the erroneous algorithm causes the drift in the altimetry to be
redoubled. A substantial drift is caused in the bias, which exhibits a negative rate
at the start of the mission before becoming more positive again after a minimum
at cycle 30. The long-term e ect of this is to cause a phantom sea level rise to
be observed. This error applies only to TOPEX data as only the TOPEX USO
is a ected. The triviality of the mistake made, along with the very slow rate at
which the oscillator drifts means that a correction is very simple. After discovery
of the error, a set of corrections were computed. Hancock and Hayne (1996)
provide such a correction on a cycle-by-cycle basis. These corrections indicate
the e ect of the error on the altimeter bias and are plotted in Figure 4.14.

The signi cant negative bias caused by the algorithm error is apparent in
the results derived here and should be reduced after correction for the algorithm
error. The trend in the algorithm error in Figure 4.14 for the same period as the
calibration is 0.2 cm/yr. Although the noise is signi cant compared to the size of
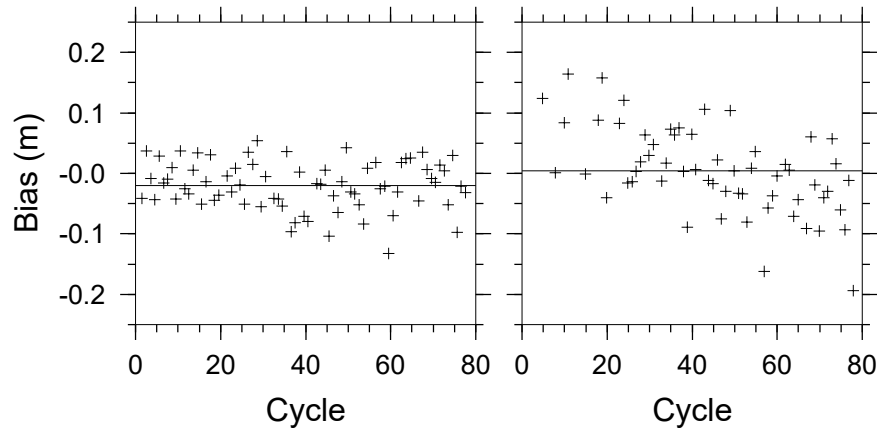
Figure 4.15: Range bias estimates for TOPEX using passes 137 (left) and 222 (right) after correction for the algorithm error. The averages are indicated by horizontal lines.

the signal which is supposed to be present in the measured bias signal, the e ect of removing the bias drift can be tested. The additive corrections to the range as given in Figure 4.14 can be applied to the biases measured in Figure 4.12. A positive change to the altimeter range corresponds to a positive change in the altimeter bias. The values in Figure 4.14 may therefore be added to the values in Figure 4.12. The resulting drift pro le for TOPEX is given in Figure 4.15. The main e ect after correction is that the range bias is much closer to zero. In fact the mean bias becomes -2.0   4.0 cm for passes of type 137 and the trend changes to -0.7   0.8 cm/yr. This range bias of -2.0 cm is adopted as the estimate for the range bias of TOPEX after correction for the USO algorithm error.

4.4   Calibration of ERS 1

The calibration principle was applied to determine the ERS 1 altimeter bias from the rst 35 day repeat multi-disciplinary phase. The sparse ground-track and short duration of the 3 day repeat ice mission made this phase unsuitable for the in situ method of calibration. The ground-track of ERS 1 during the 35 day repeat phase is shown in Figure 4.16. The smaller inter-track spacing as compared to T/P in Figure 4.3 is apparent and leads to an opportunity to consider more passes for inclusion in the calibration. The passes in the region of the Newhaven tide gauge are shown in Figure 4.17. The naming convention adopted is derived from whether a pass is east or west of the gauge (for the rst letter) and whether the pass is ascending or descending (the second letter). The number increases with distance from the gauge. Bearing in mind that unlike T/P, the ERS 1 orbit is retrograde, the ERS ascending passes go from south-east to north-west.

In this calibration the four closest passes are considered as the radial orbit
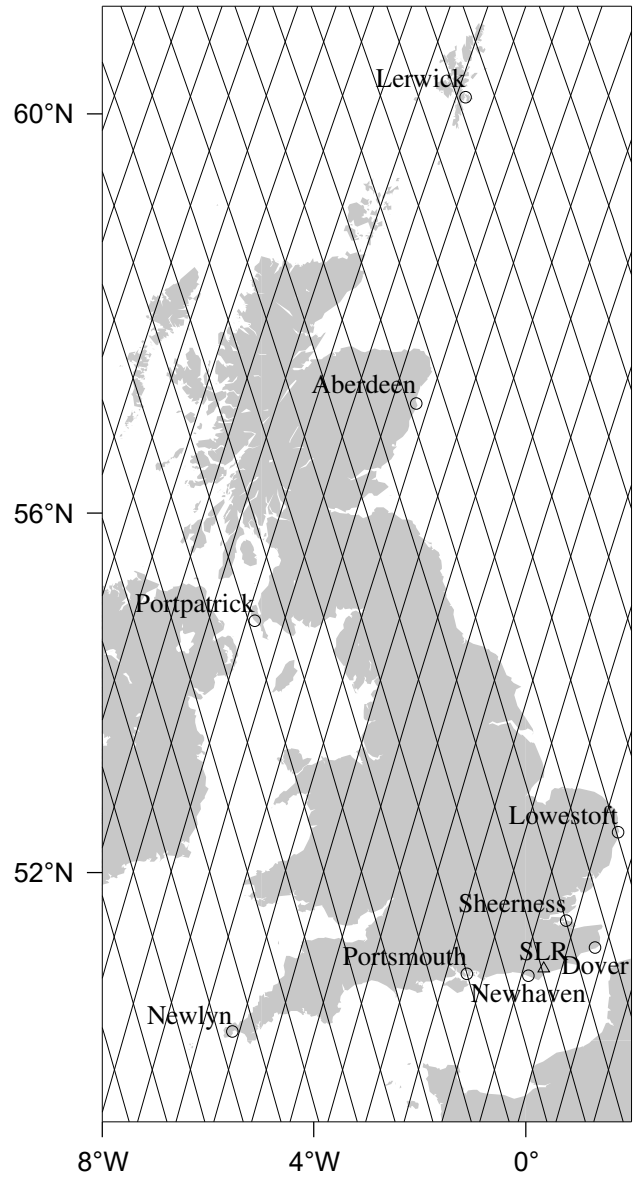
Figure 4.16: Locations of the UK tide gauges (circles) and the RGO SLR at Herstmonceux (triangle) with the ground-track of the multi-disciplinary (35 day) phase of ERS 1 overlaid.
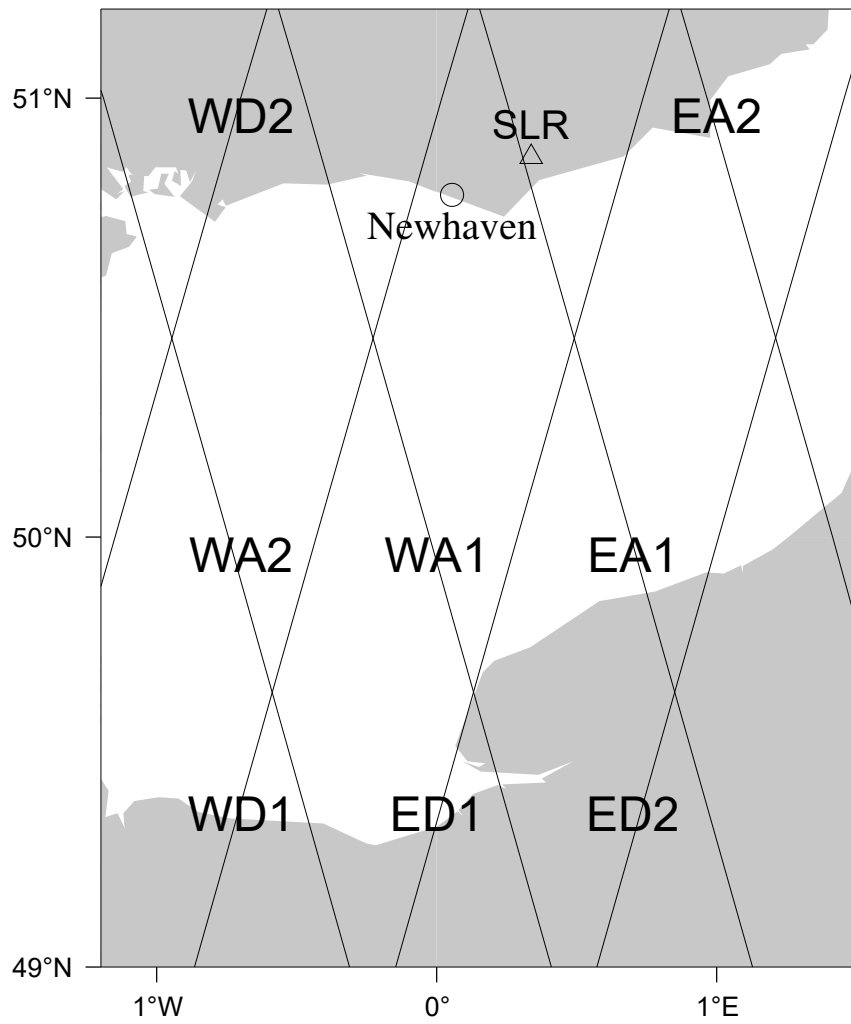
Figure 4.17: The ground-track of the multi-disciplinary phase of ERS 1 in the region of the Newhaven gauge.

Pass	D_g (km)	D_s (km)	( )	R (cm)
ED1	39	22	0.20	0.44
EA1	20	9	0.01	0.02
WD1	9	31	0.23	0.47
WA1	28	50	0.45	0.94

Table 4.6: Statistics for the four ERS 1 passes in the range bias calibration. D_g is the distance of the closest approach to the gauge, D_s is the distance of the closest approach to the SLR, is the geocentric angle of D_s and R is the typical error in the correction of the radial component of the orbit error.

correction and di erential ocean corrections will be more accurate than for those more remote from the tide gauge and tracker.

The distances from the tide gauge and the SLR to each of the four passes are given in Table 4.6. Since the PCA of the EA1 and WD1 passes to the tide gauge are located over land or very close to the coast where no altimetry would be accepted in the calibration, D_g in Table 4.6 refers to the distance between the gauge and the closest usable altimetry point on that pass.

4.4.1   Method

Altimetry data for the calibration were taken from the Ocean Product OPR02 (CERSAT, 1993). Standard editing of data was carried out, rejecting data over land. The same corrections were applied to the raw ranges as in the T/P case. The single parameter SSB model of Carnochan (1996) was adopted. This expresses the SSB as 5.95% of SWH.

The lower orbit of ERS 1 is associated with a signi cant increase in correlated error and noise in radial orbit heights. Estimation of the geographically-correlated radial orbit error from those passes with laser tracking would be unreliable because of the smaller and noisier sample, along with the variation between the four analytical passes. This precludes an estimate of the orbit error derived from passes where tracking data are available from being extrapolated to all passes, as in the case of T/P. Therefore only those passes where tracking data were available were included in the calibration. All 18 cycles of the rst multi-disciplinary phase were considered leading to 72 individual passes to be considered. Of these, suitable laser tracking and altimetry occured on 28 occasions. However, one pass had no altimetry available, the gauge was not operational for another and three resulted in spurious bias values di ering drastically from the mean, suggesting a break down in one component of the calibration. The tracking data for another pass did not span the point of closest approach of the ground-track to the SLR.
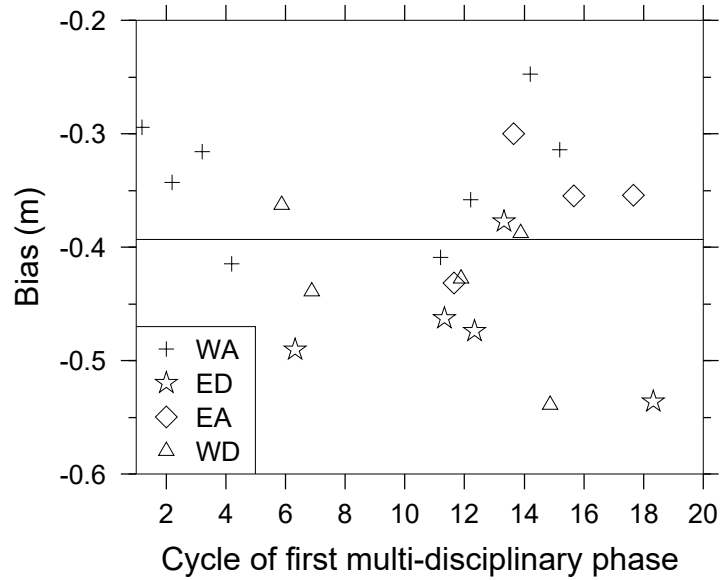
Figure 4.18: Bias estimates for the various passes of ERS 1 with the mean bias indicated by the horizontal line.

Pass type	Contributing passes	Derived bias (cm)	
ED1	5	-46.8	5.8
EA1	4	-36.0	5.4
WD1	5	-43.1	6.8
WA1	8	-33.7	5.7
All	22	-39.3	7.8

Table 4.7: ERS 1 range bias estimates.

Under these conditions the radial correction was considered unreliable and the pass was excluded from the calibration. This left 22 passes for the calibration of which there were ve of type ED1, four EA1, ve WD1 and eight WA1.

The radial corrections were calculated for each pass and the calibrations carried out, with a maximum value for R in Equation 4.4 of -20.0 cm and a mean value of -2.8 cm. The small value of the mean correction testi es to the impact of the RGO laser tracking within the long-arc orbit determinations for these near-overhead passes.

4.4.2 Bias estimate for ERS 1

The weighted mean bias for each pass type is shown in Figure 4.18. The weighted mean for each type was calculated in the same way as for T/P. Table 4.7 shows the weighted mean for each type of pass. Since the number of available passes is much smaller than the T/P case, the bias for ERS 1 is taken as the overall mean,

Component	Error contribution (cm)
Wet troposphere	0.9
Dry troposphere	0.7
Ionosphere	2.0
Sea state bias	0.9
Radial height of SLR	0.9
Range bias of SLR	1.0
Radial height of TG	0.9
Di erential models	2.8
Total	4.0

Table 4.8: Systematic error sources and estimated magnitudes in the ERS 1 range bias calibration.

namely -39.3   7.8 cm.

4.4.3 Error analysis for ERS 1 bias estimates

Table 4.8 shows the estimated systematic error contributions in the system analogous to those given for T/P in Table 4.5. Estimates are derived from Francis (1993) in the case of the media delays. The error in the ionospheric delay is larger here than in the case of TOPEX as ERS 1 lacks the dual-frequency facility. Models for the TEC of the ionosphere are relied upon for this correction. Station coordinates for the SLR are derived from satellite tracking which leads to the error in the radial height. The range bias of the SLR includes an estimate for the error in the positioning of the laser retro-re ector. The independent sea surface height will be no di erent in its accuracy when applied to ERS 1. However estimating the accuracy along the ERS 1 tracks is harder than in the case of T/P since there are insu cient passes to reliably measure the bias solution gradient along the various tracks. The mean estimated error from both passes of the T/P analysis is therefore assumed.

4.5 ERS 2 commissioning phase calibration

After its launch on 29 April 1995, ERS 2 joined its predecessor ERS 1 in the same orbital plane and thus started the so-called tandem mission. The orbit was designed to give ERS 2 the same ground-track pattern as the ERS 1 35-day repeating multi-disciplinary phase. Since ERS 1 had been returned to that orbit con guration for the second multi-disciplinary phase after the end of the geodetic

mission at the end of March that year, both satellites covered the same ground-track every 35 days. The ground-tracks of the two satellites were offset by exactly a day with ERS 2 visiting a given location 24 hours after ERS 1.

The first three cycles of ERS 2 were designated the commissioning phase during which its range characteristics were to be determined particularly in relation to ERS 1. The altimeter and the microwave radiometer were the instruments upon which the commissioning phase focused. The short lag between the ground-tracks of the two satellites was conducive to a *repeat pass* analysis whereby the differences between observations of the same location by the two satellites could be interpreted as differences in the range characteristics. This repeat pass analysis has the advantage over dual crossover analysis in that the whole ground-track can be compared between satellites instead of just the points of intersection. Also, geographically-correlated radial orbit error will not vary at common points on the ground-track for satellites in the same orbit. This obviated the need to correct for this error as is necessary in dual crossover differences.

Several studies were commissioned by the European Space Agency to carry out investigations of the difference in characteristics between the two ERS satellites during the commissioning phase. Part of the contribution of Aston to this calibration campaign involved applying the absolute calibration in the Channel as previously applied to T/P and ERS 1.

Two types of altimeter product were to be considered and calibrated. The Quick-Look Ocean Product (QLOPR) is an altimetry dataset released within a short time of collection. Here, only a minimal amount of processing of the altimetry necessary for reasonable accuracy is carried out, and the orbits are somewhat crude, perhaps without all tracking data included. The emphasis of QLOPR data is on providing the data for near real-time applications as rapidly as possible. The next data product is the Ocean Product (OPR), which is released with a longer lag after data acquisition and intended for scientific studies where accuracy is the predominant requirement and near real-time processing is not required. Both the QLOPR and the OPR products were to be considered in this calibration.

4.5.1 Calibration Method

Since the ground-track configuration of both satellites is as shown in Figure 4.16, it seems that the strategy developed for the calibration of the first multi-disciplinary phase of ERS 1 could be adopted for this new calibration. However, the reliance on the SLR at Herstmonceux is substantial as only those passes for which tracking data exist can be considered for the absolute calibration. The four passes of ERS 2 corresponding to those used in the previous ERS 1 cali-

Pass	D_g (km)	D_s (km)	( )	R (cm)
ED2	95	72	0.65	1.36
EA2	74	48	0.43	0.90
WD2	57	74	0.67	1.40
WA2	72	98	0.88	1.84

Table 4.9: Statistics for the four far ERS passes in the range bias calibration. D_g is the distance of the closest approach to the gauge, D_s is the distance of the closest approach to the SLR,   is the geocentric angle of D_s and R is the typical error in the correction of the radial component of the orbit error.

bration were investigated and it was found that of a possible 12 passes over the three commissioning phase cycles, only ve passes were tracked by the SLR. Of these ve, one pass comprised only two altimetry points. During the same period ERS 1 was tracked for seven of the possible 12 passes. The minimum zenith angle of the tracking data was excessively large in the case of two, meaning that the radial orbit correction was not reliable. Such a small number of passes undermines the con dence that can be placed in the method for determining the absolute bias as a small sample space allows the possibility for noise to skew the bias estimates. To overcome this, the next four nearest passes to the tide gauge were also considered. These are the passes labelled ED2, EA2, WD2 and WA2 in Figure 4.17. Again there exist 12 of these *far* passes for each satellite during the commissioning phase and investigation revealed that laser ranging was available for six of them in the case of ERS 2 and seven in the case of ERS 1. This time all were acceptable with small minimum zenith angles of tracking and su cient numbers of altimetry points. This added substantially to the potential dataset and it was decided to investigate these extra passes with a view to adopting them to contribute to the nal calibration estimates. An increase in the systematic errors may be o set by a increase in the dataset size and an associated reduction in the noise. From here on, the four passes closest to the gauge are referred to as the *near* passes and those farthest from the gauge are referred to as the *far* passes.

The expected noise in the radial orbit correction will of course be larger for passes which are further from the tracker. Table 4.9 gives the expected noise in the radial corrections for these new passes introduced into the calibration. As in Table 4.6, where the PCA of a pass to the gauge lies over or near land, D_g refers to the distance from the gauge to the closest usable point. This restriction applies to the EA2 and WD2 passes. The expected errors for the near passes remain the same as given in Table 4.6.

The QLOPR data were calibrated rst following the usual scheme. In situ estimates of the sea surface heights were generated as in the case of the ERS 1 rst multi-disciplinary phase except for the storm surge correction. Since the commissioning phase lay entirely within the summer season, the storm surge model was not being run by the Meteorological O ce and so this correction had to be ignored. The independent estimates of sea surface height were consequently derived by using only the geoid and ocean tide models to extrapolate from the gauge to the CP.

On examination of the altimetry of the passes for which laser range data were available, an anomalous phenomenon was noticed. During some of the passes of both ERS 1 and ERS 2, range readings appeared in pairs. Rather than a regular once-per-second range, there would be two readings separated by a small fraction of a second, followed by the normal gap of approximately a second and then another pair of observations with a short time lag between them. Later in the work it was announced that this situation was caused by mis-processing of data at the groundstation at Kiruna in Sweden. Operationally, data from di erent groundstations are merged and duplicates left out of the nal full dataset. Groundstations other than Kiruna had been processing data normally so when Kiruna and non-Kiruna data were merged to construct the full QLOPR dataset, the same altimeter points did not match exactly. This resulted in the two slightly di erent observations on the QLOPR for each true observation. This situation did not exist for all passes; only those for which Kiruna and another groundstation had been involved in the processing of those data were a ected. If no account was taken of this *ghost point* phenomenon then there was a risk of skewing the results in favour of those where the ghost points existed, in addition to corrupting the derived bias with the e ect on the range of the misprocessing at Kiruna. To compensate for this, each pass where the phenomenon prevailed was split into two passes, one containing the rst of each pair of close points, the other containing the second of each pair. Processing could then be carried out as normal on each of the two passes. The RMS about the mean of the resulting bias values within each pass was then calculated and the one with the largest RMS was rejected. Four of the ERS 2 and three of the ERS 1 passes were found to exhibit this phenomenon.

4.5.2 Calculation of QLOPR bias

The calibration of the QLOPR data for ERS 2 was based on the four near passes and the six far passes. These consisted of one each of passes of ED1, EA1, WA2 and EA2 and two each of passes WA1, WD2 and ED2. The locations of the altimeter points are shown in Figure 4.19.
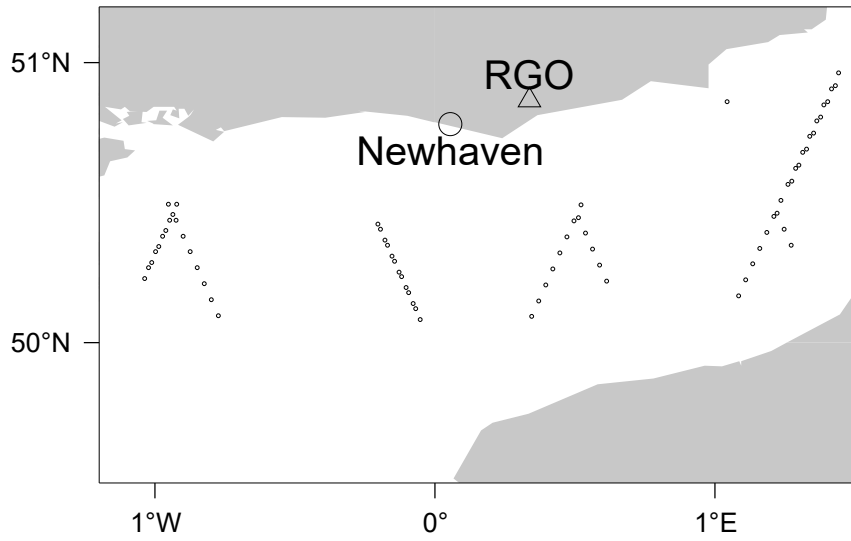
Figure 4.19: Altimeter points comprising the calibration of ERS 2 QLOPR data.

Figure 4.20: Bias estimates for ERS 2 QLOPR data using near passes and far passes respectively with the mean biases indicated by the horizontal lines.
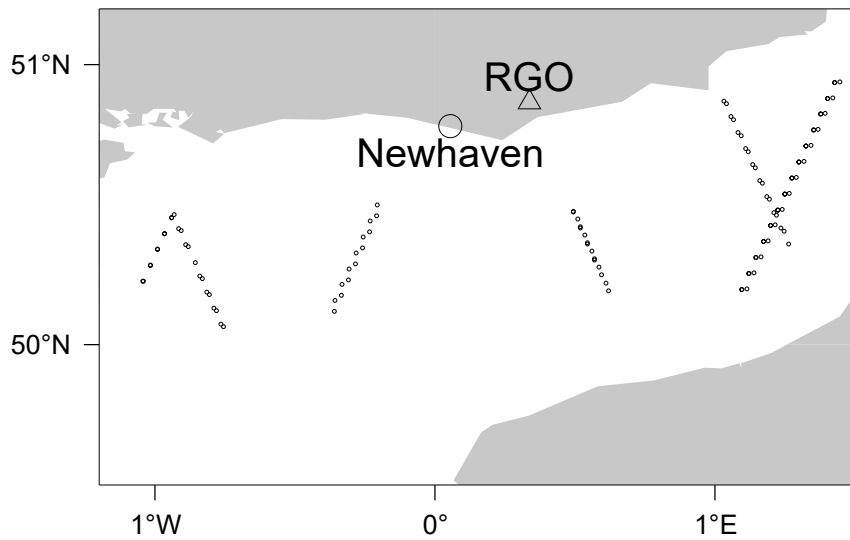
Figure 4.21: Altimeter points comprising the calibration of ERS 1 QLOPR data.
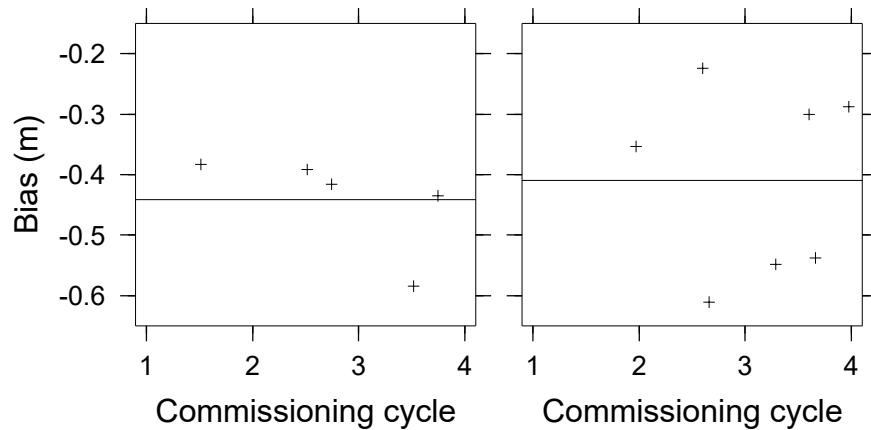
Figure 4.22: Bias estimates for ERS 1 QLOPR data using near passes and far passes respectively with the mean biases indicated by the horizontal lines.

Weighted averages were generated in the usual way and it was found that the mean bias was -41.4   9.1 cm. If the near passes or the far passes are considered alone, the weighted mean is -41.7   2.7 cm or -41.3   11.5 cm respectively. The mean values for each pass are plotted in Figure 4.20. Clearly the initial intention to reduce the uncertainty by increasing the sample size at the expense of systematic errors is not borne out by the results. Since data from the far passes have a much greater spread than those near the gauge, the RMS of the whole solution is larger than those from the near passes alone. Consequently the mean of the near passes alone is chosen to represent the derived bias estimate. The estimate for the bias of ERS 2 QLOPR altimetry is thus -41.7   2.7 cm.

In the case of ERS 1 there are   ve near passes and seven far passes. These consisted of one WD2 pass; two each of passes WD1, WA2, EA2 and ED2; and three of the EA1 pass. The locations of the altimeter points are shown in Figure

4.21. The weighted average for the near passes is -41.7   2.7 cm which is adopted as the estimate for the ERS 1 QLOPR altimetry. By comparison the bias for the far passes is -41.3   11.5 cm and for all passes it is -41.4   9.1 cm. The biases for each pass are plotted in Figure 4.22.

4.5.3   Calibration of the OPR data

Calibration of the OPR data was closely linked to the calibration of the QLOPR. Indeed the same precise orbits could be used. By this time the problem of ghost points had been solved and the extra processing required to account for the phenomenon was not required with the OPR. This time updated algorithms for the SSB were adopted. These modelled the SSB at -5.27% and -5.18% of SWH for ERS 1 and ERS 2 respectively.

4.5.4   ERS 2 bias jumps

As a result of the QLOPR calibration a series of jumps in the bias of both satellites became apparent and were characterised by Roca and Francis (1996). It was only when the two satellites could be compared using repeat pass analysis that it became apparent that the ERS 1 bias had been drifting with a step function throughout its life, and that the new satellite was also exhibiting this behaviour. This phenomenon in both instruments can be attributed to safe-hold events where an anomaly causes the satellite to shut down non-essential instruments. The reduction in power dissipation causes the temperature of the satellite to drop. When power is restored at the end of the safe-hold con guration, a new thermal equilibrium is reached and the instruments are subject to a slight change in their characteristics. In the case of the altimeter this slight change can be critical and a bias jump typically accompanies a safe-hold event. Fortunately the method of single point target response (SPTR) allows the magnitude of these jumps to be measured and corrections applied. Such corrections were supplied for each satellite and applied to the altimetry before calibration.

4.5.5   Other modi cations to the OPR data

It was reported by Stum (1996) that the o set between the centre of gravity and the radar altimeter was in error leading to range measurements being long by 2.13 cm. Further problems with the range arose from drift in the ultra stable oscillator frequency. The value used to generate the OPR data was di erent from the true value at mid-1995 causing the ERS 2 altimeter to measure long by a further 0.7 cm and ERS 1 to measure short by 2.5 cm. These errors were taking into account and corresponding corrections applied to the OPR altimetry.
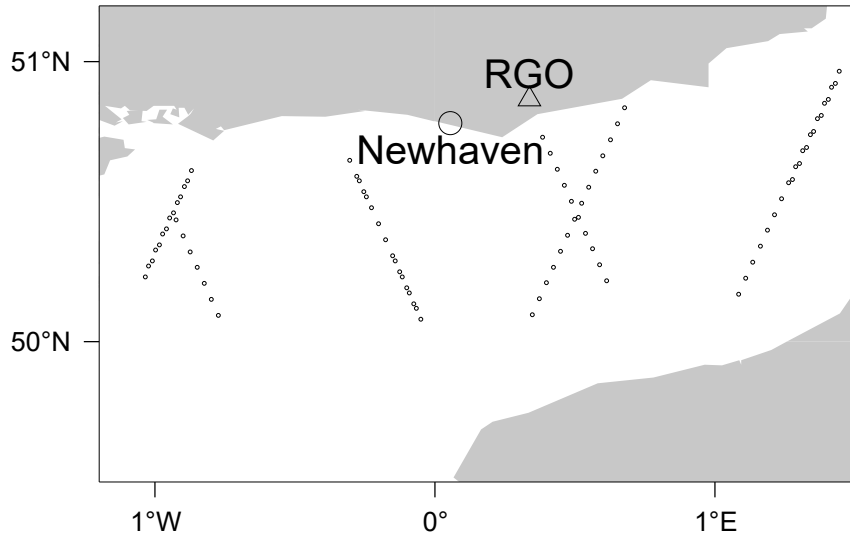
Figure 4.23: Altimeter points comprising the calibration of ERS 2 OPR data.

Study of the SWH by Cotton and Challenor (1996) had revealed that a non-linear error existed in the reported SWH values. Uncorrected this translated into error in the SSB. A suitable modification was supplied which was used to correct the OPR values of the SWH. The correction algorithm is defined as

$$
W_{cor}^{e1} = \begin{cases} 1.156 \; W_{opr}^{e1} + 0.322 & \text{if } W_{opr}^{e1} > 0.92m \\ 0.932 \; W_{opr}^{e1} + 0.527 & \text{if } W_{opr}^{e1} \leq 0.92m \end{cases}
$$

for ERS 1, where W_{opr}^{e1} is the value of SWH for ERS 1 as it appears on the OPR and W_{cor}^{e1} is its corrected value. In the case of ERS 2 the correction algorithm is

$$
W_{cor}^{e2} = \begin{cases} 1.169 \; W_{opr}^{e2} - 0.007 & \text{if } W_{opr}^{e2} > 1.24m \\ 0.955 \; W_{opr}^{e2} + 0.268 & \text{if } W_{opr}^{e2} \leq 1.24m \end{cases}
$$

with analogous notation.

4.5.6 Calculation of OPR bias

Calibration of the OPR data was based on the passes used for the calibration of the QLOPR data, since the orbits were invariant and could be interchanged. However, on examination the altimetry of one of the ERS 2 passes was no longer suitable for inclusion in the calibration. The OPR data for this type EA2 pass contained four altimetry points. In the OPR data only two points were found, one of which was too far from the gauge and thus rejected. This pass was therefore excluded from the OPR calibration. The reason for the disappearance of data was not clear but presumably the missing points in this pass had failed OPR quality control. In any case the pass was a far pass so its absence was not a serious
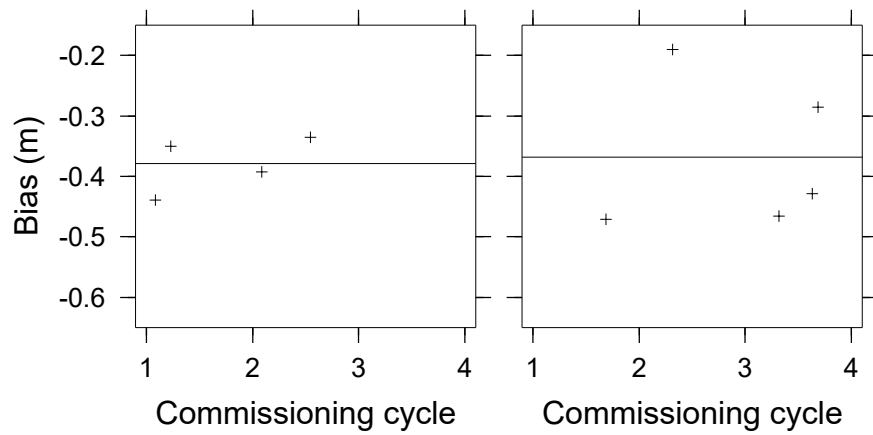
Figure 4.24: Bias estimates for ERS 2 OPR data using near passes and far passes respectively with the mean biases indicated by the horizontal lines.
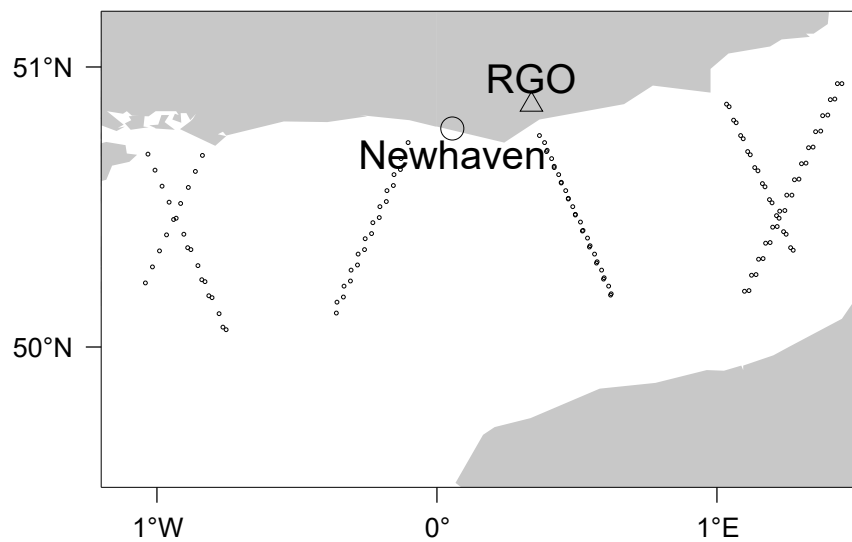
Figure 4.25: Altimeter points comprising the calibration of ERS 1 OPR data.

hindrance. The locations of the altimeter points used in the OPR calibration of ERS 2 are shown in Figure 4.23.

The weighted averages for ERS 2 were calculated and were found to be -37.9   4.0 cm, -36.9   11.1 cm and -37.3   8.8 cm for near passes, far passes and all passes respectively. The   rst of these is taken as the ERS 2 bias estimate for OPR altimetry. The mean values for each pass are plotted in Figure 4.24.

In the case of ERS 1 the passes with altimetry were the same as for the QLOPR. The locations of the altimeter points within these passes are shown in Figure 4.25. The weighted averages for ERS 1 are -41.0   6.8 cm, -40.3   14.0 cm and -40.6   11.6 cm for the near passes, far passes and all passes respectively. The   rst of these is taken as the ERS 1 bias estimate for OPR altimetry. The biases for each pass are plotted in Figure 4.26.
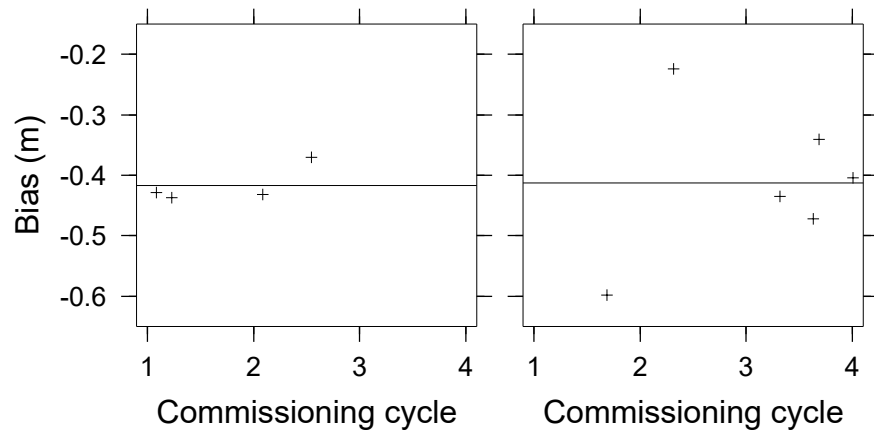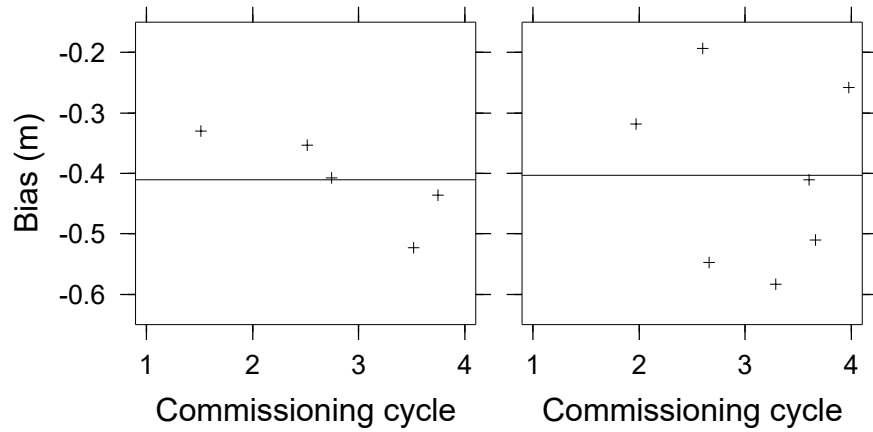
Figure 4.26: Bias estimates for ERS 1 OPR data using near passes and far passes respectively with the mean biases indicated by the horizontal lines.

4.5.7 Discussion of absolute bias determination

The range bias estimates for TOPEX and Poseidon corresponding to the version 2 GDRs are -14.7   4.0 cm and +2.3   2.2 cm respectively. The former appears to be in excellent agreement with the dedicated measurement campaign at the Harvest oil platform (Christensen *et al.*, 1994) which estimates the TOPEX bias at -14.5   2.9 cm. However the value estimated at Harvest uses the Walsh model for SSB whereas the four parameter Gaspar model has been used in the Newhaven calibration. Christensen *et al.* (1994) also estimate the bias with respect to the Gaspar model to be -17.1 cm. The disagreement may arise from the impact of conditions in the region of the calibration not being representative of the global ocean. The Poseidon bias derived from the Harvest work is +0.9   3.1 cm, this time with respect to the three parameter Gaspar model. In an experiment related to the Harvest calibration, a buoy tted with a GPS receiver was deployed to determine the in-situ ocean height. The resulting TOPEX range bias deviated very little from the main Harvest results, although there was signi cant dependence upon the GPS processing software used to derive the sea surface solution (Born *et al.*, 1994).

Further calibration of T/P has been carried out at the CNES calibration site at Lampedusa island in the Mediterranean Sea, employing a tide gauge on the nearby islet of Lampione. Despite only two passes of the satellite being available for the derivation of the TOPEX bias, the derived value is in reasonable agreement with the Newhaven work at -18.5   3.4 cm. For Poseidon, six passes were available leading to a bias estimate of 0.7   3.3 cm. These values use the same SSB model as the Newhaven bias.

The derived bias of -39.3   7.8 cm for the rst multi-disciplinary phase of ERS 1 is in good agreement with the dedicated Acqua Alta campaign of Francis

93

Comparison method	Satellites		QLOPR relative bias (cm)		OPR relative bias (cm)	
DXO	TOPEX	ERS 1	33.9	0.7	30.8	0.3
DXO	TOPEX	ERS 2	32.0	1.1	28.3	0.9
DXO	ERS 2	ERS 1	1.4	0.3	2.2	0.3
RP	ERS 2	ERS 1	1.9	0.2	1.9	0.3
ABS	ERS 2	ERS 1	2.5	8.1	3.1	7.9

Table 4.10: Comparison of relative biases for the various altimeters as derived from the dual satellite crossover (DXO), repeat pass (RP) and absolute calibration (ABS) methods.

(1992, 1993) where the value -41.5 5.2 cm was derived. This agreement is despite an older relationship between SSB and SWH, which de ned the former as 2.0% of SWH. Lam *et al.* (1993) in the precursor to the work presented here calculated the bias to be -46.0 11.0 cm. Despite a much larger uncertainty and less data, this is consistent with the more recent work presented here.

In the case of the ERS 2 commissioning phase, the results derived from this absolute calibration can be indirectly compared to the relative biases derived from other methods. For instance, a dual crossover and a repeat pass comparison were performed between the ERS satellites and each was compared using dual crossovers to TOPEX (Moore *et al.*, 1996a). Of course these comparisons yield a relative bias only, but the absolute biases from the Newhaven calibration can be easily converted into a relative bias. Table 4.10 summarises the relative biases derived from each method. Since the relative biases from dual crossovers with TOPEX are referenced to a common satellite, the relative bias between ERS 2 and ERS 1 can be derived by simple di erencing. The relative bias is thus calculated as 1.9 1.3 cm and 2.5 0.9 cm for the QLOPR and OPR data respectively. The former is in exact agreement with the corresponding value derived from repeat pass data. The mean relative bias between ERS 2 and ERS 1 derived from crossover and repeat pass QLOPR data is 1.7 cm. For the OPR data the mean relative bias is 2.2 cm. Both of these agree with the relative bias derived from absolute calibration to within a centimetre. Conversion of the ERS absolute biases to a relative bias and comparison to other methods of relative bias determination is a useful assessment of accuracy although it does not account for certain common systematic errors, such as those in ocean models or the datum position of the tide gauge or the SLR. However the results here suggest that even for a small amount of data it is possible to derive reasonable results where noise is kept under control.

Chapter 5

Bias drift determination

Knowledge of the absolute range bias associated with an altimeter is important in variability studies, allowing altimetry from different instruments to be combined. However this is not the complete solution to the problem of how to derive a global value for sea level change. It has been assumed that the bias is constant in the absolute calibration when in fact there are several potential sources of instability. The absolute calibration as performed in Chapter 4 cannot be reliably used for the detection of bias drift for a number of reasons. For instance a systematic drift in one of the ground-based instruments over time will appear as a phantom trend in the altimeter bias. This could occur if the tide gauge were subsiding, or its mechanism were degrading. Rather less likely would be a similar phenomenon in the laser ranger[1]. Additionally, the standard error of the spread of absolute bias values is such that a significant drift could be masked. How can these problems be overcome? The introduction of significantly more calibration sites would certainly address the above problems and give more confidence in a bias drift value, but sites with a configuration as ideal as that at Herstmonceux/Newhaven are comparatively rare. Still, drift is an important issue. With current estimates suggesting a sea level rise around the mm/yr level (Warrick and Oerlemans, 1990) there is a demand for more rigorous monitoring of drift in the altimeters.

The work presented in this chapter seeks to address the question of whether range bias drift in altimeters can be overcome, where the effect of the drift is to deny the resolution of sea level change.

---

[1] However a temporary anomaly in the Herstmonceux laser range readings was highlighted by careful inspection of individual satellite passes over the Channel in the absolute calibration. This error, caused by mis-processing of the laser returns, was an isolated problem and was subsequently corrected at source.

5.1 Potential sources of altimeter drift

When referring to range bias drift, any phenomenon which causes a disagreement between altimetric and true sea level must be included, in addition to purely instrumental drift which arises from changes within the altimeter. For this reason the phrase *altimetric sea level drift*, or *altimetric drift* for short, is preferred.

All components of the nal corrected altimetric sea surface height must be examined when a list of candidate sources of this drift is compiled. First, the altimeter itself is a highly precise instrument. For instance, the range bias would change by over 10 cm if for some reason the tracker started to detect the return pulse 0.3 nanoseconds earlier or later than it should. The phases of the measurement process are synchronised by the so-called ultra stable oscillator. As described in Section 4.3.12, such devices are prone to drift over the time-scale of a typical mission. This phenomenon is well-known and is usually monitored as part of the routine instrument engineering cycle. If the correction procedure is awed then the measured range will be a ected and hence the range bias will change.

The characteristics of many precise instruments will change with temperature. The thermal environment in the spacecraft is a complex system. Ine ciencies in the electrical equipment cause heat to be generated internally. This must be dissipated if it is not to build up to dangerous levels and cause damage. In an extremely rare ed atmosphere or a vacuum, neither conduction nor convection will perform this task. The thermal environment must therefore be maintained by radiating heat away. Phenomena such as solar cycles, which change the output of the sun over time and hence the energy incident upon the spacecraft, complicate this issue. The requirement to be always nadir-pointing leads to a constantly changing attitude of the craft as it describes its orbit around the Earth. This will present di erent parts of the craft to the sun and make it di cult to maintain a stable and constant temperature. This will be more extreme if the orbit causes the craft to enter Earth s shadow periodically. There is scope for the thermal pro le of the craft to change over time which may be associated with a change in the range characteristics.

Altimetric satellites often include a mode whereby an anomalous event will cause it to go into a *safe-hold* con guration with much of the instrumentation deactivated. In this case the power output will drop and cooling will occur. When the craft is reactivated the instrumentation will heat up again to the normal working temperature. As seen in the ERS 2 calibration this too could cause a random change in characteristics, as a slightly di erent thermal equilibrium is reached (see Section 4.5.4).

The raw altimeter range is corrected for various media and geophysical e ects.

Of the former, the delay due to the mass of the troposphere is modelled using global atmospheric circulation models (see Section 3.2.2). Although there will be errors in these models the overall dry mass of the atmosphere is in equilibrium so no long-term drift in the models should occur. The water vapour content of the troposphere is measured using the radiometer. This instrument could itself be unstable and induce an altimetric drift. Similarly the total electron content could be mis-modelled in the case of single frequency altimeters, particularly as the quantity is linked to solar activity. This is unlikely though, as the structure of the ionosphere is generally well understood. Dual frequency altimeters will not be a ected by ionospheric modelling errors. Of the geophysical corrections, the only possible concern involves the pole tide. However the accuracy to which it is known and the relatively short periods involved make this correction unlikely to contribute to a drift in the altimetric sea level. Also, since the pole tide acts only to change the global distribution of the xed mass of ocean, any model to correct for this should be globally coherent, and no global altimetric drift should arise from this.

Another component of the altimetric sea surface height is the orbit height of the spacecraft. Any component of the force experienced by the spacecraft which is either not modelled or is mis-modelled during orbit determination can potentially cause a systematic change in the orbit height and in turn induce a change in the range bias. The 11 year cycle of solar activity will change solar radiation pressure forces incident upon the spacecraft over this period, and may a ect atmospheric drag. If these are systematically mis-modelled then a periodic altimetric drift may arise with the same wavelength.

The above sources of altimetric drift have origins in the physics of the instrument itself, or mis-modelling of geophysical phenomena. These are somewhat di erent in nature to algorithmic changes in the way that the altimetry or corrections are generated or processed, which can also give rise to an e ect rather similar to altimetric drift. As a mission proceeds, advances in science may allow more accurate processing of the telemetry or other components of the nal altimetric sea surface height. Such changes are typically manifested as a change in the *version* of altimeter product made available to the scienti c community by the relevant agencies. If, for instance, a better model for the sea state bias is adopted, then it cannot be assumed that altimetry processed with the new algorithm will not exhibit an o set when compared to altimetry processed with the older model. Changes such as these can be considered alongside the instrumental and geophysical e ects as valid and important sources of altimetric drift.

5.2 Modelling the altimetric drift

Phenomena such as the random day-to-day changes in the thermal characteristics of the altimeter instrument may give rise to high frequency variations in the altimetric bias. As long as the result of these is simply a noisier sea surface measurement then there is no effect on the derivation of a sea level change estimate. What does affect these long-term variability estimates are any low frequency variations or trends from whatever source, from instrument switch-offs to drift in the radiometer. The former type of high frequency changes are very hard to measure as they would be indistinguishable from other sources of noise. Therefore the principal concern is the long-term trend in the altimetric bias as this is the most serious hurdle to the measurement and understanding of long-term sea level change.

5.2.1 The altimeter drift function

The altimetric drift function associated with an altimeter, , and with respect to the time t_0 is defined to be $d_{t_0}(t)$. This is the function which characterises the effect of altimetric drift, and hence can be used to remove it from altimetric sea levels. This function is defined as

$$d_{t_0}(t) = b(t_0) \quad b(t) \qquad (5.1)$$

where $b(t)$ is the altimetric range bias at time t. The value of t_0 is arbitrary and all drift values are expressed relative to the altimetric bias of at this time. It is important to remember that the altimetric drift function is not intended to explicitly combat absolute bias. The function is only ever used to relate the inherent systematic errors in altimetric measurement at some given time with those errors at another time. The function is defined in such a way that a positive value at time t means that the altimeter would measure the same sea surface to be higher at that time than at t_0. This means that if the function has a positive rate over time then the altimeter is observing a spurious rise in sea level. Altimetric sea surface heights at time t may be corrected for the effect of altimetric drift by subtracting the value of $d_{t_0}(t)$. Conversely the value may be added to the range at that time. Note carefully that this is the opposite of the conventional way of expressing absolute range bias and is chosen so that changes in the altimetric drift function will show the error in the measured sea surface height which is more tangible than the altimeter range. After correction of a set of altimetric sea levels with the drift function, all sea levels would in principle conform to the range characteristics of the altimeter at time t_0.

Since Equation 5.1 takes no account of the absolute bias, such functions cannot be used to connect two or more altimeters without further constraint. When using

altimetric drift functions to relate altimeter   to altimeter   for instance, the dual altimetric drift function d_{t_0} (t) can be de ned by adapting Equation 5.1. This becomes

$$d_{t_0} \ (t) = b \ (t_0) \quad b \ (t) \tag{5.2}$$

Similarly, this function may be subtracted from altimetric sea surface heights measured by   making them conform to the characteristics of   at time t_0.

There is no reason why the possible sources of the drift outlined above should lead to a simple function describing the drift. Indeed the jumps in altimetric bias arising from deactivations mean that continuous functions are inherently awed when used in this sense. The simplest solution of assuming a linear drift function will not necessarily resolve the full extent of the drift and could well leave signif- icant residual higher order drift in the altimetric sea level. Since high-frequency variations in the bias are not relevant to variability studies, *a priori* assumptions about the shape of the drift were avoided and the decision was made to model the phenomenon via a step function. The length of the steps must be a compro- mise between the need to have proper resolution of the drift, demanding short step lengths, and having enough observations to reliably estimate a representa- tive bias for any given step. The repeating nature of the satellites concerned means that natural step lengths are usually self-evident. For instance a bias esti- mate per ground-track cycle is a satisfactory compromise between the con icting requirements in the case of TOPEX.

If some method can be devised to estimate the altimetric drift functions then it may be possible to correct altimetric sea surfaces and bring them into a consistent reference frame, allowing true sea level variability to be measured.

5.3   Measurement of altimetric drift

Having examined the nature of altimetric drift along with possible origins, at- tention is now turned to the measurement of the phenomenon. As in the case of the absolute calibration, an independent estimator of the sea surface is required. However since it is only temporal *changes* in the altimetric sea level which are of interest, the independent estimator need only measure the same. In other words the datum height is irrelevant, and a major source of error in the absolute calibration is eliminated from this drift calibration.

Dual satellite crossovers (DXOs) are traditionally used to measure the relative bias between two altimeters in operation over a common period of time. A DXO is measured at a point of intersection between the ground-tracks of two altimeters. The di erence between the sea surface height as measured by one of the altimeters

when it reaches the point of intersection is subtracted from the sea surface height as measured by the other at the same place. This difference is termed the DXO residual. Note that the altimeters will in general reach the point of intersection at different times. Since the sea surface at the same location is measured by both altimeters, any difference between the two altimetric sea surface heights comprising the DXO may be interpreted as arising from errors in the altimetry, such as the combined effect of the absolute range bias in each altimeter.

In general, when a DXO is taken, the sea level will change between the two observations. There are many contributors to this change. The high-frequency components, such as ocean tides, can be removed using models but the longer wavelength effects such as seasonal variability and eustatic sea level change cannot easily be accounted for. To overcome this problem the time lag between the two observations making up the crossover is limited, usually to ten days at most. This restriction allows the sea level change arising from the uncorrected long-wavelength effects to be ignored as negligible. Consider the general case of a DXO between two altimeters α and β. Each will measure the sea surface height, $h(t)$, at the crossover location. Equation 3.3 may be adapted to express the components of this height after correction for the high-frequency effects to give:

$$h_{alt}^{\alpha}(t) = s(t) - b^{\alpha}(t) + \epsilon^{\alpha} + E_o^{\alpha} \tag{5.3}$$

in the case of α, where $s(t)$ is the true sea surface height, $b^{\alpha}(t)$ is the altimetric bias, ϵ^{α} is the geographically-correlated error for α and E_o^{α} is the total of the noise in the observation (other than the geographically-correlated error). The height $h_{alt}^{\beta}(t)$ may be similarly defined. The principal contribution to the geographically-correlated errors are the radial orbit errors arising from geopotential mis-modelling but may contain terms for geographically-correlated biases in the geophysical corrections applied to the raw altimeter range, such as a geographical dependence in the error in one of the geophysical corrections.

The DXO residual between the two altimeters is defined as the difference between the height observations of each altimeter at the time when each reaches the crossover point:

$$
\begin{aligned}
D^{\alpha\beta}(t_\alpha, t_\beta) &= h_{alt}^{\alpha}(t_\alpha) - h_{alt}^{\beta}(t_\beta) \\
&= [s(t_\alpha) - b^{\alpha}(t_\alpha) + \epsilon^{\alpha}] - [s(t_\beta) - b^{\beta}(t_\beta) + \epsilon^{\beta}] + E_o \\
&= s(t_\alpha) - s(t_\beta) + b^{\alpha}(t_\alpha) - b^{\beta}(t_\beta) + \epsilon^{\alpha} - \epsilon^{\beta} + E_o
\end{aligned}
$$

where E_o is the total of residual errors in the observation, equal to the difference between E_o^{α} and E_o^{β}. This residual may be related to the altimetric drift functions

(Equations 5.1 and 5.2) if it is rewritten as

$$D\ (t\quad t\ ) = s(t\ )\quad s(t\ ) + [b\ (t_0)\quad b\ (t\ )]\quad [b\ (t_0)\quad b\ (t\ )] +$$
$$+ E_o$$
$$= s(t\ )\quad s(t\ ) + d_{t_0}(t\ )\quad d_{t_0}\ (t\ ) +\qquad\qquad + E_o \qquad (5.4)$$

In Equation 5.4, the terms for the long-wavelength variability are problematic in that they cannot be recovered independently of the drift functions. In general it is hard to correct for these variability terms. At any given location there may well be a multitude of components from seasonal and semi-annual to annual, bi-annual and many less well-characterised signals. In particular the eustatic change is a hurdle since if it is not accounted for it will corrupt the bias drift functions and deny the opportunity to measure this signal with the corrected altimetry. The impact of this error in traditional DXOs is usually reduced by introducing the restriction of having the two observations comprising each DXO very close together in time. If the measurements are limited to be close to each other in time, variation in the sea surface can either be removed with tide models for instance, or assumed to be negligible. A maximum lag of 10 days is su cient for most of the ocean but this may have to be reduced in areas of extreme variability around major ocean currents. With a suitably short maximum time lag it may be assumed that $s(t\ )\quad s(t\ )$. However, as a consequence of the temporal proximity of the observations, coupled with the long-wavelength nature of the altimetric drift, the bias terms will be very nearly constant over the time period. Since observations over such short time periods cannot resolve a separate rate of change in each altimetric drift, it must be assumed that $d_{t_0}(t\ )\quad d_{t_0}(t\ )$ and $d_{t_0}\ (t\ )\quad d_{t_0}\ (t\ )$. Under these conditions Equation 5.4 reduces to

$$D\ (t\quad t\ )\quad s(t\ )\quad s(t\ ) + d_{t_0}(t\ )\quad d_{t_0}\ (t\ ) +\qquad + E_o$$
$$d_{t_0}(t\ )\quad d_{t_0}\ (t\ ) +\qquad + E_o$$

Here the terms $d_{t_0}(t\ )$ and $d_{t_0}\ (t\ )$ are inseparable and only the di erence between the two as a function of time may be recovered. This is unsatisfactory since the objective of measuring the altimetric drift in both altimeters independently of the sea level variability is not achieved.

It is apparent that traditional DXOs are limited in that the change in relative bias over time cannot be resolved into the independent drift contributions of each altimeter. In addition to this, and more importantly, the third unknown of the true sea level change cannot be determined.

5.3.1 Gauge-augmented altimetric measurements

The above crossover technique is commonly used to measure the relative bias between two altimeters and how it varies over time. Altimeters may only be compared in this way when they overlap in time. As described above, altimeters cannot be used to distinguish bias drift and sea level change. However the principle can be extended to overcome this limitation. With care, ocean variability can be measured independently using tide gauges and then removed from altimetric difference observations such as DXOs. To do this it must be assumed that long-term sea level variability has a large spatial wavelength and hence that the variability measured at a gauge accurately represents the variability at a nearby sub-satellite point. A quantification of *nearby* remains to be determined. The altimetric drift could then be measured by comparing altimeter observations of the sea surface height at a particular location. If a differential correction is derived from a nearby tide gauge and removed from the altimeter difference then any trend should represent altimetric drift. This can be seen as a generalisation of the traditional DXO, where instead of assuming that the sea surface variability is negligible, it is accounted for via a tide gauge. Note that as only changes in the altimetric bias are of interest, no correction for the mean sea surface between the gauge and the sub-satellite point is required. This obviates the need for an accurate geoid model, an important source of error in the absolute calibration.

This principle of augmenting altimetric measurements with tide gauge differences can be applied to the DXO residual given in Equation 5.4. First a tide gauge difference is defined as

$$G(t - t') = g(t) - g(t') \tag{5.5}$$

where $g(t)$ is the reading of some tide gauge at time t. If the gauge is close to a crossover location then the variability measured at the gauge will be related to the variability observed by the altimeter:

$$G(t - t') + E_g = s(t) - s(t') \tag{5.6}$$

where E_g is the amount by which the gauge is in error in estimating the variability measured by the altimeter. A *gauge augmented altimeter difference* is defined to be the difference between the altimeter difference and the gauge difference, combining Equations 5.4 and 5.6 as follows:

$$
\begin{aligned}
D'(t - t') &= D(t - t') - G(t - t') \\
&= [s(t) - s(t') + d_{t_0}(t) - d_{t_0}(t') + \ldots + E_o] \\
&\quad - [s(t) - s(t') - E_g] \\
&= d_{t_0}(t) - d_{t_0}(t') + \ldots + E_T \tag{5.7}
\end{aligned}
$$

where E_T is the total error other than the geographically-correlated error, equal to the combined contributions of E_o and E_g.

Inspection of Equation 5.7 reveals that the two drift functions can now be separated by choosing altimeter observations with a long time lag. This will form the basis of the inter-altimeter calibration.

5.3.2   Radial orbit error

The presence of the orbit error terms in Equation 5.7 presents a potential problem. For now it is assumed that   and   , the terms for geographically-correlated error are purely of radial orbit error origin. From orbit theory the radial orbit error arising from geopotential mis-modelling,   , is correlated with location and varies with ascending or descending satellite pass. This error may be expressed as

$$
= \begin{cases} {}_f + {}_v & \text{if the pass is ascending} \\ {}_f - {}_v & \text{if the pass is descending} \end{cases}
$$

where $_f$ is the mean error for ascending and descending passes (the geographically-correlated error) and $_v$ is the variation from the mean for a given ascending or descending pass (the geographically anti-correlated error) (Tapley and Rosborough, 1985). Introducing this into Equation 5.7 will give four forms depending on the ascending/descending configuration of each pass. These are

$$D_D^A(t - t') = d_{t_0}(t) - d_{t_0}(t') + (_f - _f) + (_v + _v) + E_T; \tag{5.8}$$

$$D_A^D(t - t') = d_{t_0}(t) - d_{t_0}(t') + (_f - _f) - (_v + _v) + E_T; \tag{5.9}$$

$$D_A^A(t - t') = d_{t_0}(t) - d_{t_0}(t') + (_f - _f) + (_v - _v) + E_T; \quad \text{and} \tag{5.10}$$

$$D_D^D(t - t') = d_{t_0}(t) - d_{t_0}(t') + (_f - _f) - (_v - _v) + E_T \tag{5.11}$$

where the A and D labels on D indicate whether the pass contributed by that satellite is ascending or descending respectively. These equations show that while the variable parts of the geographically-correlated error may be recovered from the system, the   xed parts cannot. In fact the term ($_f$ - $_f$), which is constant, cannot be separated from the bias term and this di erence will necessarily corrupt the bias functions derived at that location. Without an independent indicator of the   xed orbit error term, this error in the solution cannot be overcome. One way of combating this error is to estimate the bias functions at as many locations as possible using di erent tide gauges, since the   xed correlated orbit error term varies with location and has a global mean of zero. Another issue is that of the variable parts of the orbit error. Ground-track patterns are such that for two prograde satellites, DXOs involving one ascending and one descending pass are

much more common than those involving two ascending or two descending. This may mean that while many observations may be available following the form of Equations 5.8 and 5.9, observations following the form of Equations 5.10 and 5.11 are sparse or non-existent in the region of a tide gauge. If any combination of prograde or retrograde satellites is examined it transpires that two of Equations 5.8 – 5.11 will describe the great majority of the DXO observations, leaving few observations to separate $_v$ and $_v$. However, even if only observations of the most numerous forms are considered, the sum of the variable components of the geographically-correlated orbit error, ($_v$ $_v$) can still be recovered. Although the two components cannot be recovered separately, the resolution of the drift functions is not compromised.

A special case of this inter-altimeter calibration arises in the case of ERS 1 or Geosat. These missions were split into phases with different orbit characteristics and hence a change in the ground-track pattern and geographically-correlated radial orbit error. It is of interest to relate these phases to one another for the purposes of variability studies. In fact this scenario is indistinguishable from the multi-satellite case described above. The separate phases of the mission may be linked in exactly the same way using single satellite crossovers in the place of DXOs.

5.4 The single altimeter case

In the previous section, the relating together of two distinct altimeter instruments has been considered. This is critical for overcoming the problems of bias drift in each instrument and the bias offset between them. Also valuable is the ability to measure the altimetric drift of an altimeter in isolation. This can be regarded as a quality control for altimeters. Indeed Mitchum (1994) has drawn the analogy between the role of tide gauges in providing a check of satellite altimetry and the use of tide poles to monitor the accuracy and drift in tide gauges. As the tide pole provides a low resolution measure of the sea surface, albeit with a high noise component compared to the tide gauge, it is able to highlight trends and jumps in the gauge measurement. So the tide gauges cannot provide the spatial coverage of altimetry but can detect an altimetric trend in the locality. Satellite altimetry has brought many breakthroughs in the field of ocean science but the temptation to ignore tide gauges must be resisted.

5.4.1 Single satellite crossovers

DXOs are not the only way of looking at common points on the ocean with altimeters. The ground-track of a single altimeter will also have many intersections.

This is the basis of the single satellite crossover (SXO) which is effectively a special case of the DXO Equations 5.8 and 5.9, since SXOs must always comprise one ascending and one descending pass for a single satellite in a fixed ground-track. These two DXO equations are adapted to define S, the gauge-augmented SXOs for an altimeter :

$$
\begin{aligned}
S_D^A(t_1\ t_2) &= d_{t_0}(t_1)\quad d_{t_0}\ (t_2) + (\ _f\qquad_f) + (\ _v +\ _v) + E_T \\
&= d_{t_0}(t_1)\quad d_{t_0}(t_2) + 2\ _v + E_T; \quad \text{and} \quad\quad (5.12) \\
S_A^D(t_1\ t_2) &= d_{t_0}(t_1)\quad d_{t_0}\ (t_2) + (\ _f\qquad_f)\quad (\ _v +\ _v) + E_T \\
&= d_{t_0}(t_1)\quad d_{t_0}(t_2)\quad 2\ _v + E_T \quad\quad\quad (5.13)
\end{aligned}
$$

In this case the orbit error is less of a problem in that the fixed portion vanishes and the variable part may be recovered.

5.4.2 Repeat passes

The final type of common altimetric sea surface observation is the repeat pass (RP). This applies to measurements made by an altimeter along the repeating ground-track each time it passes over the same point. For the moment RP differences are considered since these are related to Equations 5.10 and 5.11. These equations may be adapted to define R, the gauge-augmented RP difference for an altimeter . In fact both degenerate into the same expression:

$$
R(t_1\ t_2) = d_{t_0}(t_1)\quad d_{t_0}(t_2) + E_T
$$

So in this case the orbit error is removed from the system altogether.

RP observations do not need to be compared in pairwise differences since the principle lends itself to the generation of time series. The sea surface heights which are measured each time the ground-track reaches some specified location will be related. For an altimeter the RP height, $H\ (t)$, is defined. This is essentially the sea surface height observed by the altimeter at that time. Note carefully the distinction between the RP difference, as defined above, and the RP height. The components of the RP height are derived from Equation 5.3:

$$
H\ (t) = s(t)\quad b\ (t) +\quad + E_o
$$

This may be rewritten in the form of the altimetric drift function of as follows:

$$
\begin{aligned}
H\ (t) &= s(t) + b\ (t_0)\quad b\ (t)\quad b\ (t_0) +\quad + E_o \\
&= s(t) + d_{t_0}(t)\quad b\ (t_0) +\quad + E_o
\end{aligned}
$$

The gauge-augmented RP height is generated using a reading from a nearby tide gauge. This is defined to be

$$H(t) = H(t) \quad g(t)$$
$$= s(t) + d_{t_0}(t) \quad b(t_0) + \quad g(t) + E_o \tag{5.14}$$

Again, it is hoped that the gauge will observe the same variability as the altimeter, albeit with some error. However since no difference is taken in this case there will in general be a non-zero datum offset for the signals from the altimeter and the gauge. In the case of the altimeter this offset will be the mean sea surface since no account is taken of the topography between the gauge and the RP. The signals in Equation 5.14 may be broken into their components as follows:

$$H(t) = [s_c + s_v(t)] + d_{t_0}(t) \quad b(t_0) + \quad [g_c + g_v(t)] + E_o \tag{5.15}$$

where s_c and g_c are the constant datum offsets for the altimeter and the gauge signals respectively while $s_v(t)$ and $g_v(t)$ are the signals overlayed on these offsets. In Equation 5.15 the terms s_c, $b(t_0)$, and g_c are all constants and so may be grouped together into a single term, say. This leaves the gauge-augmented RP height in the form

$$H(t) = s_v(t) \quad g_v(t) + d_{t_0}(t) + \quad + E_o$$

Since the gauge and the altimeter are intended to measure the same signal, this may be simplified to

$$H(t) = d_{t_0}(t) + \quad + E_T \tag{5.16}$$

where E_T accounts for the altimeter noise and the discrepancies between the variabilities measured by the gauge and the altimeter.

To summarise, two forms of gauge-augmented RP are derived. The first is the RP difference involving two altimeter measurements in which all correlated error cancels. The second form is the RP height, several of which are used to generate a time series. In this case the correlated error cancels apart from a constant offset which may be eliminated by removing the average of the series.

5.5   A strategy for altimetric drift measurement

A complete set of expressions to characterise the signals present in gauge-augmented altimeter observations of all types has been derived above. This theory may now be applied to the real altimeters. The first step towards putting these principles into practice is to find a suitable set of tide gauges to use. These must be

subject to quality control to purge potential sources of systematic error from the drift solution. Such a suitable set is derived in Chapter 6.

In Chapter 7 gauge-augmented SXOs are employed to estimate the altimetric drift function for the TOPEX mission and thus perform an *intra-altimeter* drift calibration. This is the special case which is simpler than the general case but allows some important methods to be developed and tested. This is followed up in Chapter 8 with an application of the general case to TOPEX and ERS 1 using gauge-augmented RPs and DXOs. An *inter-altimeter* drift calibration is thus performed on these altimeters.

Chapter 6

Inter-comparison of tide gauges and altimetry

A set of tide gauges is needed to facilitate the determination of altimetric bias drift. A candidate tide gauge will potentially be used to provide a reference sea surface height against which altimeter-derived sea surface heights can be compared. The typical altimeter range will be taken at some distance from the tide gauge so a suitable gauge must be able to estimate variability reliably in the surrounding ocean. There are several potential problems which may prevent a gauge from doing this accurately. These problems are considered in this chapter.

A scheme for assessing the degree to which time-series of individual tide gauges represent the variability in the surrounding ocean is designed. This scheme is applied to the tide gauges of the World Ocean Circulation Experiment using comparisons with the TOPEX altimeter. A set of tide gauges considered to be reliable for altimetric calibration is derived along with a subset considered particularly suitable for the calibration of TOPEX.

6.1 Requirements of tide gauges for altimetric bias drift determination

Certain characteristics of a tide gauge are desirable if it is to successfully calibrate satellite altimeters. The properties are identi ed as follows.

6.1.1 Mean sea surface between gauge and altimeter point

The mean sea surface in the vicinity of the gauge may change, seasonally or otherwise, due for example to the variation in the geostrophic balance. Freshwater in ux from rivers near a gauge can modify the salinity or temperature, and hence the density, of the surrounding water with a seasonal cycle or a long-term trend,

causing a similar cycle or trend in the gauge time series. This in ux would not in general a ect an altimeter point and so comparisons of the gauge and altimeter time series would result in a trend on top of any altimetric drift.

6.1.2   Independent drift

Tide gauges are susceptible to systematic drift in the measured time series of sea surface heights. One potential source of drift is when the mechanism of the tide gauge degrades. For instance the stilling well family of gauge can su er from fouling of the inlet hole which will reduce the response time of the measurement. Problems like this should be spotted if a regular visual check is made with a tide pole. The tide pole time series, although much noisier than the gauge series should not show a trend over time with respect to the gauge series. The tide pole check should also be used to span any replacement of the gauge. As mentioned below, if the gauge device is replaced, care must be taken that the new gauge has the same zero level as the old one.

A major source of corruption of tide gauge sea levels arises from vertical displacement of the ground upon which the gauge is installed. If the height of the mounting changes then the gauge will observe this in the resultant time series. Sources of vertical movement include volcanic activity, crustal dynamics, plate tectonics and post-glacial rebound (PGR) in addition to more mundane phenomena such as vandalism or other interference at the gauge site. PGR is strongly related to latitude and is mainly signi cant only in the higher latitudes.

In recent years GPS has been used to monitor the vertical stability of tide gauges with the aim of removing datum motion e ects from the sea level series allowing the true sea level signal to be determined. Carter *et al.* (1989) and Carter (1994) highlight the need for this work and lay out the requirements of a GPS campaign to monitor a gauge. This work is still at an early stage and is unlikely to be carried out on a signi cant number of the gauges suitable for altimeter calibration work for several years. Until that goal is realised, alternative means of quality control must be found.

6.1.3   Data availability

The data must be available over the time for which calibration is required. A gauge can only contribute to calibration during the time in which it is operational and the data made available. With many national and international organisations cooperating to provide a global dataset, many problems can arise in the operation of the gauge or the dissemination of the data. Calibration can be carried out across a drop-out in data availability, for instance when two altimeters whose

missions are separated in time are compared. In this case care must be taken that no o set occurs across the drop-out, for instance if the tide gauge is replaced and the datum of the new instrument is not levelled to the same reference as the old instrument.

6.2   The WOCE tide gauges

The World Climate Research Programme (WCRP) is an umbrella organisation of the World Meteorological Organization, the International Council of Scienti c Unions and the Intergovernmental Oceanographic Commission of the United Nations Educational, Scienti c and Cultural Organisation. The WCRP exists to model climate processes involving the oceans, atmosphere, ice (sea and land) and land surface, along with the interactions which arise between them. Assessing and predicting the in uence of human activities on this dynamic system is a major component of their remit. In the 1980 s the WCRP conceived the World Ocean Circulation Experiment (WOCE) with the remit to improve models of global ocean circulation and in particular to increase understanding of the role of circulation in climate. The eld phase of the programme commenced in 1990 and was scheduled to end in 1997. This phase exists to collect observational data of various parameters linked with circulation. These parameters include hydrography, ocean current, temperature, salinity and sea level. Under the last of these categories, a number of tide gauges have been selected to provide in-situ sea level observations. At the time that this work commenced, there were 94 tide gauges available in the *fast-release* WOCE dataset. These were all considered for use in altimeter calibration.

As the work proceeded, more gauges were added to the set and the time series of the existing gauges were extended. Although the extended datasets were assimilated in to the calibrations, new tide gauges were not subsequently included in this calibration work.

Most of the tide gauges in the WOCE dataset were not installed speci cally for the WOCE. These gauges were already operational, having been installed by national and other authorities for the study of sea level. The primary implication of a gauge being adopted by the WOCE was that the data would be processed and made widely available with a short lead time. For this reason the datasets of many of the gauges span much longer than the seven years of the experiment, some going back for several decades or longer. The gauges are distributed globally, being installed on both mid-ocean islands and continental coasts bordering the ocean basins. Although there is a bias in favour of installations in the Paci c ocean, the Atlantic and Indian oceans have signi cant numbers of gauges. Figure
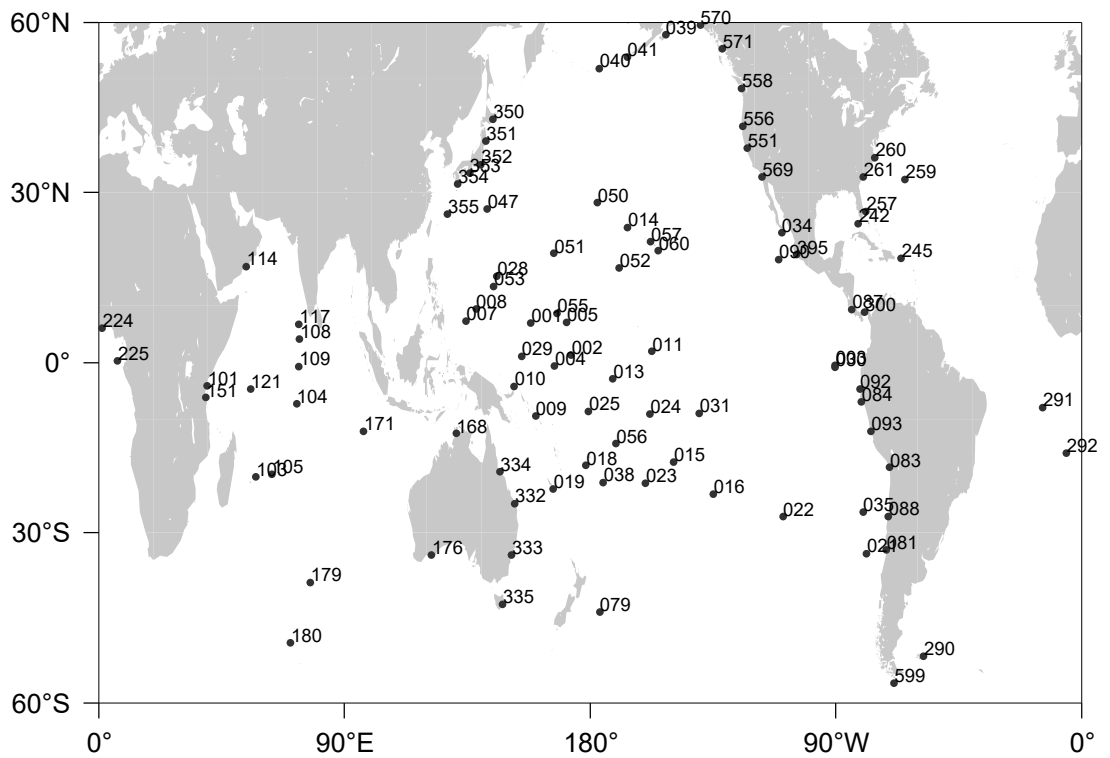
Figure 6.1: Locations and codes of all the tide gauges in the WOCE dataset.

6.1 shows the global distribution of the 94 gauges in the WOCE dataset along with the unique identi cation code of each as assigned by the WOCE.

The times for which data is available for each gauge are shown in Figure 6.2. In most cases coverage is good and all gauges are in operation for at least some of the period since 1985 when the main altimetric satellites have been in operation.

Data for each gauge is made readily available via File Transfer Protocol on the internet, with a lead time of less then three months from when the observation is taken. Three resolutions of data are produced (WOCE, 1995). The most basic dataset comprises time series of raw readings taken every hour. No averaging or ltering is applied to these values and so they will observe all oceanographic e ects including all tidal constituents. The next level is the daily series which consists of a value for each day centred on noon, generated by applying a Bloom eld convolution lter (Bloom eld, 1976) to 119 hourly values. Finally all the hourly values for a particular month are combined with a simple geometric average to give a single monthly value which provides the nal level of dataset. These processing steps are carried out before the data is distributed and three separate les are made available for each gauge, corresponding to the three resolutions.

The WOCE tide gauges are concentrated in the lower latitudes. In fact those installed on islands in the open ocean extend no further than 50 in the northern or southern hemisphere. PGR should not therefore cause signi cant corruption of the WOCE gauge data, for the island gauges at least. The ICE 4G(M2) model for
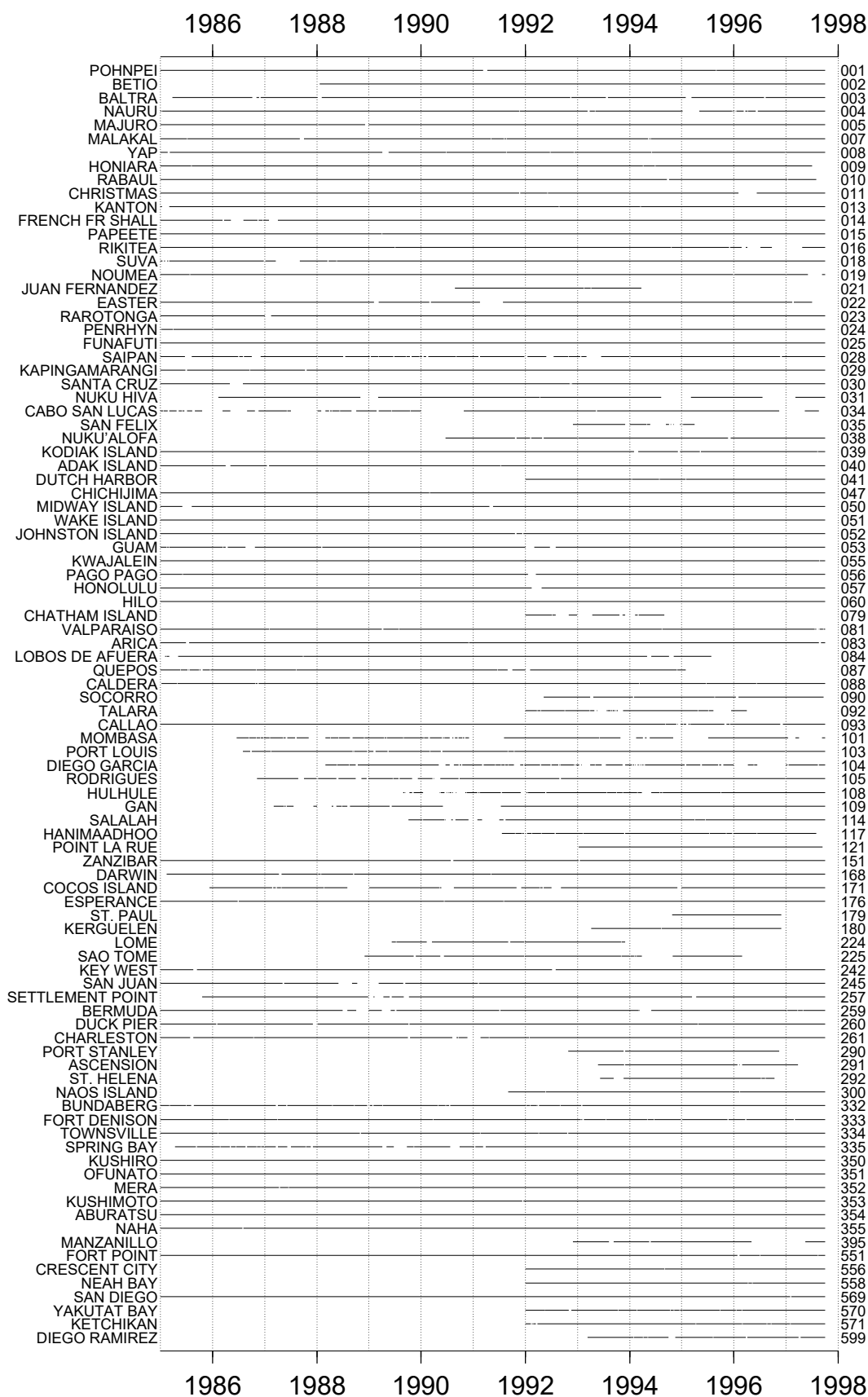
Figure 6.2: Times since 1985 during which the different gauges in the WOCE dataset are operational and the data available. The names of the tide gauges are shown on the left and the codes are given on the right.

PGR-driven sea level rate as given in Rapp and Zhang (1996, Figure 5) is derived from the ICE 4G loading model and the mantle viscosity model of Peltier and Jian (1996). Since the areas of high expected PGR activity from this model do not coincide with the locations of WOCE gauges, con dence is high that any e ect of this phenomenon in corrupting comparisons with altimetry will be minimal.

6.3 Matching the gauge and altimeter observations

The aim is to estimate the variability observed by the altimeter as accurately as possible. The corrections applied to the altimeter and the processing carried out on the tide gauge readings are important to maximise the accuracy of this estimate.

6.3.1 Astronomical tide

The astronomical tide is observed by the altimeter and the tide gauge, but this e ect cannot be assumed to be equal at the altimetry point and the tide gauge. The amplitude and phase of the various constituents may well vary between the two locations. Steps must therefore be taken to reduce the error which would corrupt the comparisons if the tide were ignored.

One method of harmonising the altimeter and gauge readings to account for astronomical tide is to correct both using a model. A potential problem arises in this scheme in that the accuracy of global astronomical tide models is at a minimum near land. The altimetry which contributes to the construction of the models is likely to be sparse in the region of islands, making the models less reliable in those areas. In addition, The constituent harmonics of the tidal models are less likely to apply near land as the assumptions used to construct the model are disrupted. Also, local e ects can potentially reduce the accuracy of global models. For instance if a gauge is installed near a lagoon or in a harbour with a narrow opening, the tidal harmonics observed by the gauge may well be out of phase with the surrounding ocean and hence the model values. These e ects will not have impact on the surrounding open ocean where the altimetry to be calibrated is likely to be taken, so the global models for the astronomical tide will be more representative of the astronomical tide.

A possible solution to this problem would involve correcting the tide gauge readings for short periodic tides independently of the global tidal models. The time series of *daily* tide gauge readings in the WOCE dataset is ltered using 119 hourly values. In essence this smoothes the signal, removing short periodic

tidal signal. If the altimeter is corrected for short periodic tides using a global tidal model then the altimeter and the gauge will in principle observe only the long periodic tides. Although these too will differ between the two locations, long periodic tides are simpler than their short periodic counterparts, have larger spatial wavelength, will not be significantly affected by the phase lags caused by local land and coastal features and are much smaller in amplitude. For these reasons, not correcting for the long periodic tides in the altimeter and the gauge is an acceptable approximation.

6.3.2 Loading tide

The ocean loading tide is observed by the altimeter but not the tide gauge since the land on which the gauge is mounted, being at the coast, is subject to vertical displacement due to the weight of water on the Earth s crust. Correction of altimeter ranges for this quantity is therefore required to unify the two instruments in this respect.

6.3.3 Body tide

Similarly the tide gauge will not observe the body tide in its time series whereas the altimeter will. The altimeter is therefore corrected for this effect to unify the observations for this effect.

6.3.4 Pole tide

Whereas the altimeter observes the geocentric pole tide, the tide gauge observes only the oceanic response. Trupin and Wahr (1990) show that the oceanic and the solid Earth components of the pole tide are in equilibrium with the forcing polar motion, and that as a consequence they are in phase with each other. As an approximation in this work, the altimetry can be corrected for the geocentric pole tide and the tide gauge left uncorrected. In this case the tide gauge will observe the oceanic part of the pole tide response. The amplitudes involved are small and if they are significant they will only serve to increase noise, given the relatively short wavelengths and reasonable geographical spread involved.

6.3.5 Inverse barometric effect

The tide gauge and the altimeter both observe the depression of the sea surface due to variations in atmospheric pressure. Although the pressure variations will not be identical at both locations it is an acceptable approximation to correct neither. The models and available data for values of atmospheric pressure are

unlikely to provide a useful differential correction between the two locations for this effect. Again, the gradient of atmospheric pressure variations between gauge and altimeter point will usually be small enough to obviate the need for such a correction and the errors arising will be noise rather than systematic.

6.3.6 Storm surge

The tide gauge readings will be susceptible to the observation of storm surges which will not appear in the open ocean where altimeter observations are made. This will particularly apply to gauges which are necessarily installed at the coast where the build-up of water will be most pronounced under the right conditions. In general no models are available for the storm surge in the regions of the WOCE tide gauges so this effect must be ignored as a source of noise. The substantial depth of the ocean basins in which the island gauges are installed means that this quantity as observed by those gauges will be insignificant.

6.4 Gauge assessment

A strategy is devised for identifying a core set of the WOCE tide gauges which most accurately measure variability in the surrounding open ocean. First, all continental tide gauges are rejected and only the gauges installed on islands away from continental land mass are considered. This is because the complex tidal regimes and other oceanographic effects present in the continental shelf regions will certainly reduce the reliability of gauges in those regions when used to estimate this variability. Mitchum (1994) demonstrates that the continental coast gauges exhibit poor agreement with altimetry. The WOCE data set includes 53 island gauges. In this case the problem of storm surge is reduced as the effect around small islands will be less than that in coastal regions.

6.4.1 Quantification of the gauge accuracy

The accuracy at which the gauge estimates the variability in the surrounding open ocean must be quantified. There are several candidates for this purpose, namely

the correlation between the true variability and the gauge estimate,

the root mean square (RMS) of the difference between the two values, and

the rate at which the difference between the two values changes over time.
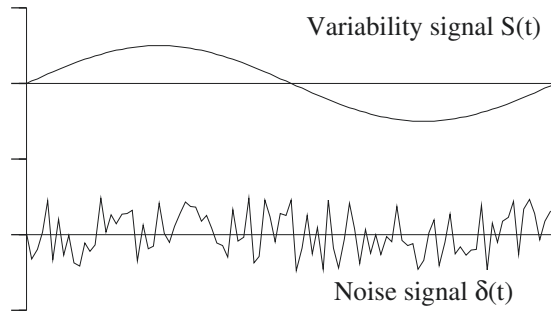
Figure 6.3: The simulated variability signal $S(t)$ and the random noise signal $\delta(t)$, both in arbitrary units.
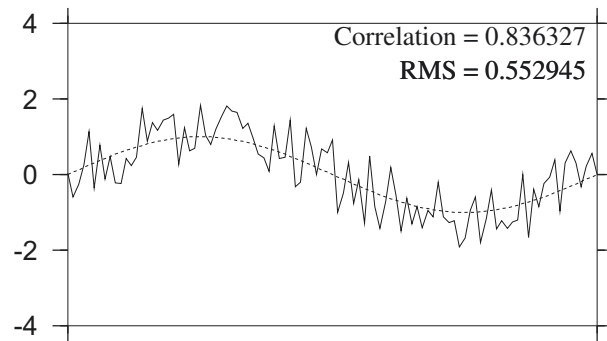
Figure 6.4: The variability signal corrupted by the noise signal (solid line) as compared to the uncorrupted variability (dashed line), all in arbitrary units.
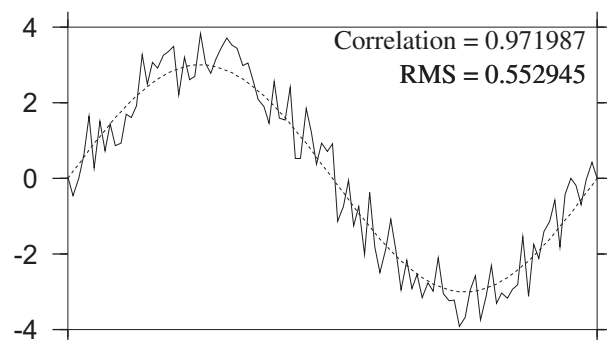
Figure 6.5: The variability signal amplified by a factor of three and corrupted by the noise signal (solid line) as compared to the uncorrupted amplified variability (dashed line), all in arbitrary units.

Consider a gauge which estimates a large sea surface variablity at a point in the open ocean, where the average reading is in error by a given amount. Also consider another gauge which estimates a smaller variability at a nearby point where again the average reading is in error by the same amount. The correlation between the signal observed by the gauge and the true variability signal will be higher for the gauge estimating the larger variability. In other words the correlation is a function of the amplitude of the signal. Thus the correlation between the gauge and ocean signals is not a good indicator of the quality with which the tide gauge measures the variability at the point in the open ocean. To illustrate this, a simple sinusoidal variability signal $S(t)$ is generated along with a random noise signal $\epsilon(t)$ taken from a uniform distribution. These are shown in Figure 6.3. Figure 6.4 shows the signal $S(t)$ along with the signal $S(t) + \epsilon(t)$, simulating the noisy estimate of the variability by a tide gauge. In this case the correlation is 0.836 and the RMS is 0.553. Figure 6.5 shows the similar case where this time $S(t)$ is amplified by a factor of three. This time the correlation is 0.972. Of course the RMS remains the same at 0.553. Both gauges measure the variability equally well which is indicated by the RMS. It would be misguided to reject a gauge purely on the basis of it having a low correlation coefficient with the altimetry as this measure does not provide a consistent indicator of the accuracy. On the other hand the RMS does not have this limitation and is therefore chosen as having the desired properties of a quality indicator.

Any apparent systematic trend in the gauge estimate could be indicative of one of the problems such as degradation of the gauge mechanics or PGR or other geological process. The magnitude of a trend in the error measuring the sea surface is thus also accepted as a quality indicator.

6.4.2 Choice of altimeter

An independent estimator of the sea surface height with which to compare the tide gauge readings is required. Although altimetry is what will ultimately be calibrated, with care it can be used at this stage to compare with the tide gauges. The TOPEX altimeter was chosen for this role for the following reasons. First, the higher orbit of T/P along with the quality and extent of its tracking systems means that the noise in the radial component of the computed orbits will be much less than that of ERS 1. For instance, errors due to mis-modelling of the atmospheric drag will be much less for T/P. Note that the intention is to make comparisons which are essentially repeat pass in nature. As explained in Section 5.4.2 the geographically-correlated radial errors in the orbit, in particular those arising from geopotential mis-modelling, will not therefore affect the comparisons, as an offset in the mean of the altimeter sea surface heights can be removed and

will have no e ect on the RMS di erence, trend or correlation.

The shorter repeat period of T/P is useful since comparisons can be made at a small number of speci c points on the ground-track near the tide gauge. The resultant dataset will be su ciently large for meaningful statistical analysis of the gauge and altimeter time series to be carried out. This fact was also signi cant in choosing TOPEX as a base altimeter for comparison with tide gauges.

Sea surface measurements from TOPEX are to be compared to the readings of the tide gauges. It may be argued that this is best carried out at the points of closest approach of the ground-tracks to the gauge, or on the line of latitude that the gauge lies. This will in general result in the best possible agreement between the gauges and the altimeter. However the gauges will not just be employed to augment repeat pass measurements, which may be taken at any latitude within the inclination of the satellite. They will also be required to augment single and dual satellite crossovers. The luxury of being able to choose the best location for optimum agreement with tide gauge data does not exist in the case of these observations. It was decided to use the crossover points on the TOPEX ground-track in the region of the tide gauge to compare the altimetry to the tide gauge data. This will give a better indication of how representative each tide gauge is of variability in the surrounding ocean.

6.5   Method

In this analysis, the analytical ground-track of T/P was considered in the region of each of the 53 island tide gauges in the WOCE set. The identities of the four analytical T/P passes, two ascending and two descending, forming the smallest diamond surrounding the gauge were determined. TOPEX altimetry from these passes from the rst 130 cycles of the mission were extracted in the region of the gauge. All Poseidon data were rejected on the grounds that its altimetric bias characteristics di er from those of TOPEX.

Raw altimetry was corrected as described above. The tide model of the Center for Space Research (CSR) version 3 was employed. The software implementing this model has the advantage that it splits the long and short periodic components, the long periodic constituents being generated from equilibrium theory and the short periodic constituents generated from orthoweights. This allowed the long periodic components to be excluded from the altimetric correction. The loading tide correction can be made in the same step, as this quantity is included in CSR model.

The intersections of the four analytical passes at each gauge lead to four analytical crossover locations, which can be conveniently identi ed by the compass
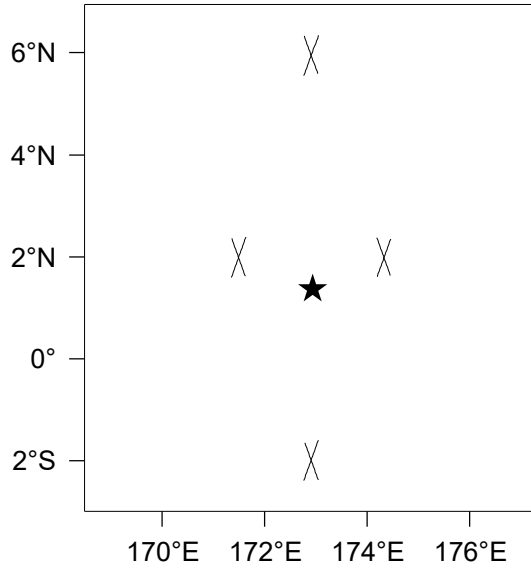
Figure 6.6: WOCE tide gauge number 2 at Betio island, along with the crossovers between the four enclosing T/P passes. The gauge is identi ed by the star.

directions. For example, a typical con guration is given in Figure 6.6. The example given is gauge 2 at Betio. The four enclosing passes are ascending passes 123 and 199; and descending passes 110 and 34. In this case the *South* crossovers can be formed between pass 199 of any cycle and pass 34 of any cycle. Orbit perturbations from cycle to cycle dictate that the location of each particular crossover will vary depending upon which cycles are chosen, but will always lie within a few kilometres of the general analytical position. Since 130 cycles have been considered, in principle it is possible to generate 16900 crossovers at each general crossover location. In fact the rejection of Poseidon data ensures that there is a maximum of only 119 cycles since the 11 T/P cycles 20, 31, 41, 55, 65, 79, 91, 97, 103, 114 and 126 are dedicated to Poseidon operation. A full TOPEX dataset will therefore yield just over 14000 crossovers.

A particular analytical crossover location at a given gauge will involve two passes, p_1 and p_2, one ascending and one descending. Each SXO residual will involve the ground-track intersection of pass p_1 of a speci ed repeat cycle c_1 with pass p_2 of a speci ed repeat cycle c_2. The term $X_{p_1 p_2}(c_1 \ c_2)$ is de ned to be the crossover residual between pass p_1 of cycle c_1 and pass p_2 of cycle c_2. The altimeter measurements must be interpolated to the point of intersection of these two particular satellite passes to generate the crossover residual. The term $t_{p_1 p_2}(c_1 \ c_2)$ is de ned to be the time during pass p_1 of cycle c_1 that the satellite ground-track reaches the point of intersection of that pass with the ground-track of pass p_2 of cycle c_2. The crossover residual can thus be expressed as

$$X_{p_1 p_2}(c_1 \ c_2) = h(t_{p_1 p_2}(c_1 \ c_2)) \quad h(t_{p_2 p_1}(c_2 \ c_1)) \tag{6.1}$$

119

where $h(t)$ is the altimetric sea surface height interpolated to time t. The tide gauge difference of Equation 5.5 can be used as a comparison. In particular the gauge difference

$$G_{p_1 p_2}(c_1, c_2) = g(t_{p_1 p_2}(c_1, c_2)) - g(t_{p_2 p_1}(c_2, c_1)) \qquad (6.2)$$

will be related to the crossover difference of Equation 6.1 since in principle both should measure the same variability.

6.5.1 Independent crossover residuals

In principle SXOs may be taken between all possible pairs comprising one ascending and one descending pass at each analytical crossover location. This would generate up to 14000 residuals as explained above. It is possible to utilise all these residuals to generate statistics and eventually to derive an estimate for the altimetric drift function. However this must be avoided since there is heavy dependence between the residuals derived in this way. To illustrate this, consider the case where two arbitrary ascending passes are picked at an analytical crossover location. Each may be used to generate SXOs with all the descending passes at that analytical location. If the two resulting series are compared then apart from a constant offset between them, they will be found to be very similar. This offset arises primarily from the noise in the altimetric sea surface heights as measured by the two ascending passes. A small amount of signal will be introduced since the exact locations of the SXOs will vary slightly in each case. Thus it cannot be assumed that all crossover residuals generated at an analytical crossover location are independent. This is intuitive when it is considered that the full crossover dataset at an analytical crossover are generated using up to 119 ascending and up to 119 descending passes and yet may be used to derive up to 14000 residuals. Care must be taken in the next section so that the altimetry is fully exploited but only independent crossovers are used.

6.5.2 Generation of independent crossover time series

Two series of independent crossover differences can be generated at each analytical crossover location, one involving all ascending passes and the other involving all the descending passes. The first series is generated by picking a cycle m to give

$$X_{p_1 p_2}(i, m) \quad i = 1, \ldots, 130$$

where m is chosen such that the crossover yield is maximal. The second series is generated by choosing a cycle n to give

$$X_{p_2 p_1}(i, n) \quad i = 1, \ldots, 130$$

where n is again chosen for an optimal yield. The gauge difference series associated with these crossover series are be similarly constructed.

Since each gauge contributes four analytical crossover locations involving two ascending passes, a_1 and a_2 say, and two descending passes, d_1 and d_2 say, there will be eight crossover series and eight associated gauge difference series associated with each tide gauge. These will be

$$
\begin{aligned}
&X_{a_1 d_1}(i\ r_1) &&G_{a_1 d_1}(i\ r_1);\\
&X_{d_1 a_1}(i\ r_2) &&G_{d_1 a_1}(i\ r_2);\\
&X_{a_2 d_1}(i\ r_3) &&G_{a_2 d_1}(i\ r_3);\\
&X_{d_1 a_2}(i\ r_4) &&G_{d_1 a_2}(i\ r_4);\\
&X_{a_1 d_2}(i\ r_5) &&G_{a_1 d_2}(i\ r_5);\\
&X_{d_2 a_1}(i\ r_6) &&G_{d_2 a_1}(i\ r_6);\\
&X_{a_2 d_2}(i\ r_7) &&G_{a_2 d_2}(i\ r_7); \quad \text{and}\\
&X_{d_2 a_2}(i\ r_8) &&G_{d_2 a_2}(i\ r_8)
\end{aligned}
$$

where r_n are the reference cycles and $i = 1$ 130.

6.5.3 A crossover determination algorithm

Since the position of each crossover in any of the above crossover series will in general be unique, each pair of satellite passes for which a crossover is required must be interpolated together to generate that particular residual. In this work the crossover residual for each pair of passes is found as follows. The ground-track expressed in latitude, longitude and time, of each pass is obtained in the region of the region of the expected crossover location. For each is found a cubic polynomial to express the longitude as a function of latitude. The roots of the polynomial difference are found and thus the approximate time of the crossover in each pass is found. The four altimeter observations each side of the approximate crossover time in each pass are then interpolated again and a more accurate estimate of the location of the crossover is found along with estimates of the time that each of the two passes reaches the crossover location. The eight sea surface heights in each pass are interpolated to the corresponding time of the crossover using a cubic polynomial. The difference between these two heights is interpreted as the crossover residual.

6.5.4 Tidal Aliasing

Precise satellite orbit computations must include a dynamic model for the ocean tides in the calculation of the gravitational attraction of the Earth. Of course

there will be errors in these tidal models which will a ect the generated orbits. Marshall *et al.* (1995) establish that these model errors will interact with the orbital characteristics of T/P and cause orbital resonance perturbations. Each tidal constituent will cause a di erent error frequency which will be aliased into collinear altimeter observations of a given point on the ocean. The principal lunar and solar tides, M_2 with a period of 12.421 hours and S_2 with a period of 12.000 hours are in general the predominant tidal constituents and so will cause orbit errors of the largest amplitudes. To account for these errors which may be present in the time series derived above, harmonics with the frequencies corresponding to the aliasing periods of two principal tidal constituents are removed from each time series. As the error will vary with geographical location, a di erent harmonic must be found at each crossover of each gauge. The aliasing periods for the M_2 and the S_2 tidal constituents are 62.1 days and 58.7 days respectively (Marshall *et al.*, 1995). A least squares numerical solver is employed. When solving for harmonics in this way, the mean constant signal must be removed from the observations or incorrect harmonics of larger amplitudes will result. Each crossover location contributes a time series of ascending passes and a time series of descending passes, each of which will be a ected by the same amplitude and phase of orbit error at the speci ed frequencies. However, each of the time series may be o set from each other in the height domain. To account for this fact an o set for each series was introduced so that the harmonics described the true signal present in the combined series. Thus the function t at each crossover location was

$$f(t) = \quad _1\cos\frac{2\ t}{62\ 1} + \quad _2\sin\frac{2\ t}{62\ 1} + \quad _3\cos\frac{2\ t}{58\ 7} + \quad _4\sin\frac{2\ t}{58\ 7} + O_{a\ d}$$

where t is the time of the observation. The o set $O_{a\ d}$ is constant for both series but can vary between the ascending and the descending pass series. These o sets along with $_1$, $_2$, $_3$ and $_4$ are solved for. A harmonic with freedom in amplitude and phase expressed as

$$f(\ ) = A\cos\ + B\sin$$

can be rewritten in the form

$$f(\ ) = \quad \cos(\quad)$$

where

$$= \tan^{-1}\frac{B}{A}$$

and

$$= \quad \overline{A^2 + B^2}$$

TG	South			East			North			West		
	Obs.	S2	M2	Obs.	S2	M2	Obs.	S2	M2	Obs.	S2	M2
001	208	1.9	1.4	205	1.0	2.3	215	1.9	1.2	217	1.8	0.8
002	212	0.1	0.4	219	1.0	0.3	219	0.8	2.3	211	0.3	0.6
003	211	0.8	1.5	207	1.3	0.7	210	1.7	1.0	217	0.9	0.8
004	177	0.9	1.7	180	1.1	1.9	163	0.9	2.8	172	0.6	2.2
005	215	0.3	2.0	223	0.3	0.6	220	0.2	0.5	217	0.6	1.9
007	212	0.7	2.4	206	1.2	0.8	216	0.5	0.7	218	0.8	2.4
008	209	1.7	1.7	207	1.8	0.5	223	1.7	0.7	221	1.1	1.4
009	205	1.8	1.6	171	2.4	1.2	214	1.3	2.4	218	0.5	1.3
010	166	2.0	4.2	216	0.4	1.6	214	0.3	0.9	216	0.6	1.6
011	217	0.7	0.9	91	1.7	2.1	213	0.7	1.8	214	1.3	0.3
013	225	0.5	1.2	220	0.7	0.3	219	1.0	0.6	228	0.6	0.5
014	219	1.3	1.9	228	2.3	1.1	222	1.3	4.1	221	1.3	1.5
015	228	1.6	1.8	227	1.8	0.8	228	2.0	1.3	228	1.2	0.7
016	211	1.3	1.3	206	1.5	1.1	200	0.7	2.0	208	0.3	1.4
018	218	1.6	2.7	218	0.7	0.9	171	0.9	2.5	222	2.1	1.4
019	174	1.8	0.8	192	1.7	0.5	190	0.7	3.1	202	0.2	1.2
021	93	0.1	1.6	97	0.8	0.6	99	2.0	0.4	94	0.8	0.4
022	213	1.3	0.2	215	0.6	1.0	227	1.0	0.7	220	0.6	1.1
023	216	2.7	0.6	220	2.3	0.8	226	1.8	2.2	228	2.0	0.6
024	229	2.0	0.6	218	1.4	0.5	221	1.8	1.9	223	1.1	0.7
025	222	1.0	0.5	223	1.4	1.3	221	1.1	0.9	219	0.2	1.5
028	201	2.5	1.8	194	1.7	1.6	197	1.7	1.2	185	1.7	2.2
029	216	2.9	4.1	212	0.9	1.5	225	0.6	0.4	216	0.2	1.2
030	221	0.8	1.3	219	1.2	0.5	220	1.7	0.3	225	0.7	0.9
031	118	1.8	1.4	38	3.8	3.2	103	1.5	0.1	114	1.1	0.8
035	113	1.0	1.4	110	1.8	3.7	111	0.6	0.4	113	0.3	1.2
038	217	0.8	1.0	219	2.1	2.9	222	2.6	1.5	223	1.4	0.4
047	182	0.8	2.1	204	0.8	4.5	209	2.8	3.8	219	1.7	3.0
050	223	1.8	2.5	227	1.0	1.2	223	2.5	0.2	229	0.5	1.5
051	228	1.8	3.1	226	1.2	0.9	219	1.5	3.0	221	2.0	2.9
052	223	2.4	3.2	228	1.0	4.1	207	1.3	3.4	225	3.3	2.5
053	223	1.1	1.6	222	1.7	1.1	225	0.6	0.4	208	0.7	1.2
055	205	1.1	1.0	213	0.9	1.2	220	1.0	0.6	227	0.9	0.1
056	227	1.8	1.2	217	1.3	1.1	212	1.2	0.6	211	1.7	0.9

TG	South			East			North			West		
	Obs.	S2	M2	Obs.	S2	M2	Obs.	S2	M2	Obs.	S2	M2
057	226	1.2	0.6	226	1.0	0.5	220	0.8	0.3	218	1.1	0.7
060	228	1.0	0.7	227	1.8	2.3	213	2.0	3.1	225	2.3	1.2
079	85	2.4	0.9	88	1.9	1.5	87	2.6	2.1	83	1.0	0.7
103	193	0.9	1.2	228	3.0	2.0	222	2.4	1.1	207	2.8	2.7
104	153	2.5	1.8	153	0.8	0.7	154	2.4	2.6	152	1.5	0.5
105	217	1.7	1.7	214	0.4	1.8	202	0.8	1.5	216	1.7	0.1
108	164	2.0	0.9	184	2.8	0.3	178	0.3	0.6	188	0.9	0.1
109	224	3.1	4.4	223	1.5	0.9	215	0.8	0.8	221	2.3	0.5
117	204	1.7	0.6	195	1.0	1.0	210	3.4	1.5	219	1.5	0.7
121	200	2.1	0.6	203	1.4	1.4	202	1.0	1.2	207	1.3	1.3
171	224	1.9	1.3	229	2.0	3.0	222	1.7	0.6	220	1.6	0.4
180	185	0.8	1.3	62	4.2	2.2	181	1.5	3.1	180	0.7	1.1
245	231	1.2	0.8	221	0.5	1.1	218	1.4	0.5	231	0.2	2.7
259	143	1.3	2.2	140	2.6	3.2	118	1.7	0.9	146	0.4	0.6
290	93	1.5	2.5	85	1.4	6.6	84	1.2	3.2	8	22.5	25.4
291	159	0.8	0.4	160	0.8	0.5	158	1.3	0.8	157	1.3	0.3
292	140	0.4	0.7	143	0.6	0.8	145	1.2	1.0	142	0.6	0.7
335	221	0.9	0.5	227	0.1	3.5	225	0.9	5.5	0	0.0	0.0
355	200	2.7	2.3	180	2.2	2.3	220	1.8	3.1	206	1.1	0.9

Table 6.1: Amplitudes, in centimetres, of the harmonics removed from the time series to account for resonant orbit error arising from mis-modelling of the S_2 and M_2 semi-diurnal tides. The number of observations contributing to each solution is also shown.

This alternative form allows the amplitudes of the resultant harmonics to be extracted. The amplitudes for each crossover location of each gauge, along with the number of observations contributing to the solution are shown in Table 6.1.

The table shows that in most cases the amplitudes of the harmonics are very small and of the order of 1 1.5 cm. The large values for the *West* crossover of gauge 290 are due to only eight values being available. If this location is excluded then the mean harmonic amplitudes are 1.35 cm for the S2 alias period and 1.46 cm for the M2 alias period. A larger value for the M2 correction implies a larger error in the M2 component of the tidal model used in orbit generation. This is consistent with the dominance of this tide in most regions. The accuracy of the radial orbits derived from independent quality control suggest that these values should be small so where the value exceeds about 3 cm and the sample is large, other signal is probably being absorbed by the solver. This other signal is

most likely to arise from the break down of the tide model near land.

The harmonic for each crossover location is constructed from the values $_1$, $_2$, $_3$ and $_4$ and are removed from both crossover series at that crossover location.

6.5.5 Derivation of the quality statistics

There are now up to eight crossover series and the associated gauge difference series for each tide gauge. Sets of quality ratings could be derived for each series pair which would give rise to sets of eight quality values per gauge. Since the initial intention is to classify a gauge as either good or bad, only one set of quality ratings per gauge is desired. This could be achieved by somehow averaging the eight crossover series together to make one representative series. For instance, a representative series comprising one averaged crossover value and one averaged gauge value per cycle could be calculated and the statistical analysis performed on these series. However, this hypothetical approach would introduce smoothing and could result in misleading quality ratings. A more realistic alternative is to perform the statistical analysis on the combined data from the eight series without averaging.

A realistic statistical analysis cannot be performed without taking into account the possible offset between the crossover and the gauge series. Each crossover series is generated by differencing the same pass of each cycle with a given reference pass. Any offset in the reference pass will offset the series by that amount. The same applies to each gauge series since each reading is referenced to an arbitrary datum. These offsets will artificially enlarge RMS values if not accounted for. In addition, since in general the offsets will be different for each of the eight series at each gauge, the correlations and slopes will also be affected. To account for these arbitrary offsets, each of the eight crossover series and the eight corresponding gauge series at each tide gauge is normalised to ensure a zero average in each.

Once the mean has been removed from each series, rejection of anomalous points can take place. The point-wise difference between each crossover series and its associated gauge series is taken. If any such difference exceeds 25 cm then the corresponding members of the crossover and gauge series are rejected. The number of crossover observations dropped by 3.3% from 42538 to 41131 when this rejection filter was applied.

The quality indicators for each gauge are generated using all eight filtered crossover time series associated with that gauge. First, the RMS difference between the combined crossover series and their associated gauge series at that tide gauge is calculated. Any trend in the series is calculated by subtracting the ap-

TG	Obs.	RMS (cm)	Slope (cm/yr)	Corr	TG	Obs.	RMS (cm)	Slope (cm/yr)	Corr
292	570	3.37	1.17	0.75	4	692	7.51	1.27	0.36
291	634	5.12	0.14	0.46	60	893	7.60	0.47	0.43
13	892	5.24	0.61	0.66	104	612	7.68	0.51	0.60
30	885	5.25	0.25	0.62	290	270	7.72	-1.06	0.77
3	845	5.33	0.33	0.60	57	890	7.76	-0.87	0.47
15	911	5.41	1.05	0.43	7	852	7.77	1.73	0.67
109	883	5.76	-0.13	0.62	29	869	7.84	2.31	0.64
79	343	5.87	-0.74	0.83	16	825	8.14	-1.66	0.44
21	383	5.90	-4.52	0.59	9	808	8.37	-1.02	0.75
55	865	5.99	0.18	0.59	38	881	8.48	-0.31	0.45
24	891	6.11	-0.79	0.49	171	895	8.60	-0.63	0.65
22	875	6.16	0.76	0.57	28	777	8.62	2.75	0.62
31	373	6.30	-0.25	0.28	56	867	8.66	1.57	0.08
10	812	6.44	-3.05	0.77	103	850	9.21	1.65	0.56
121	812	6.45	-1.67	0.64	19	758	9.32	0.35	0.37
2	861	6.48	1.31	0.40	14	890	9.38	-0.58	0.51
25	885	6.50	-1.24	0.62	259	547	9.53	-0.42	0.67
245	901	6.58	0.36	0.64	18	829	9.56	-1.20	0.41
1	845	6.60	-0.26	0.68	335	677	9.57	-1.37	0.71
35	447	6.86	-1.14	0.20	23	890	9.63	-1.29	0.27
5	875	7.03	0.16	0.50	52	883	9.73	0.66	0.46
180	608	7.30	0.53	0.79	105	849	9.90	2.61	0.47
117	828	7.34	0.15	0.61	50	902	10.10	1.14	0.48
108	714	7.34	-0.59	0.57	47	814	10.36	0.61	0.64
11	735	7.38	0.31	0.57	51	894	10.80	0.52	0.34
53	878	7.41	-1.86	0.72	355	806	10.99	0.49	0.60
8	860	7.49	0.69	0.64					

Table 6.2: Quality assessment statistics for each tide gauge. The columns show the tide gauge number, the number of observations contributing to the statistics and the three quality statistics for that gauge.

propriate gauge series from each crossover series and then performing a linear regression. The mean rate is calculated over all tide gauges and removed from each trend so that the effect of altimetric drift may be counteracted. The correlation between the combined crossover and gauge series pairs is calculated at each gauge for information only. The results of this are shown in Table 6.2. Each gauge is identified by its WOCE code in the first column. The number of observations available for analysis is given in the second column, the RMS difference between the crossover series and the gauge series is given in centimetres in the third column, the normalised rate of the difference between the two, in centimetres per year, is shown in the fourth column and the correlation coefficient between the gauge and the altimeter is given in the fifth column. The entries are sorted by increasing RMS.

Figure 6.7 shows how the agreement between the series varies between the different series at a typical tide gauge. In this case, gauge 13 at Kanton is shown. The trends are calculated without removal of the mean trend. The location of the Kanton gauge is shown in Figure 6.8. All series show reasonable agreement between the instruments, although the agreement is worst at the south crossover, despite the fact that the north crossover is nearly 200 km more remote than the south crossover. Since altimeter series at the other crossovers are in excellent agreement with the gauge, the disagreement at the south crossover must be due to oceanographic signal in the region of that crossover. Given that Kanton island is surrounded by open ocean, the reason for this discrepancy is not known. The signal may be the signature of the El Nino Southern Oscillation event of 1992 or it could be related to variability in ocean currents around the south crossover.

The details of some atypical gauges are shown. Figure 6.9 shows the overall solution for gauge 355 at Naha. Although the variability is not great and seems to be dominated by a semi-annual signal, the gauge s measurement of the variability is poor. The overall RMS difference is 10.99 cm which is highest of all gauges included in the exercise. Figure 6.10 shows the region in which the gauge is located. The approximate distances from the gauge to the South, East, North and West crossovers are 295 km, 334 km, 76 km and 306 km respectively. Inspection of the series for the North crossover reveals that the agreement is extremely poor at this point, with an RMS of over 11 cm. The other three crossovers, although poorly correlated with the altimeter, are not as extreme as the North crossover. The North crossover is the main contribution to the large overall RMS for this gauge. By comparison, gauge 53 at Guam accurately measures high variability. Figure 6.11 gives the solution for this gauge and shows the many frequencies of variability present in the signal. The region of this gauge is given in Figure 6.12. This time the approximate distances from the gauge to the South, East, North
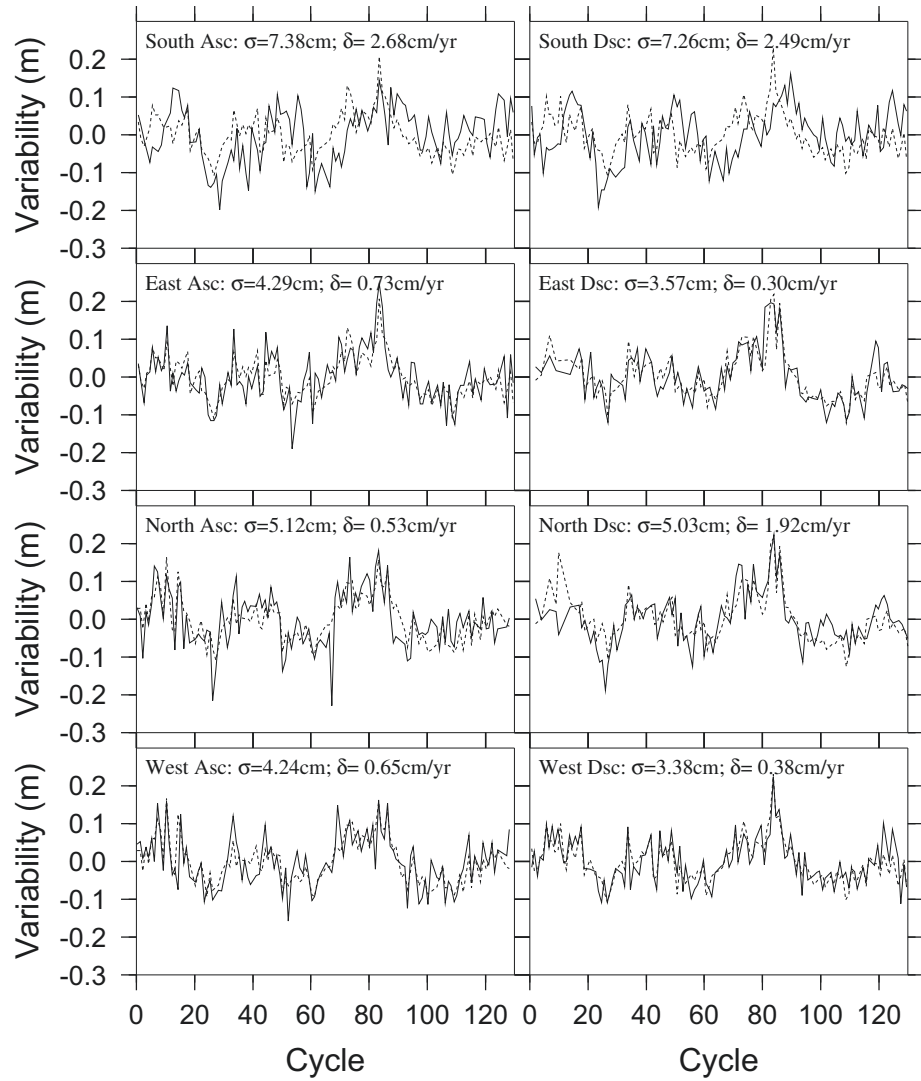
Figure 6.7: Comparison between the eight time series for the tide gauge (dashed line) and the altimeter (solid line) at gauge 13 (Kanton). Each graph shows the RMS difference (σ), in centimetres, between the two series and the slope (δ) in cm/yr of the difference between the two signals.
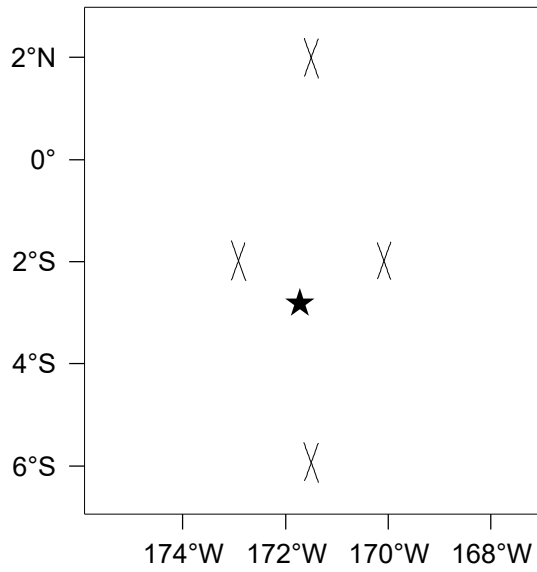
Figure 6.8: The location of gauge 13 (Kanton) along with the crossovers between the four enclosing T/P passes. The gauge is identi ed by the star.
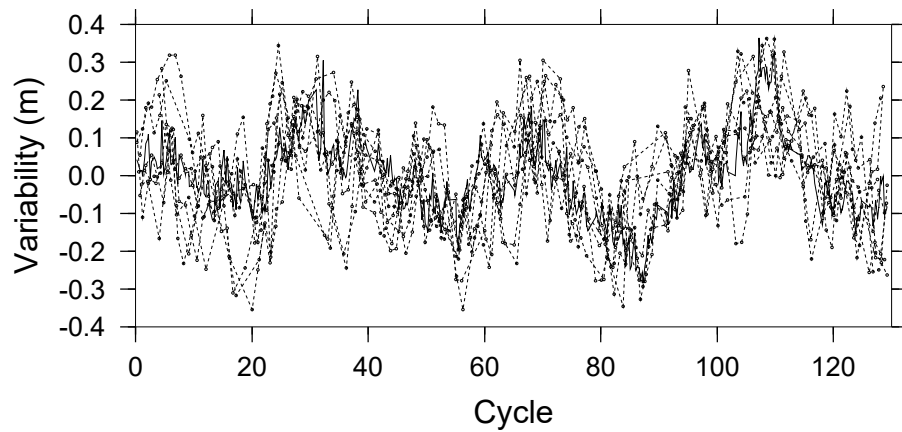
Figure 6.9: The tide gauge time series (solid line) and all eight altimeter time series (dotted lines) at gauge 355 (Naha).
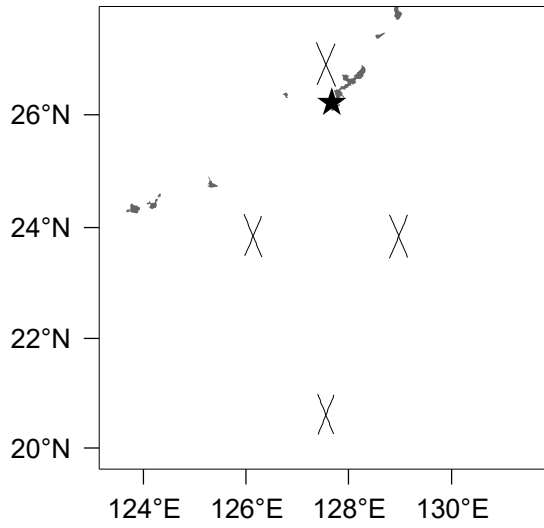
Figure 6.10: The location of gauge 355 (Naha) along with the crossovers between the four enclosing T/P passes. The gauge is identi ed by the star.
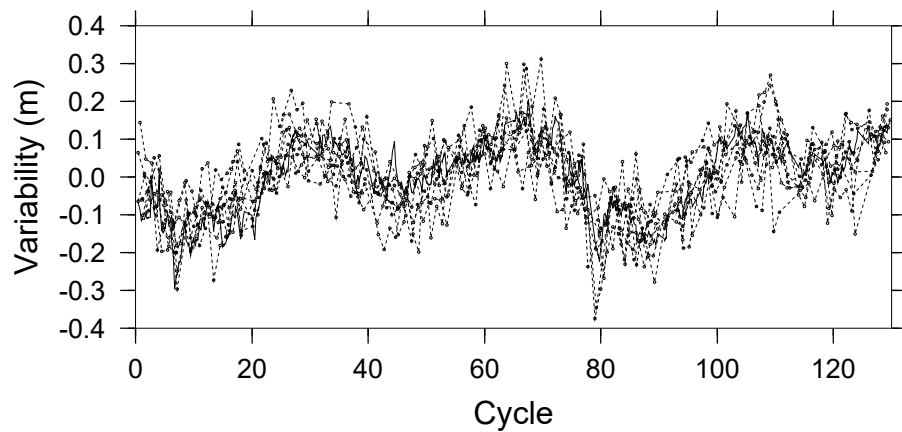
Figure 6.11: The tide gauge time series (solid line) and all eight altimeter time series (dotted lines) at gauge 53 (Guam).
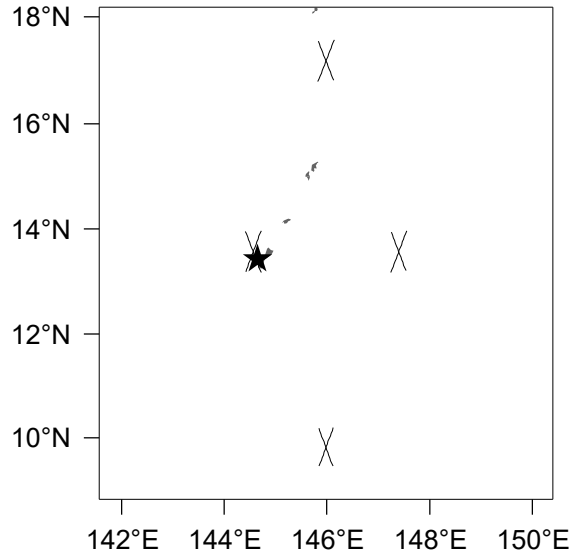
Figure 6.12: The location of gauge 53 (Guam) along with the crossovers between the four enclosing T/P passes. The gauge is identi ed by the star.
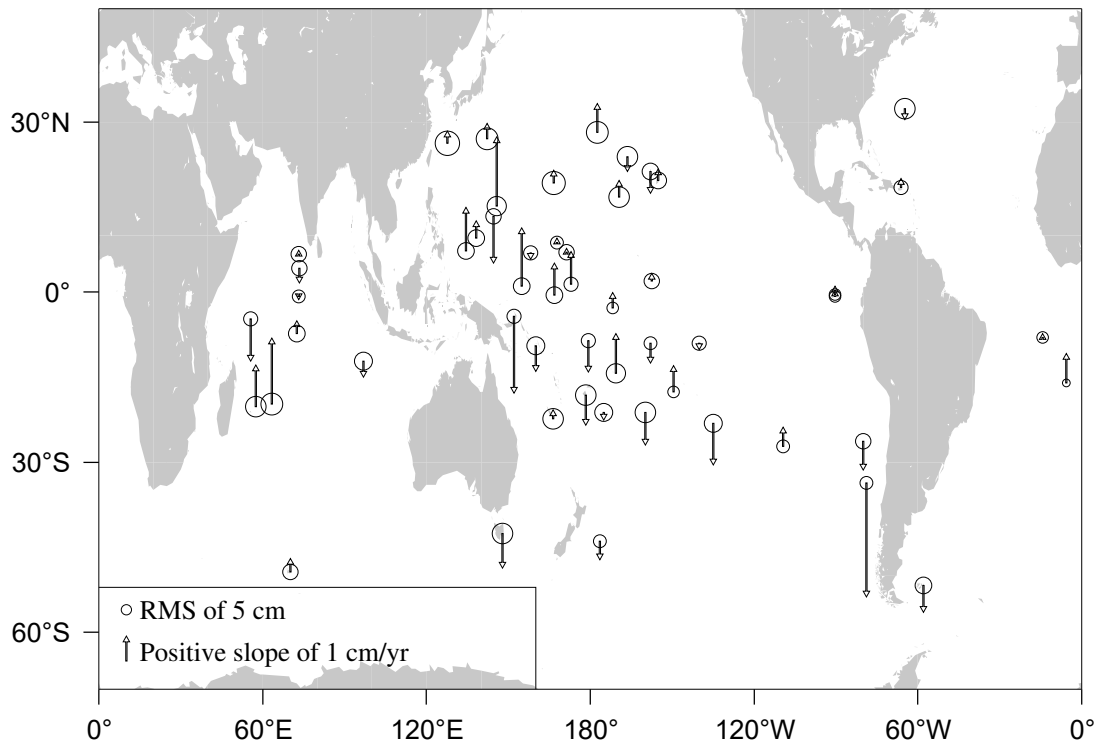
Figure 6.13: The geographical distribution of gauge quality. The length of the arrows represent the normalised slope of the di erence between the crossover and the gauge series. The size of the circles represent the RMS of the di erence between the crossover and the gauge series.

and West crossovers are 428 km, 298 km, 440 km and 18 km respectively. The RMS difference is typical in this case and stands at 7.41 cm.

6.6 The core gauge dataset

Quality measures for each of the 53 island gauges have now been derived as given in Table 6.2. The trend and RMS measured at each gauge are plotted on Figure 6.13. The selection of gauges is based primarily on the slope. Gauges which exhibit a large trend with respect to the crossovers are potentially more dangerous as these are more likely to corrupt bias drift estimates. Therefore any gauge which exhibits a slope with a magnitude greater than 3 cm/yr when compared with the crossovers is rejected. With this criterion, two gauges are lost. These are 10 and 21 at Rabaul and Juan Fernandez respectively.

The RMS of the difference between the crossover and the gauge series is also important although it is possible that a high value of noise in the comparison between the gauge and the crossovers could be due to noise in the altimeter. To reject those gauges with a high RMS is reasonable when using those gauges to calibrate TOPEX although this criterion is not easily extended to other altimeters. Setting a cut-off RMS is hap-hazard at best and arbitrary at worst. The relatively small number of candidate tide gauges means that only a small number of them may be rejected. However if ones in serious disagreement with the altimetry are accepted, there is an increased risk of erroneous drift estimates. If gauges where the RMS is greater than 10 cm are rejected then only four gauges are lost. These are 47, 50, 51 and 355 at Chichijima, Midway Island, Wake Island and Naha respectively.

Looking for a connection between the rejected gauges is risky with such small numbers. However the four gauges rejected on the basis of RMS are all in the Northern Pacific, suggesting a high degree of variability in the sea surface topography in that region, possibly linked to ocean currents. The two rejected for having a large trend are both close to large land masses at continental margins. The associated risk of tectno-geological activity could give rise to a non-zero gauge datum rate. In the case of gauge 10 at Rabaul, East of New Guinea, the gauge lies on a narrow straight between New Britain and New Ireland which opens it to speculation. For instance a change in the circulation pattern in that area could change the transport through the straight gradually over time. This scenario could be associated with a gradual trend in the difference between the gauge readings and the variability in the surrounding ocean.

In conclusion, it is decided that WOCE gauges 10 and 21 are unsuitable for altimetric calibration owing to their significant vertical instability. In addition to
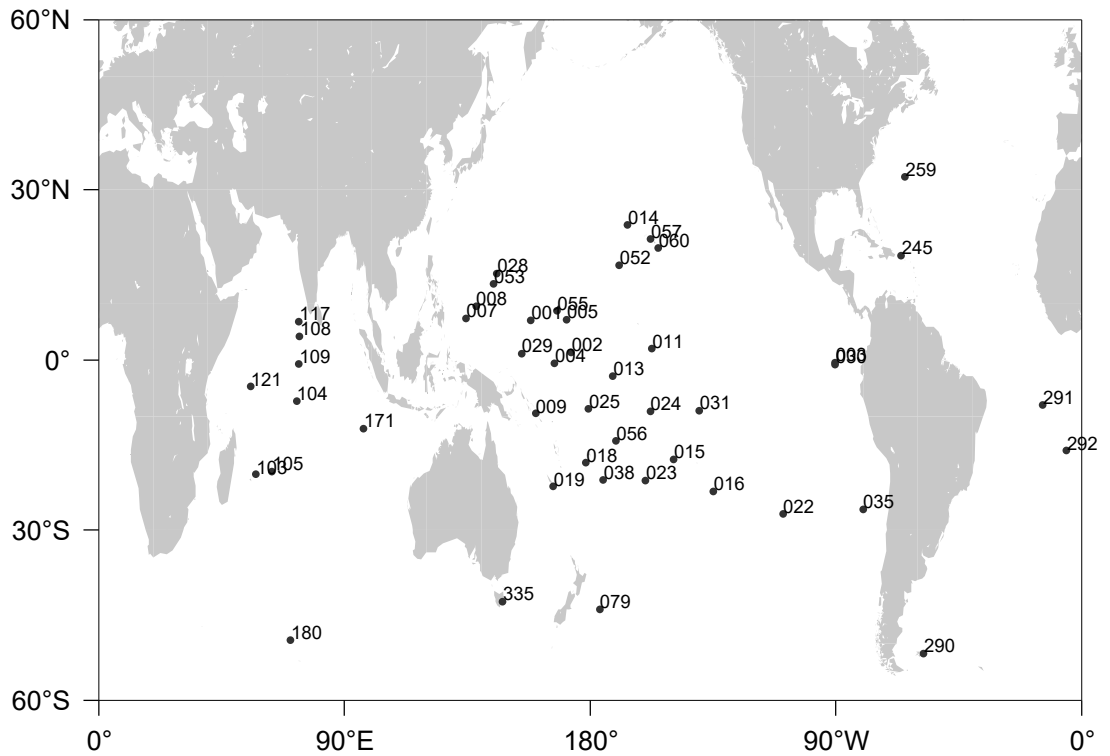
Figure 6.14: Locations and codes of tide gauges in the   nal set accepted for altimeter comparisons.

this, gauges 47, 50, 51 and 355 are considered unsuitable for calibration of TOPEX as the comparisons between these gauges and TOPEX are highly noisy. This cannot be automatically generalised to other altimeters though, as the respective contributions of the altimeter and the gauge to the noise cannot be determined. However care should be taken when using these four gauges in other situations. This leaves 47 WOCE tide gauges suitable for calibration of TOPEX, the accepted set of which is shown in Figure 6.14.

Chapter 7

Intra-altimeter calibration of TOPEX

As a by-product of the assessment of tide gauges in the last chapter, a set of crossovers in the vicinity of tide gauges have been produced, along with associated tide gauge di erences. If they are combined with the gauge di erences, the crossovers may now be employed to estimate an altimetric drift function for TOPEX.

The tide gauges designated as suitable for calibration in the last chapter are taken as a starting point, and additional quality control is applied to the individual crossover series to exclude anomalies not identi ed earlier. A method of nding the altimetric drift function best described by the available observations is developed and applied to the suitable data. The resulting drift function for TOPEX is compared to that predicted to be induced by the algorithm error in the processing of the USO data. The e ect of this is removed from the drift function and the impact of the drift implied by the internal calibration mode of the instrument is assessed. Finally an altimetric drift function for Poseidon is estimated, although this is hindered by the lack of data for this instrument.

7.1 Measurement of drift

Ultimately $d^T(t)$, the altimetric drift function for TOPEX, is sought. Recall from Section 5.2.1 that this is to be modelled as a step function with each parameter applying for 9.9156 days and corresponding to a ground-track cycle. At each island tide gauge in the WOCE set, up to eight series have been derived, two at each of the four enclosing analytical crossover locations corresponding to the ascending and descending passes at that location. In principle, each of these will measure this altimetric drift function. Of course the noise arising from mis-modelled oceanographic signals, orbit perturbations, altimeter range noise and

media mis-modelling will mask the drift in any given series. By merging the signals in some way, an estimate for the function can be derived.

7.1.1 A scheme for merging series

From the previous chapter there is a dataset of SXO observations and gauge difference observations following the forms of Equations 6.1 and 6.2 respectively. Recall that these are grouped into sets with a common reference pass and that a common reference pass applies to all ascending or all descending passes at each analytical crossover location. The SXO observations may thus be expressed as $X_{p_1p_2}(c\ r_i)$ where r_i is the reference pass corresponding to the analytical crossover location and whether p_1 is ascending or descending for that particular observation. This crossover observation is associated with the gauge difference $G_{p_1p_2}(c\ r_i)$. The crossover and gauge differences from Equations 6.1 and 6.2 may be combined to derive the gauge-augmented crossover difference:

$$
\begin{aligned}
X_{p_1p_2}(c\ r_i) &= X_{p_1p_2}(c\ r_i) \quad G_{p_1p_2}(c\ r_i) \\
&= [h(t_{p_1p_2}(c\ r_i)) \quad h(t_{p_2p_1}(r_i\ c))] \quad [g(t_{p_1p_2}(c\ r_i)) \quad g(t_{p_2p_1}(r_i\ c))]
\end{aligned}
\tag{7.1}
$$

Equations 5.12 and 5.13 show how gauge-augmented SXOs relate to the altimetric drift functions. If p_1 is assumed to be an ascending pass this relationship may be applied in this case as follows:

$$
X_{p_1p_2}(c\ r_i) = d_{t_0}^T(t_{p_1p_2}(c\ r_i)) \quad d_{t_0}^T(t_{p_2p_1}(r_i\ c)) + 2 \quad {}_v^T + E
\tag{7.2}
$$

where ${}_v^T$ is the variable part of the geographically-correlated orbit error for T/P at that location. Now, pass p_1 of cycle c will in general appear only once in the set of SXO observations at that analytical crossover location unless it is itself a reference pass. Conversely, pass p_2 of cycle r_i will contribute to up to 120 crossovers since it is a reference pass. This means that if Equation 7.2 is used in its current form as the basis of a solution for the drift parameters then the recovered parameters will be heavily biased by any error in the reference cycles. To overcome this problem, it is first noted that the term $h_{p_2p_1}(r_i\ c)$ in Equation 7.1 will vary only slightly over all gauge-augmented SXO residuals to which it contributes. This is due to slight changes in crossover location from one cycle to the next which mean that the reference pass is interpolated to a slightly different point in each case, usually within a few kilometres. The term $h_{p_2p_1}(r_i\ c)$ may therefore be approximated by a term, ${}_i$ say, which is held constant over $X_{p_1p_2}(c\ r_i)$ for $c = 1 \quad 130$. This removes the dependence on the term $d_{t_0}^T(t_{p_2p_1}(r_i\ c))$ in Equation 7.2 which becomes

$$
X_{p_1p_2}(c\ r_i) = d_{t_0}^T(t_{p_1p_2}(c\ r_i)) \quad {}_i + 2 \quad {}_v^T + E
$$

where the slight noise arising from variation in the crossover location is absorbed into E to preserve the strict equality. In this equation both i and $\frac{T}{v}$ are constants within sets of SXO residuals with a common reference pass. Since they cannot be recovered separately, they may be merged into one offset, h_i say:

$$X_{p_1p_2}(c\ r_i) = d_{t_0}^T(t_{p_1p_2}(c\ r_i))\quad h_i + E \tag{7.3}$$

where

$$h_i = \ _i\quad 2\ \frac{T}{v}$$

Although p_1 was assumed to be an descending pass, repeating these derivations in the case of a descending pass p_1 yields an identical expression for $X_{p_1p_2}(c\ r_i)$ where this time the offset is given by

$$h_i = \ _i + 2\ \frac{T}{v}$$

It is possible to take all the gauge-augmented crossover observations with a common reference pass and estimate the h_i which applies to that set of observations by finding the mean value. This may then be removed from the series. An estimate for each step in the altimetric drift function may then be derived by averaging all the observations at all locations which involve that step. This is not robust if it is the case that there is missing data. For instance, if amongst the observations with a common reference pass, the values that would estimate the lowest values in the drift are missing, solving for and removing h_i for the existing observations in that set would lower the existing observations too far. Such a situation may arise if the tide gauge is not operational for all 130 cycles of TOPEX. To avoid the possibility of this skewing, a least squares solution scheme is developed.

By rearranging Equation 7.3, a suitable observation equation may be constructed:

$$X_{p_1p_2}(c\ r_i)\quad [d_{t_0}^T(t_{p_1p_2}(c\ r_i))\quad h_i] = E$$

The best solution in the least squares sense will minimise $\quad E^2$ over all observations. Since no two observations will involve the same two parameters, this observation equation gives rise to a complicated set of normal equations which must be solved. The derivation of the normal equations in the general case of inter-altimeter calibration is presented later. Therefore a similar derivation is not presented here and the interested reader is directed ahead to Section 8.3.

Since there is no inherent mechanism to constrain the drift function with respect to the offset parameters, a Lagrangian multiplier is employed in the least squares solution to constrain the sum of all the parameters comprising the altimetric drift function to be zero. A singular matrix is therefore avoided.

7.1.2 Data acceptance criteria

The work in the previous chapter involved deriving a core set of tide gauges which are in principle suitable for calibrating any altimeter. An acceptable method here would involve only using observations derived with gauges from that core set. However in the course of deriving this core set of tide gauges, each of the eight individual sets of observations at each gauge has been considered, and quality measures may easily be derived for each of these. This extra knowledge can be further applied to preclude series where the altimeter exhibits extreme deviation from the tide gauge readings. Thus gauges where one or two series are particularly poor but the overall agreement is generally good may be selectively rejected. This phase of quality control acts in addition to the exclusion of observations involving the six gauges already classified as unreliable. To carry out this quality control, the RMS between the gauge and the altimeter is derived for each of the eight series at each gauge. Any location where the RMS difference between the combined altimetry and the gauge series was less than 12 cm was accepted. As the typical statistic here involves only one eighth of the observations that were used to derive the overall RMS and slope for each tide gauge, the noise levels are much higher, and no attempt is made to reject on the basis of any trend in the series. This additional quality control resulted in the exclusion of 11 series, on top of all series associated with gauges 10, 21, 47, 50, 51 and 355.

7.1.3 Data dependence

Consider the eight gauge-augmented crossover sets associated with a particular gauge. At the north crossover for instance, there will be a set of descending passes. Each time the altimeter contributes a value in this series, a short time later it will contribute a value to the descending series at the east crossover. The time taken for the sub-satellite point to travel from the north crossover to the east crossover in any given cycle will be at a maximum of about 80 seconds at the equator. Since the ground-track density increases in the higher latitudes, the time taken for this journey will be much less away from the equator. Since many sources of error in the system will have decorrelation times much longer than a minute or so, the series at these two locations will not be truly independent measures of the altimetric drift. Although it might reasonably be believed, for instance, that errors in the wet tropospheric path delay or the electro-magnetic bias would totally decorrelate between these two close observations, it requires a larger stretch of the imagination to believe that, for instance, secular radial orbit error could be unrelated between the two locations. Of the eight series surrounding a given gauge, correlation due to short time lags will also apply
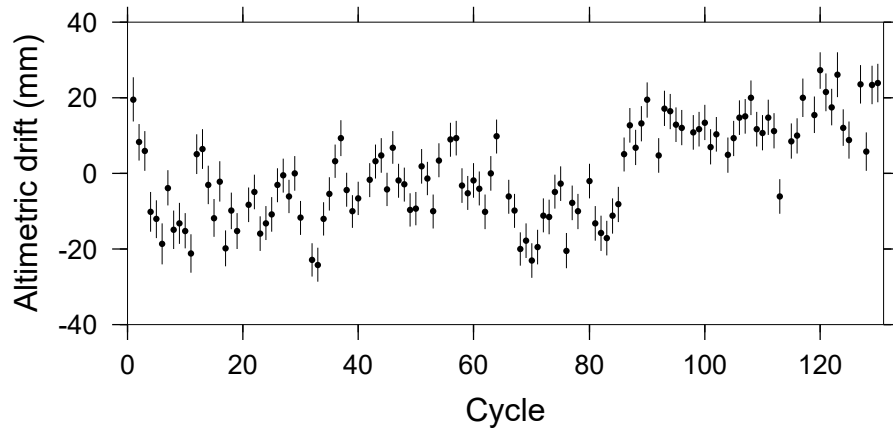
Figure 7.1: The estimated altimetric drift function of the TOPEX altimeter. The bars indicate the standard error of each parameter. The drift shown corresponds to error in the observed sea surface height.

between the north ascending and the west ascending series; the south ascending and the east ascending series; and the south descending and the west descending series.

If not addressed, this dependence will result in standard errors which are underestimates of the full impact of noise on the system and give con dence in the solution which is unduly high. To account for the dependence, the dependent series can be combined before the nal solution is generated. This will yield a maximum of four independent estimates of the drift for each gauge.

The same precaution against biasing the merged series in the case of missing data must be taken when merging two crossover series together. Essentially the same least squares system is used as was derived in Section 7.1.1 for deriving the altimetric drift function, although only two o sets will be recovered as opposed to over 400. Where one of the series to be merged has been rejected, through quality control, the accepted series is taken as the merged series, and no actual merging is carried out.

7.2 Results

The above method of merging dependent gauge-augmented crossover series was applied to all accepted TOPEX data and a nal estimate of the altimetric drift function was derived. The solution for $d^T(t)$ thus obtained is shown in Figure 7.1. The measures taken to use independent estimates of the drift ensure that the error bars are realistic.

Recall from Section 5.2.1 that the drift function expresses changes in the altimetric sea surface over time. The drift estimate in Figure 7.1 suggests that the altimeter is measuring shorter as time goes on. Note that the reference time

to which all values in the Figure are related is arbitrary since the mean value is constrained to be zero. Correction of TOPEX altimetric sea surfaces with this function will in principle remove the effect of altimetric drift but the corrected heights will not conform to the characteristics of the altimeter at any time in particular.

7.2.1 The first eight cycles

Hancock and Hayne (1994) explain how the first eight T/P cycles are affected by many manœuvres, safe-holds, attitude control problems and frequent switches between operation of TOPEX and Poseidon. These lead to reduced accuracy in the altimeter ranges, in the case of the mispointing; and to less reliable orbit heights, since orbit determination is less accurate under extensive manœuvre conditions. Consequently the noise level in observed sea surface heights during this period is significantly higher than later in the mission. This noise would be manifested as errors in the bias drift measured here. Therefore there is no reason for the altimetric bias, as it is defined here, to remain stable during each cycle in this period. Consequently a representative bias value for each cycle is likely to be unrealistic. The much reduced availability of TOPEX data during these eight cycles also compromises the ability to resolve the bias drift accurately during this period. The estimates for the first eight cycles are therefore included for reference only. In fact further investigation of the values in Figure 7.1 reveals that the RMS spread of the eight bias values during this phase is nearly 10 mm, substantially more than the RMS during any other period of eight cycles after this period.

The drift estimates shown in Figure 7.1 show a distinct trend. Up to cycle 65 there appears to be a slight rise, then there is a sudden drop of 10–15 mm. After another approximately 20 cycles the drift jumps up again and continues the previous positive trend at an accelerated rate. A significant range of values are covered, from a minimum of less than -20 mm just after the start to a maximum of nearly 30 mm towards the end of the first 130 cycles. This was surprising when first derived since this implies that the altimeter-observed sea level rate is too positive. If this is the case, any sea level rate derived from TOPEX must be corrected for this drift. Although the shape of the solution does not suggest linearity, a linear regression of the bias estimates was performed giving a trend of 8.6 ± 0.9 mm/yr, if the first eight cycles are excluded. The uncertainty shown is one standard error. This is a very significant drift, implying a large error in the instrument.

Figure 7.2: The estimated altimetric drift function of the TOPEX altimeter after removal of the e ect of the USO algorithm error.

7.2.2 The oscillator algorithm error

The announcement of the bias drift induced by mishandling of the drift in the USO (see Section 4.3.12) came in July 1996, while this work was in progress. The general shape of the drift given in Figure 4.14 has some similarities to the drift measured in Figure 7.1. Indeed, it seems to be the predominant signal in the series.

To test whether the USO algorithm error explains the signal in the altimetric drift that has been measured, the correction for the error can be applied to the drift solution of Figure 7.1. The supplied corrections in Figure 4.14 consist of additive adjustments to the altimeter range. For a given sea surface height, an increase in the altimeter range is manifested as a decrease in the apparent sea surface height. The adjustments suitable for additive correction of the range must therefore be subtracted from the sea surface heights in Figure 7.1 to simulate correction of the altimeter ranges for the USO algorithm error.

Figure 7.2 shows the bias drift solution from Figure 7.1 after removal of the e ect of the USO drift as given in Figure 4.14. An o set is included to give a mean value of zero. Although this shows signi cant residual signal, the linear trend now diminishes. Linear regression of the bias estimates of cycle nine onwards gives a slope of 0.1   0.9 mm/yr which is shown as the solid line on Figure 7.2. Since this is indistinguishable from zero, this implies that after correction of the USO algorithm error, sea level rates observed by the altimeter are *true* sea level change, within the context of this calibration.

The residual signal present in Figure 7.2 is worthy of some investigation. A spectral analysis is performed on the signal, excluding the rst eight cycles, and the resulting harmonic amplitudes shown in Figure 7.3. The largest signals are the bi-annual, annual and a curious peak at 5 cyc/yr corresponding to a
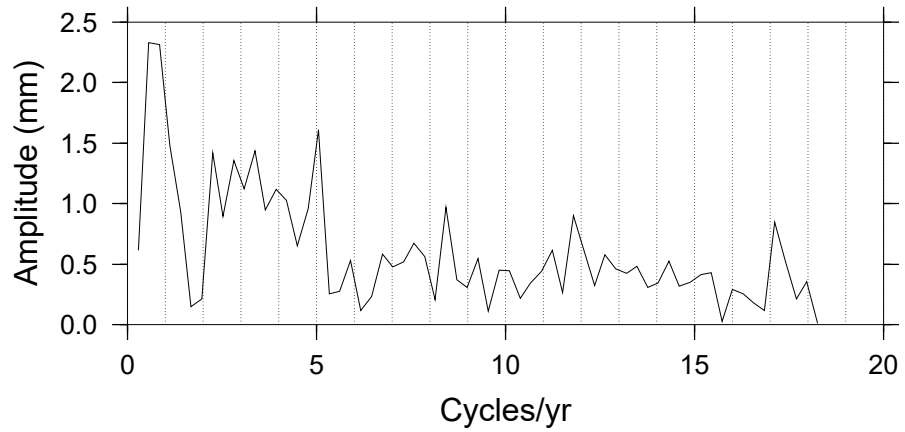
Figure 7.3: Power spectrum of the residual signal in the TOPEX altimetric drift function after removal of the effect of the USO algorithm error.

wavelength of just over 70 days. These demonstrate that the comparison of altimeters and tide gauges is susceptible to errors but comfort can be drawn from the fact that the largest amplitude is only 2.3 mm. Seasonal variability in circulation and freshwater influx for example may well be causing the mean sea surface between the gauges and the altimeter points to be time dependent, especially in the cases of the annual signal. Reassuringly, a local minimum is reached around the six cycles per year point, corresponding to the harmonics removed to account for the resonant orbit error arising from mis-modelling of the M_2 and S_2 tidal constituents. This process will of course remove signals at this wavelength whatever the source. Although it is not anticipated that the altimetric drift will contain cycles of this wavelength, their unintentional removal if they exist would not have a significant impact on the ability of the corrected altimeter to measure sea level change.

7.2.3   The internal calibration

TOPEX has a built-in facility to monitor instrumental sources of range bias drift. Hayne *et al.* (1994) explain this *internal calibration* which has two modes, namely Cal-1 and Cal-2. The former is important for bias drift in that it aims to quantify the effect of changes in the internal path delay of the instrument along with changes in the ability to measure the radar backscatter cross-section of the ocean. Together the two phases last about four minutes and they are usually carried out twice a day. Since it requires suspension of normal range measurements, internal calibration is usually scheduled to take place over land to mitigate loss of ocean data.

Hayne *et al.* (1994) and their regular updates give the correction to the TOPEX altimeter range measurements required to remove the drift measured

141

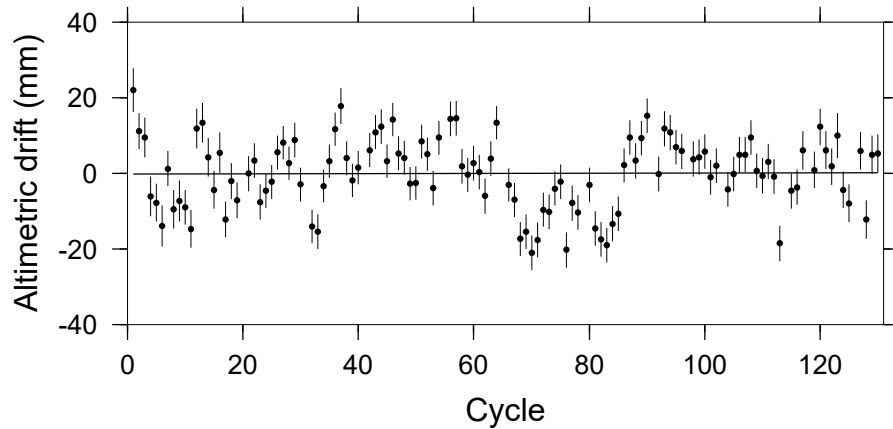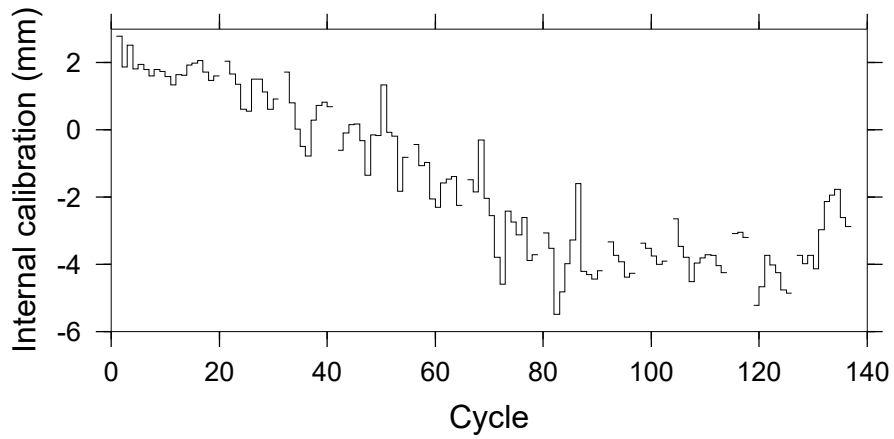Figure 7.4: Corrections to TOPEX range derived from the internal calibration.
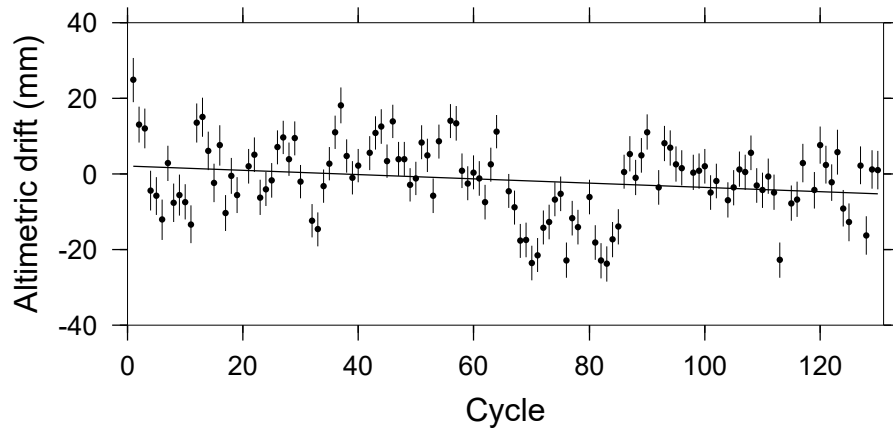
Figure 7.5: The estimated altimetric drift function of the TOPEX altimeter after removal of the e ect of the USO algorithm error and correction for the internal calibration.

by the internal calibration processes. The corrections required are given in Figure 7.4. These are in the same sense as the USO algorithm error correction.

These corrections are not applied to the data records distributed by the agencies involved and they were not applied at any stage in the processing of the data here. The altimetric bias drift estimates derived here should therefore independently measure this instrumental phenomenon. This is tested by removing the values given in Figure 7.4 from the altimetric drift pro le in Figure 7.2. The result of this is shown in Figure 7.5. A regression applied to the drift estimates after cycle eight indicates that a trend is present in the altimetric bias of -2.1   0.9 mm/yr. This trend is shown as the solid line on Figure 7.5.

7.2.4   The Poseidon altimetric bias drift

Although Poseidon did not contribute to the selection of suitable tide gauges, there is no reason why the altimetric drift of this instrument cannot be measured

142
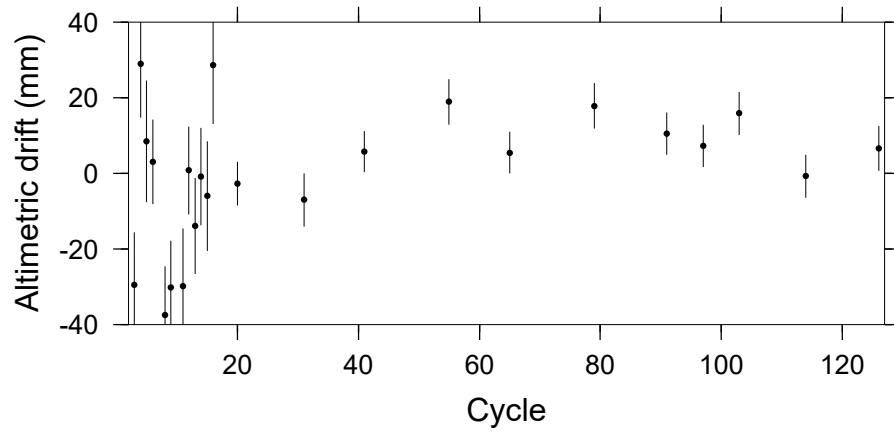
Figure 7.6: The estimated altimetric drift function of the Poseidon altimeter.

Figure 7.7: Number of independent observations contributing to each parameter of the Poseidon altimetric drift function.

in the same way. All available Poseidon data were selected at the same calibration points as for TOPEX and processed in the same way with the same correction applied. Again a reference cycle was chosen and eight altimeter series per gauge generated which were then combined to make four independent estimates of the bias drift per gauge. The gauges accepted as reliable in the TOPEX comparison were adopted in this case. The sparsity of Poseidon data hindered quality control comparisons for individual series. Figure 7.6 shows the solution derived from the combined solution of all these series.

The number of observations making up the solution is much smaller since the Poseidon altimeter is operational only about 10% of the time. Figure 7.7 shows the observations contributing to the drift estimate for each cycle. This can be compared to the contributions to TOPEX given in Figure 7.8. This detracts from the reliability of the solution. In fact the sparsity of data at the start of the mission before cycle 20 suggests that little confidence can be placed in these values, a suggestion which is born out in the solution with large error bars and unreasonable erratic behaviour of the drift during this period.
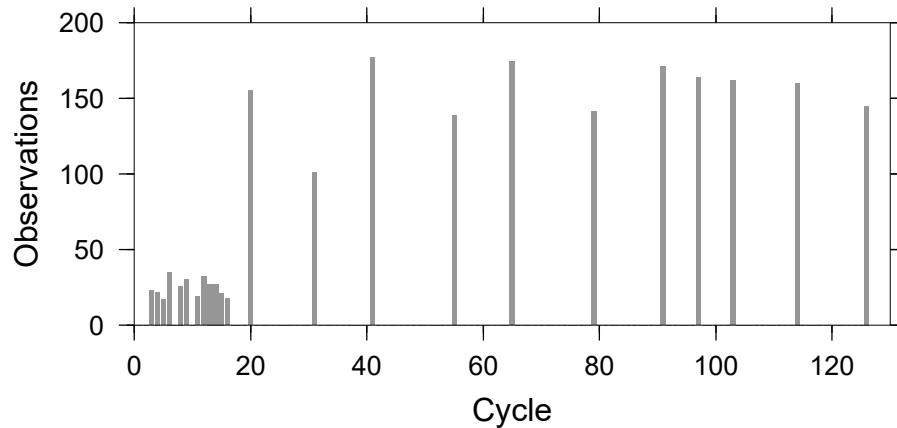
143
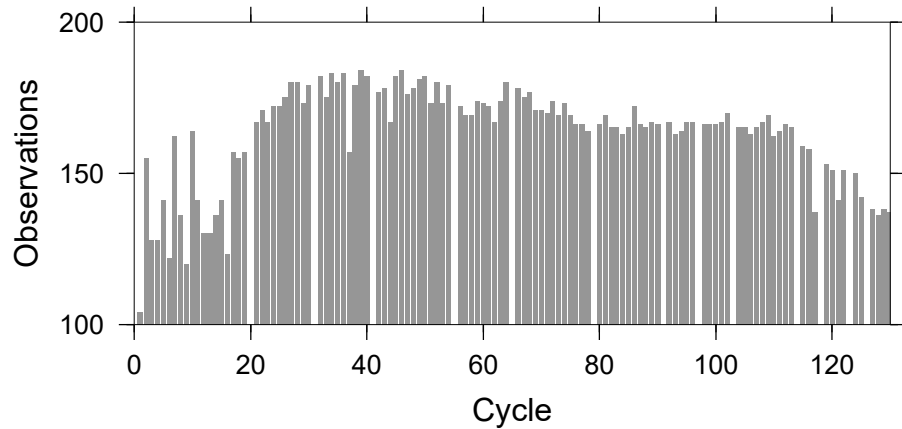
Figure 7.8: Number of independent observations contributing to each parameter of the TOPEX altimetric drift function.

If the cycles with less than 50 observations are ignored and a regression performed on the bias values then an increase in measured sea level, or a decrease in altimetric bias, of 3.0 ± 2.7 mm/yr is obtained. This is surprisingly large, considering that no error similar to the USO algorithm error in TOPEX has been found for Poseidon. The values for cycles 20 and 31 are much lower than those later in the mission. If these are ignored then a regression suggests that the bias is decreasing by -2.4 ± 3.1 mm/yr for this phase. The inconsistency suggests that the low availability of data denies the accurate resolution of the Poseidon altimetric drift.

7.3 Discussion

On first inspection, Figure 7.5 seems to suggest that applying the correction derived from the internal calibration introduces an altimetric drift. One possible interpretation is that the internal calibration is flawed and is measuring a spurious drift. However changes in the internal path delay will certainly change the bias of the instrument, so assuming that these changes are measured correctly by the internal calibration, rejection of the corrections derived from this mode on the basis if these results alone is erroneous. It seems likely that the residual altimetric drift after application of the internal calibration is caused by one of the other sources of drift highlighted in Chapter 6, perhaps from a non-zero total vertical gauge motion.

Mitchum (1997a) suggests that a phenomenon such as instability in the radiometer would lead to an error in the correction for the water content of the troposphere which changes over time. This would in turn induce an altimetric drift. Some such effect could explain the drift seen in Figure 7.5. However, the high water content of the troposphere in the tropics as compared to that in the

144

higher latitudes complicates the issue. This is because there is no reason to assume that this hypothetical instability in the radiometer should be the same for all values of water content. The geographical concentration of gauges in the lower latitudes does not evenly sample the full range of possible values of water content. If this scenario were the case then the altimetric drift derived from this work would be valid only in the tropics. Any relationship between the water vapour content and the instability in the radiometer could be con rmed by analysis of the drift as a function of latitude, however this is hampered in this case by the lack of gauges in the higher latitudes and the concentration of available gauges to within 25 of the equator.

The important implication of the work in this chapter is that e ective quality control of altimeters using an independent reference is critical. Augmenting altimetric sea surface measurements with tide gauge readings has allowed an estimate for the altimetric drift functions of TOPEX and Poseidon to be recovered. Validation of the TOPEX function against the altimetric signal expected to arise from the USO algorithm error suggests that this method is sensitive enough to detect drift and allow suitable corrections to be made. The tide gauges selected to correct the altimeter-observed sea surface heights have performed well, suggesting that they may be suitable for application to other altimeters.

Chapter 8

Inter-altimeter calibration

Having investigated the feasibility of using tide gauges to monitor drift in a single altimeter, attention is now turned to the multi-altimeter case. This involves the linking of more than one altimeter for the purpose of combating the e ect of relative bias, in addition to altimetric drift. Here a method of inter-altimeter calibration is applied to the TOPEX and the ERS 1 instruments. Although there is substantial temporal overlap between the two missions, there is heavy reliance on tide gauge augmented dual satellite crossovers with very long time lags, as would be the case if two disjoint missions were to be inter-calibrated.

8.1   Strategy

ERS 1 and TOPEX are to be inter-calibrated. Whereas the T/P satellite is in a constant orbit and is thus straightforward to handle, the various phases of the ERS 1 mission cause changes in the ground-track pattern. Since RP height measurements will be relied upon to constrain the drift within each altimeter, the ice and geodetic phases of ERS 1 are a complication. They can be treated as separate altimeters and linked by DXOs to TOPEX and other phases within ERS 1. However the sparse ground-track of the ice phase along with its short duration mean that the altimetry in the region of tide gauges is sparse. The geodetic phase on the other hand is spatially dense but its non-repeating nature precludes the use of RP height observations. These phases were excluded to keep the experiment as simple as possible. Therefore the contribution of ERS 1 to this calibration is limited to the rst and second multi-disciplinary phases only.

There is no reason to depart from the method employed in Chapter 7 of using the four enclosing T/P passes at each gauge. To use the same convention with the denser ERS 1 ground-track would not be optimal since the repeat period is 3.5 times as long and several other passes appear within the diamond described by the enclosing T/P ground-track at each gauge. Instead the four ascending and
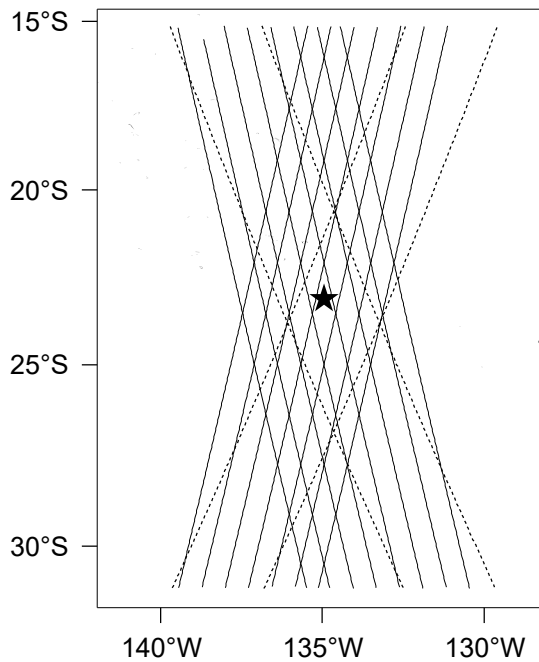
Figure 8.1: The T/P (dashed lines) and ERS 1 (solid lines) ground-tracks in the region of WOCE tide gauge 16 at Rikitea in French Polynesia (star).

four descending passes each side of the gauge are chosen. This choice of ERS 1 passes is based on the desire to include a similar amount of altimetry from each satellite. Consider the ascending passes to the east of a tide gauge for instance. In 35 days, ERS 1 will have described each of the four ground-tracks exactly once. By comparison T/P will have described its one ascending pass either three or four times. This configuration thus ensures that a similar amount of ERS 1 and T/P altimetry is included. Of course the times during which Poseidon is operational will mean that up to 10% of the TOPEX altimetry will not be present. However it is anticipated that the noisier nature of ERS 1 will lead to more rejection of the available data. The favouring of ERS 1 passes counteracts this. A typical configuration is given in Figure 8.1 for gauge 16 at Rikitea.

From the two sources of altimetry, RP heights and DXO measurements can be derived. Each of these are of course augmented with variability corrections from the corresponding tide gauge. The RP heights are used primarily to fix the drift within each altimeter and the DXO measurements are used to fix each altimeter relative to the other and account principally for relative range bias. Again the assumption is that ocean variability is removed by the tide gauge and so changes in the measured sea surface height are due to the altimetric drift.

To generate the RP heights, the altimetry from each pass is interpolated to the latitude of the corresponding tide gauge. This leads to four and 16 series of RP heights for TOPEX and ERS 1 at each gauge respectively. Unlike crossovers, RP heights observe the mean sea level and so each series will contain a constant

o set. This will in general vary for each RP height. The main component of this o set is the geoid height above the reference ellipsoid. The magnitude of this can be several dozens of metres so this quantity must be modelled or the resulting drifts and standard errors will be meaningless. Geographically-correlated orbit error will also appear in the RP heights. However this will be indistinguishable from the o set and will be absorbed into that quantity.

DXO observations will not observe the mean sea surface. However the geographically-correlated orbit error will not be absorbed elsewhere and will appear in the residuals. If not modelled adequately then the variable part of this error will corrupt the solution. The quality of T/P orbits are such that the radial orbit error of ERS 1 will dominate. Since the JGM 3 geopotential model will be used for the T/P orbits it is assumed that the contribution of T/P radial orbit error to the DXO residuals is negligible and dominated by that of ERS 1. While this quantity may be ignored for T/P, to do the same in the case of ERS 1 has the potentially to cause signi cant corruption in the solution, particularly in the relative o set between the altimetric drift solution for each altimeter. The approach used is to assume that for each gauge, the magnitude of the ERS 1 radial orbit error is constant over all DXOs associated with that gauge. In addition, recall from Equations 5.8   5.11 that the xed part of the correlated radial orbit error may not be recovered separately from the di erence between the drift solution for each altimeter, without arti cial constraint. The approximation is made that the radial orbit error at a given gauge is purely the variable contribution of the ERS 1 error. This means that the xed portion will corrupt the o set between the drift solution for each altimeter. Thus this method is based on the assumption that the xed part of the ERS 1 radial orbit error will average to zero over all tide gauges in the solution.

DXOs between an ascending pass and a descending pass are to be included in the solution, since these are the most common type. The inclusion of DXOs between two ascending or two descending passes, which are much less common than the rst type, was also considered. Since this would not increase the number of parameters recoverable from the system it was decided to exclude this second type of DXO from the solution. Although inclusion would yield more observations, this advantage was not deemed to override the resulting additional complexity.

8.2   The altimetric drift functions

As in the intra-altimeter calibration of T/P, the drift of TOPEX is modelled as being constant over each 9.9156 day cycle. The 35 day repeat period of the

multi-disciplinary phases of ERS 1 is a long time over which to assume that the bias is constant as it will not resolve changes which may be significant and have a shorter wavelength. The connection between bias drift steps and orbit cycles must be lost. A 10 day step length seems at first to be a sensible approach. However some *a priori* knowledge of what the drift may be doing would be useful. From Section 4.5.4 it is known that certain anomalies, in particular safe-hold events, are associated with sudden discontinuities in the bias characteristics. A list of dates on which such phenomena occured was available and it was decided to employ these times as a starting point for the altimetric drift step function boundaries. Since several weeks can elapse between consecutive safe-hold events in some cases, the longer ones must be broken down to maintain a reasonable resolution of altimetric drift. An upper limit of 10 days was therefore placed on a single step in the model of the ERS 1 drift and the longer periods were split into several distinct steps not exceeding 10 days in length. A lower limit of five days was allowed for any single step in the model. Where two consecutive safe-hold events occured within five days, the period between them was subsumed into an adjacent segment. The altimetric drift function for ERS 1 was thus split into 125 steps, 74 for the first multi-disciplinary phase and 51 for the second.

8.3   The solution scheme

From the gauge-augmented altimetric observations it is hoped that parameters describing the drift functions may be recovered. In particular $d_{t_0}^T(t)$ and $d_{t_0}^{E\,T}(t)$ for TOPEX and ERS 1 respectively are desired. These are modelled via step functions so in the case of $d_{t_0}^T(t)$ for instance, one parameter per step must be recovered. These parameters are defined here to be

$$d_i^T \quad \text{for} \quad i = 1 \quad P$$

where P is the number of steps in this function, equivalent to the number of TOPEX cycles in the calibration. If r_i is defined to be the time of the ith step then the function is defined as

$$d_{t_0}^T(t) = \begin{array}{ll} d_1^T & \text{if} \quad r_0 \quad t < r_1 \\ d_2^T & \text{if} \quad r_1 \quad t < r_2 \\ \vdots & \\ d_P^T & \text{if} \quad r_{P\,1} \quad t < r_P \end{array}$$

Similarly for $d_{t_0}^{E\,T}(t)$, the parameters are defined to be

$$d_i^E \quad \text{for} \quad i = 1 \quad Q$$

where Q is the number of steps in this function. If s_i is defined to be the time of the ith step then the function is defined as

$$d_{t_0}^{E\ T}(t) = \begin{array}{lll} d_1^E & \text{if} & s_0 \le t < s_1 \\ d_2^E & \text{if} & s_1 \le t < s_2 \\ & \vdots & \\ d_Q^E & \text{if} & s_{P-1} \le t < s_Q \end{array}$$

In addition to the parameters for the drift functions, an offset for each RP location must be recovered. For the TOPEX RPs these are defined to be

$$\beta_i^T \quad \text{for} \quad i = 1 \ldots B$$

where B is the number of TOPEX RP locations. For ERS 1 RPs the offsets are defined to be

$$\beta_i^E \quad \text{for} \quad i = 1 \ldots C$$

where C is the number of ERS 1 RP locations. Finally, terms for the variable part of the geographically-correlated orbit error of ERS 1 at each tide gauge must be recovered. These are defined to be

$$\gamma_i \quad \text{for} \quad i = 1 \ldots G$$

where G is the number of tide gauges.

There are four basic classes of observation from which the bias drift functions, and the other parameters defined above, may be estimated. The first, Φ^1, is the gauge-augmented DXO between TOPEX and ERS 1 where TOPEX contributes an ascending pass and ERS 1 contributes a descending pass. The residual is always calculated here by subtracting the ERS 1 sea surface height from the TOPEX sea surface height. This observation involves a drift parameter for each altimeter, and an orbit error term. The set of all DXO residuals of this type may be partitioned according to which of these parameters each observation is associated with. So Φ_{tegi}^1 is defined to be the ith DXO observation of type Φ^1 which involves the parameters d_t^T, d_e^E and γ_g. The notation N_{teg}^1 is defined as the number of observations involving these three parameters.

It is prudent to introduce some supporting notation at this point. Consider the number of observations of type Φ^1 which involve d_t^T and d_e^E (with no discrimination on the choice of orbit error parameters). This number is given by the expression

$$\sum_{i=1}^{G} N_{tei}^1$$

150

For brevity the notation N^1_{te} is adopted as shorthand for this summation. A similar notation, N^1_t for instance, is adopted to refer to the double summation, which in this case is essentially all observations of type $\cdot^1$ involving the parameter d^T_t. All notations of these forms are taken to be similarly de ned.

Returning to the observation $\cdot^1_{tegi}$, it is apparent from Equation 5.8 that each DXO residual of this type may be related to the corresponding parameters by the observation equation

$$\cdot^1_{tegi} = d^T_t \quad d^E_e + \quad_g + E^1_{tegi} \tag{8.1}$$

where E^1_{tegi} is the noise in this observation. To nd the solution best described by the observations in the least squares sense, the expression

$$I = \sum_{teg}\sum_{i=1}^{N^1_{teg}} [E^1_{tegi}]^2$$

$$= \sum_{teg}\sum_{i=1}^{N^1_{teg}} [\cdot^1_{tegi} \quad (d^T_t \quad d^E_e + \quad_g)]^2 \tag{8.2}$$

must be minimised over all observations of type $\cdot^1$. This is equivalent to nding the stationary point. To this end, partial derivatives of I with respect to each parameter in turn are taken. First, the partial derivative with respect to an arbitrarily picked TOPEX drift parameter, d^T say, is

$$\frac{\partial I}{\partial d^T} = \begin{array}{ll} \sum_{eg}\sum_{i=1}^{N^1_{teg}} 2[\cdot^1_{tegi} \quad (d^T_t \quad d^E_e + \quad_g)] & \text{if} \quad t = \\ 0 & \text{if} \quad t = \end{array}$$

$$= \sum_{eg}\sum_{i=1}^{N^1{}_{eg}} 2[\cdot^1{}_{egi} \quad (d^T \quad d^E_e + \quad_g)]$$

It will become apparent that a factor of 2 is common throughout all normal equations which are to be derived, so it is cancelled henceforth. The expression

$$\frac{\partial I}{\partial d^T} = 0$$

must be satis ed for the stationary point to be found. This yields the normal equation

$$\sum_{eg}\sum_{i=1}^{N^1{}_{eg}} d^T \quad \sum_{eg}\sum_{i=1}^{N^1{}_{eg}} d^E_e + \sum_{eg}\sum_{i=1}^{N^1{}_{eg}} {}_g = \sum_{eg}\sum_{i=1}^{N^1{}_{eg}} {}^1{}_{egi}$$

which may be expressed more succinctly as

$$\sum_{i=1}^{N^1} d^T \quad \sum_{e}\sum_{i=1}^{N^1{}_{e}} d^E_e + \sum_{g}\sum_{i=1}^{N^1{}_{g}} {}_g = \sum_{eg}\sum_{i=1}^{N^1{}_{eg}} {}^1{}_{egi}$$

A normal equation of this form is generated for all $= 1 \quad P$.

The quest for the stationary point in the expression I of Equation 8.2 continues with partial derivatives of the expression with respect to each ERS 1 drift parameter being taken. For an arbitrary parameter d^E this is

$$\frac{\partial I}{\partial d^E} = \begin{cases} \sum_{eg} \sum_{i=1}^{N^1_{teg}} 2[\,{}_{tegi} \quad (d_t^T \quad d_e^E + \quad {}_g)] & \text{if} \quad e = \\ 0 & \text{if} \quad e = \end{cases}$$

$$= \sum_{tg} \sum_{i=1}^{N^1_t{}_g} 2[\,{}_t{}_{gi} \quad (d_t^T \quad d^E + \quad {}_g)]$$

Equating to zero in the same way, this eventually yields the normal equation

$$\sum_t \sum_{i=1}^{N^1_t} d_t^T + \sum_{i=1}^{N^1} d^E \sum_g \sum_{i=1}^{N^1{}_g} {}_g = \sum_{tg} \sum_{i=1}^{N^1_t{}_g} {}_t{}_{gi}$$

for $= 1 \quad Q$ where again the factor of 2 is cancelled.

Finally, the partial derivative of I with respect to an arbitrary orbit error term, say, is

$$\frac{\partial I}{\partial} = \begin{cases} \sum_{te} \sum_{i=1}^{N^1_{teg}} 2[\,{}_{tegi} \quad (d_t^T \quad d_e^E + \quad {}_g)] & \text{if} \quad g = \\ 0 & \text{if} \quad g = \end{cases}$$

$$= \sum_{te} \sum_{i=1}^{N^1_{te}} 2[\,{}_{te}{}_i \quad (d_t^T \quad d_e^E + \quad)]$$

which yields the normal equation

$$\sum_t \sum_{i=1}^{N^1_t} d_t^T \sum_e \sum_{i=1}^{N^1{}_e} d_e^E + \sum_{i=1}^{N^1} = \sum_{te} \sum_{i=1}^{N^1_{te}} {}_{te}{}_i$$

for $= 1 \quad G$.

Now the second basic class of observation, ^{2}, is considered. This is similar to the class ^{1} in that it comprises DXO observations. The difference arises in that ERS 1 contributes the ascending pass and TOPEX contributes the descending pass. Equation 5.9 may be applied to derive the observation equation

$$_{tegi}^2 = d_t^T \quad d_e^E \quad {}_g + E_{tegi}^2$$

with notation analogous to the case of the ^{1}. This is identical to Equation 8.1 apart from the sign of the orbit error term. The derivation may be repeated to yield the normal equations

$$\sum_{i=1}^{N^2} d^T \sum_e \sum_{i=1}^{N^2{}_e} d_e^E \sum_g \sum_{i=1}^{N^2{}_g} {}_g = \sum_{eg} \sum_{i=1}^{N^2_{eg}} {}_{egi}^2$$

152

for $\phi = 1 \ldots P$ and

$$\sum_{t}\sum_{i=1}^{N_t^2} d_t^T + \sum_{i=1}^{N^2} d^E + \sum_{g}\sum_{i=1}^{N^2_g} \phi_g = \sum_{tg}\sum_{i=1}^{N_t^2{}_g} \phi^2_{t\,gi}$$

for $\phi = 1 \ldots Q$ and

$$\sum_{t}\sum_{i=1}^{N_t^2} d_t^T + \sum_{e}\sum_{i=1}^{N^2{}_e} d_e^E + \sum_{i=1}^{N^2} \phi = \sum_{te}\sum_{i=1}^{N^2_{te}} \phi^2_{te\,i}$$

for $\phi = 1 \ldots G$. Again a common factor of 2 has been implicitly cancelled from each of these.

The third basic class of observation is ϕ^3, the TOPEX RP height. An observation of this type involves a TOPEX drift parameter and an offset parameter. Again, these observations may be partitioned according to the parameters they involve. The term ϕ^3_{tki} is defined to be the ith observation of type ϕ^3 which involves the parameters d_t^T and ϕ_k. Using notation reminiscent of the DXO observations, N^3_{tk} is adopted to represent the number of observations of type ϕ^3 involving these two parameters. Equation 5.16 may be employed to relate such observations to the corresponding parameters. This relationship is expressed by the observation equation

$$\phi^3_{tki} = d_t^T + \phi^T_k + E^3_{tki}$$

where E^3_{tki} is the noise in this observation. Again the expression

$$I = \sum_{tk}\sum_{i=1}^{N^3_{tk}} [E^3_{tki}]^2$$

$$= \sum_{tk}\sum_{i=1}^{N^3_{tk}} [\phi^3_{tki} - (d_t^T + \phi^T_k)]^2 \tag{8.3}$$

must be minimised. The partial derivative of this expression with respect to an arbitrary TOPEX drift parameter d^T is

$$\frac{\partial I}{\partial d^T} = \begin{cases} \displaystyle -\sum_{k}\sum_{i=1}^{N^3_{tk}} 2[\phi^3_{tki} - (d_t^T - \phi^T_k)] & \text{if } t = \\ 0 & \text{if } t \neq \end{cases}$$

$$= -\sum_{k}\sum_{i=1}^{N^3{}_k} 2[\phi^3{}_{ki} - (d^T - \phi^T_k)]$$

After elimination of the factor of 2, the normal equation is found to be

$$\sum_{i=1}^{N^3} d^T - \sum_{k}\sum_{i=1}^{N^3{}_k} \phi^T_k = \sum_{k}\sum_{i=1}^{N^3{}_k} \phi^3{}_{ki}$$

153

for $\quad = 1 \quad P$.

The partial derivative of I in Equation 8.3 with respect to the arbitrary o set parameter $\quad^T$ is

$$\frac{\quad I}{\quad^T} = \sum_{t}\sum_{i=1}^{N^3_{tk}} 2[\quad^3_{tki} \quad (d^T_t \quad \quad^T_k)] \qquad \text{if} \quad k =$$

$$0 \qquad\qquad\qquad\qquad \text{if} \quad k =$$

$$= \sum_{t}\sum_{i=1}^{N^3_t} 2[\quad^3_{t\ i} \quad (d^T_t \quad \quad^T)]$$

This yields the normal equation

$$\sum_{t}\sum_{i=1}^{N^3_t} d^T_t \quad \sum_{i=1}^{N^3} \quad^T = \sum_{t}\sum_{i=1}^{N^3_t} \quad^3_{t\ i}$$

for $\quad = 1 \quad B$.

The nal class of observation, $\quad^4$, is related to $\quad^3$, except that it involves ERS 1 RPs. Again Equation 5.16 may be employed to relate an observation $\quad^4_{eki}$ to the parameters d^E_e and $\quad^E_k$. The relationship is

$$\quad^4_{eki} = d^E_e + \quad^E_k + E^4_{eki}$$

with analogous notation. This yields the normal equations

$$\sum_{i=1}^{N^4} d^E \quad \sum_{k}\sum_{i=1}^{N^4_k} \quad^E_k = \sum_{k}\sum_{i=1}^{N^4_k} \quad^4_{ki}$$

for $\quad = 1 \quad Q$ and

$$\sum_{e}\sum_{i=1}^{N^4_e} d^E_e \quad \sum_{i=1}^{N^4} \quad^E = \sum_{e}\sum_{i=1}^{N^4_e} \quad^4_{e\ i}$$

for $\quad = 1 \quad C$.

8.3.1 Weighting of observations

Four sets of normal equations have been derived corresponding to the four types of observation available. To recover all ve sets of parameter in a single process involves a combined solution of the normal equations corresponding to these observation types. Since a common factor of 2 has been eliminated throughout, the normal equations with common parameters may be grouped. If the observations used to estimate the parameters are not weighted in any way then the model will be extremely biased in favour of the DXO observations at the expense of those of the RP type. To illustrate this, consider that at each tide gauge there are

four RP series consisting of up to 149 cycles of TOPEX altimetry. In the case of ERS 1 there are 16 RP series, each containing up to 31 cycles. On average 26 of the 32 possible DXO sets were within range and contained data. Each of these contains up to 4600 DXO observations. So a typical gauge contributes up to 600 TOPEX RP observations, 500 ERS 1 RP observations and 120,000 DXO observations. Clearly the DXOs must be down-weighted if they are not to dominate the solution. ERS 1 altimeter observations are more noisy than those of TOPEX so ERS 1 observations can be down-weighted. By assigning ERS 1 RP observations a weight equal to half that of TOPEX RP observations, the latter are encouraged to slightly modify the ERS 1 drift solution via DXOs, while the converse is discouraged. To have the same impact as ERS 1 RP observations, the weight of DXO observations would have to be $w_E \frac{500}{120000}$ where w_E is the weight assigned to ERS 1 RP observations. However the noisier nature of DXOs along with the significant orbit error component means that RP observations are more trusted. It is preferable to leave the RP observations to solve for the intra-altimeter drift and let the DXOs find the relative bias. Consequently a weight of $w_E \ 10^{-4}$ is assigned to DXO observations.

The normal equations for the combined solution including the weights may now be constructed. For instance, in the case of an arbitrary TOPEX drift parameter. d^T say, the normal equation is

$$
\sum_{i=1}^{N^1} w_D + \sum_{i=1}^{N^2} w_D + \sum_{i=1}^{N^3} w_T \quad d^T
$$

$$
\sum_e \left(\sum_{i=1}^{N^1_e} w_D + \sum_{i=1}^{N^2_e} w_D \right) d^E_e
$$

$$
+ \sum_g \left(\sum_{i=1}^{N^1}{}_g w_D \sum_{i=1}^{N^2}{}_g w_D \right) {}_g + \sum_k \sum_{i=1}^{N^3_k} w_T \quad {}^T_k
$$

$$
= \sum_{eg} \sum_{i=1}^{N^1_{eg}} w_D \ {}^1_{egi} + \sum_{i=1}^{N^2_{eg}} w_D \ {}^2_{egi} + \sum_k \sum_{i=1}^{N^3_k} w_T \ {}^3_{ki}
$$

for $= 1 \quad P$ where w_D, w_T and w_E are the weights assigned to the DXO observations, the TOPEX RP observations and the ERS 1 RP observations respectively. The other ve sets of normal equations may be similarly constructed.

8.3.2 Implementation issues

Inspection of the normal equation sets reveals that implementation of the system in the form of a numerical matrix inversion problem will result in a symmetric matrix. The numerical solution may thus be derived significantly faster by

employing an algorithm optimised for such a symmetric matrix. This is important bearing in mind that there are over 1300 parameters to be recovered. The Cholesky factorisation method is such an algorithm and was adopted in this case, leading to substantial time savings over general matrix inversion algorithms. It was important to take the extra time required to invert the matrix rather than simply solve by back-substitution, so that the covariance matrix could be obtained for estimation of the standard errors associated with the parameters.

8.3.3 Further constraint

The drift estimator as defined here cannot be recovered without further constraint. This is due to the fact that the two sets of offset parameters, δ_i^T and δ_j^E, can be recovered relative to each other but there is no mechanism to restrict them within any absolute frame. To overcome this, one of the drift parameters must be constrained. In this case the first available TOPEX drift parameter, that corresponding to cycle seven, was constrained to be zero. Thus a singular matrix was avoided.

8.4 Method

When this work commenced the version 3 GDRs of T/P altimetry were available up to cycle 171. Although cycles 1–6 were not readily available in this format it was decided to use this altimetry as it is the most accurate available. In any case the missing first six cycles constitute most of the unreliable initial eight cycles (see Section 7.2.1). The JGM 3 geopotential model is used to generate the ephemerides in this dataset, so the geographically-correlated radial orbit errors can be expected to be very low. This dataset has the effect of the USO algorithm error removed (see Section 4.3.12) and the altimetry is modified to reflect the internal calibration (see Section 7.2.3). All available TOPEX altimetry is extracted in the region of each gauge for the four passes corresponding to that gauge. Only TOPEX data are selected since Poseidon has been shown to be too sparse for reliable comparison. Of the 165 cycles, 16 are devoted to Poseidon cycles leaving 149 TOPEX cycles in this calibration. TOPEX altimetry is corrected for the same phenomena as in the intra-altimeter calibration.

All 18 cycles of the first multi-disciplinary phase of ERS 1 were available along with the first 13 cycles of the second multi-disciplinary phase. Altimetry for the earlier phase is available in the form of version 3.0 OPRs. However an updated data production method had been achieved in time for the second multi-disciplinary phase and altimetry from this phase is only available in the form of newer version 6.0 OPRs, which is the current standard for ERS 2 altimetry.

Re-processing of the earlier phases with the version 6.0 OPR method has not been done and is not likely to be carried out by the agencies responsible for dissemination of data. This leaves the reliability of the unification of altimetry from the two phases open to question since modification of algorithms used to generate ranges and geophysical corrections can also change the altimetric bias. This does not preclude the inclusion of both multi-disciplinary phases in this experiment. In fact it is a valuable validation of the two datasets, allowing any inherent difference between them to be quantified. Altimetry from the eight chosen ERS 1 passes at each gauge were taken from the OPRs with the same standard corrections applied in the case of TOPEX.

The radial orbit heights appearing on the ERS 1 OPRs were replaced with those calculated at the Delft University of Technology (DUT). These are precise orbits calculated using the Delft Gravity Model 4 (DGM 4), a refinement of JGM 3, converged using observations from tracking systems, crossover residuals and altimeter heights. The accuracy of these orbits is expected to be significantly superior to that of the OPR orbits.

Again tide gauges from the WOCE fast release dataset are used. As a starting point those considered reliable in Chapter 6 are included. In particular gauges 10 and 21 are excluded since they have been shown to exhibit a significant trend in comparison with altimetry. The four gauges considered unreliable on the basis of excessive noise in the comparisons with the altimetry are not precluded here. If the source of noise were in the altimetry rather than the tide gauge time series then the newer version GDRs may prove to be more reliable. Therefore 51 gauges are adopted, comprising the 53 originally considered with 10 and 21 excluded. This will be qualified by quality control of the altimetry series to check for instability not detected in the earlier work.

The area of interest must somehow be restricted to prevent DXOs being taken at excessive distance from the gauge. This is achieved simply by masking all altimeter observations at latitudes more than 8 different from the latitude of the appropriate tide gauge.

8.4.1   An algorithm for repeat pass heights

RP heights may be derived for each appropriate pass of each altimeter. This is achieved by interpolating the sea surface heights of that pass to the same latitude as the tide gauge. This is chosen in preference to interpolation to the point of closest approach since variability is likely to be more correlated meridionally than zonally (Mitchum, 1994). Four altimetry values each side of the required latitude were taken and interpolated with a low order polynomial. The pass was rejected if the time spanned by the eight observations exceeded 20 s or if less than eight

altimetry points were available. In this way a time series of sea surface heights was derived for each analytical pass of each altimeter.

8.4.2   Dual satellite crossovers

DXOs were generated at each gauge using all possible pairs of T/P and ERS 1 passes. These are split into sets comprising all the DXOs at a given analytical DXO location. In principle 32 DXO sets are expected at each gauge since the two ascending T/P passes will generate a DXO set with each of the descending ERS 1 passes and vice-versa. In practice the number of DXO sets at a gauge is less than this since some of the analytical DXO locations will lie too far from the gauge and out of the area of interest.

The same crossover determination algorithm as had been employed for single satellite crossovers in the intra-altimeter calibration case was used. For consistency with the solution scheme developed above, all DXOs were generated by subtracting the ERS 1 sea surface height from the TOPEX sea surface height.

8.4.3   Additional quality control

RP heights were subject to checks for suspicious behaviour. Only those TOPEX series where data were present for at least 100 of the possible 149 cycles were accepted. The slope of the series after augmentation with gauge data was calculated for each series. It was noticed in the case of TOPEX that some of the series exhibited extremely steep slopes of the order of 10 cm/yr. On inspection this was found to be due to anomalous data at the start or the end of the mission. In particular gauge 35 at San Felix exhibited this behaviour in that the difference between the gauge and the altimeter sea surfaces deviated by over a metre from the mean for that series. This phenomenon appeared in all four TOPEX series at that gauge suggesting that the gauge was at fault. A more robust method for determining the slope was devised to overcome the effect of this sort of problem.

For each set of RP heights at a given location, an initial estimate of the mean sea surface was derived by calculating the mean height after exclusion of the outer quartiles. This estimate was then used to reject any values in the full dataset for that series which deviated by more than 15 cm from this mean sea surface estimate. A linear regression was performed on the accepted values to estimate the trend between the altimeter and the gauge.

The mean trend for all TOPEX RP series was found to be -0.47 cm/yr. This was subtracted from the trend for each series and any which then had a trend greater than 2.0 cm in magnitude were rejected. This resulted in the loss of only six series. In fact all four of the series at the San Felix gauge were rejected
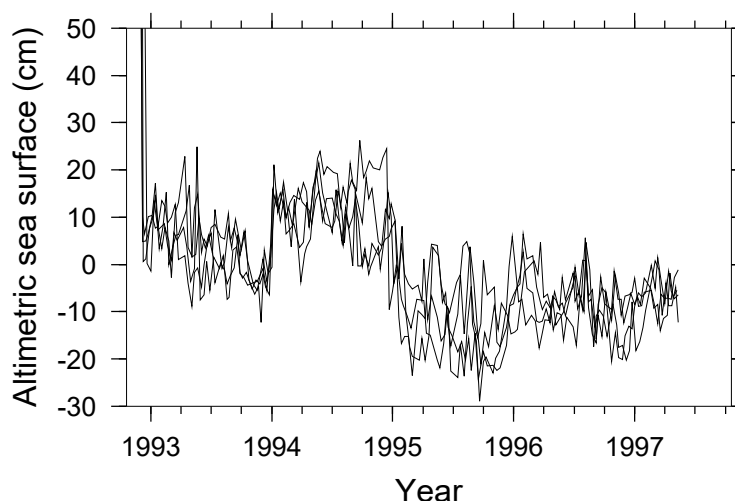
Figure 8.2: Gauge-augmented altimetric sea surface heights for the four RP series at gauge 35 (San Felix).

by this method suggesting that, in addition to the highly spurious values at the start, there is also significant cause for concern throughout the period of interest. The gauge-augmented sea surface heights for the four RP locations are given in Figure 8.2. This shows that the disagreement between the gauge and the altimeter may be partly due to a bi-annual signal amongst other things. The origin of this signal is open to debate. As a precaution, all observations involving this gauge were excluded from the calibration, leaving a total of 50 gauges. This gauge was not rejected from the earlier calibration work because not enough data after the sudden jump in early 1995 were included to affect the quality statistics significantly.

It is difficult to perform a similar quality control on the ERS 1 RP series since each typically has far fewer cycles of data than the T/P case. An attempt was made nevertheless. For a RP series, at least 20 of the possible 31 cycles had to be present for that series to be included. This time a mask of 20 cm was used to reject values with a large RMS variation from the initial mean sea surface estimate. This was not an easy choice to make and in the end became a compromise between minimising the data lost and insulating the system from bad observations. The mean slope over all ERS 1 RP series was calculated to be +1.89 cm/yr. However the small amounts of data involved in each series meant that no satisfactory rejection on the basis of slope could be performed. Nine series were lost through the rejection of series exhibiting substantial noise.

Despite this quality control some of the accepted series still exhibit significant noise. Therefore when fitting the observations to the model, it is prudent to apply a rejection filter where observations which vary excessively from the expected value are excluded. A naive approach to this, where all RP series are treated
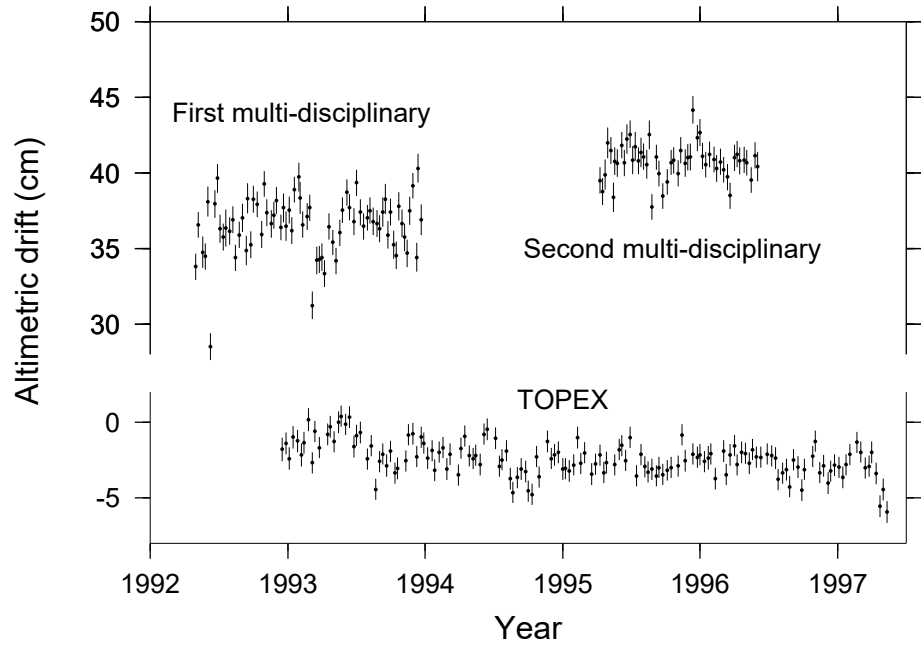
159

Figure 8.3: The combined altimetric drift solution for ERS 1 and TOPEX derived from the inter-altimeter calibration. Note the discontinuity in the vertical scale.

in isolation, risks biasing the model when data are missing and the trend is signi cant. This is a particular risk in the case of the break between the two multi-disciplinary phases of ERS 1 where the jump may be signi cant. The introduction of *a priori* information into the model in the form of an initial guess at the altimetric drift function of each altimeter, along with estimates of the mean sea surface o set for each RP series, avoids the risk of such skewing. This involves using the output of the model as input for a re nement and the system thus becomes iterative. To prime the model, the mean sea surface estimates calculated in the quality control phase were adopted for the initial iteration and each drift function was assumed to be the zero function.

8.5 The drift solution

Data tting was performed iteratively with the o sets, drift and ERS 1 orbit error output from one iteration being used as the input to the next. This was repeated until convergence was achieved. The converged solution contained 550639 DXOs, 20194 ERS 1 RPs and 19198 TOPEX RPs.

Figure 8.3 shows the solution for the altimetric drift functions of TOPEX and ERS 1 after convergence. These are the two functions $d_{t_0}^T(t)$ and $d_{t_0}^{E\,T}(t)$ where t_0 is the seventh cycle of TOPEX. In particular the solution must de nitely not be interpreted as absolute bias, although this is tempting since the absolute bias of TOPEX in the version 3 GDRs is anticipated to be around zero.
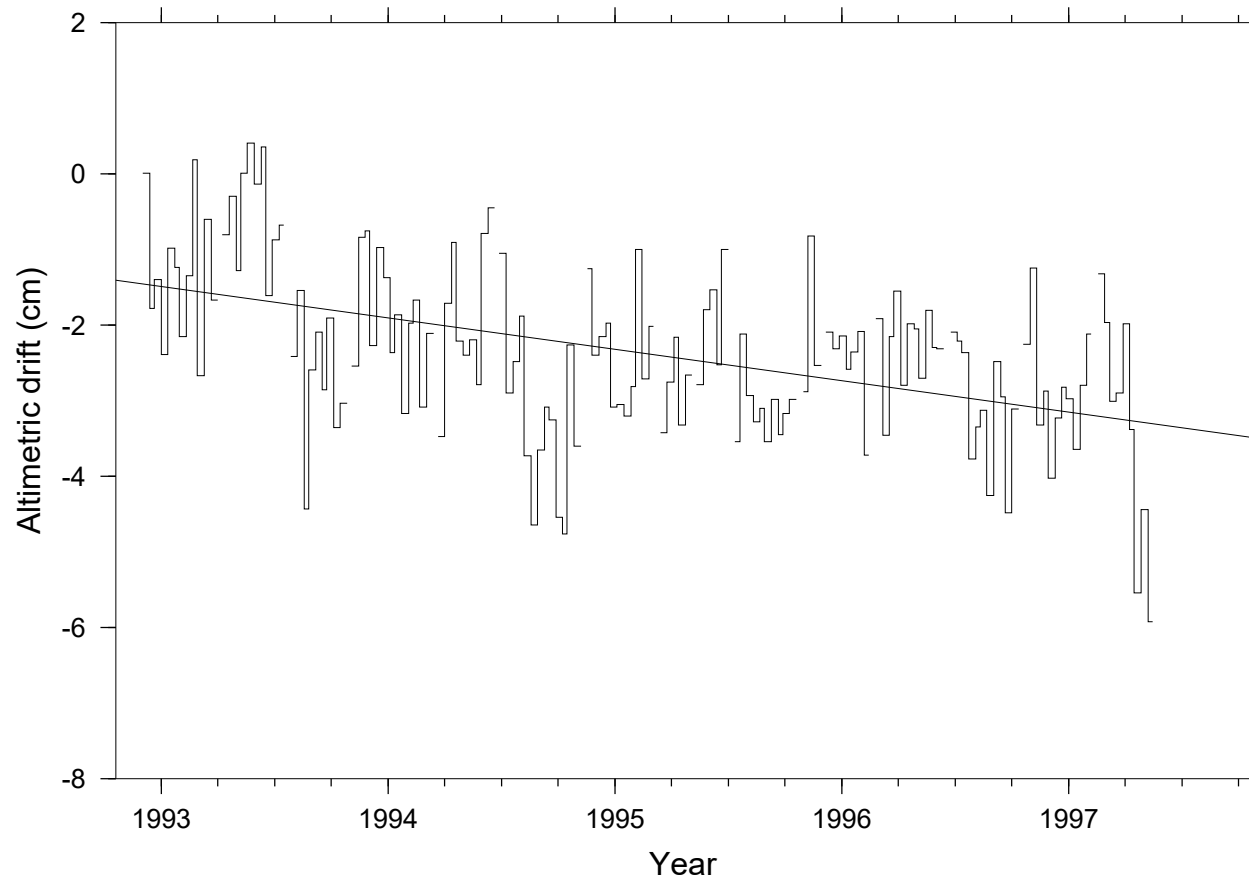
Figure 8.4: The estimated altimetric drift function of TOPEX as derived from the inter-altimeter calibration. The continuous line shows the best fit regression.

Figure 8.5: The estimated altimetric drift of the ﬁrst multi-disciplinary phase of ERS 1 as derived from the inter-altimeter calibration. The continuous line shows the best ﬁt regression and the light vertical lines indicate the safe-hold events.
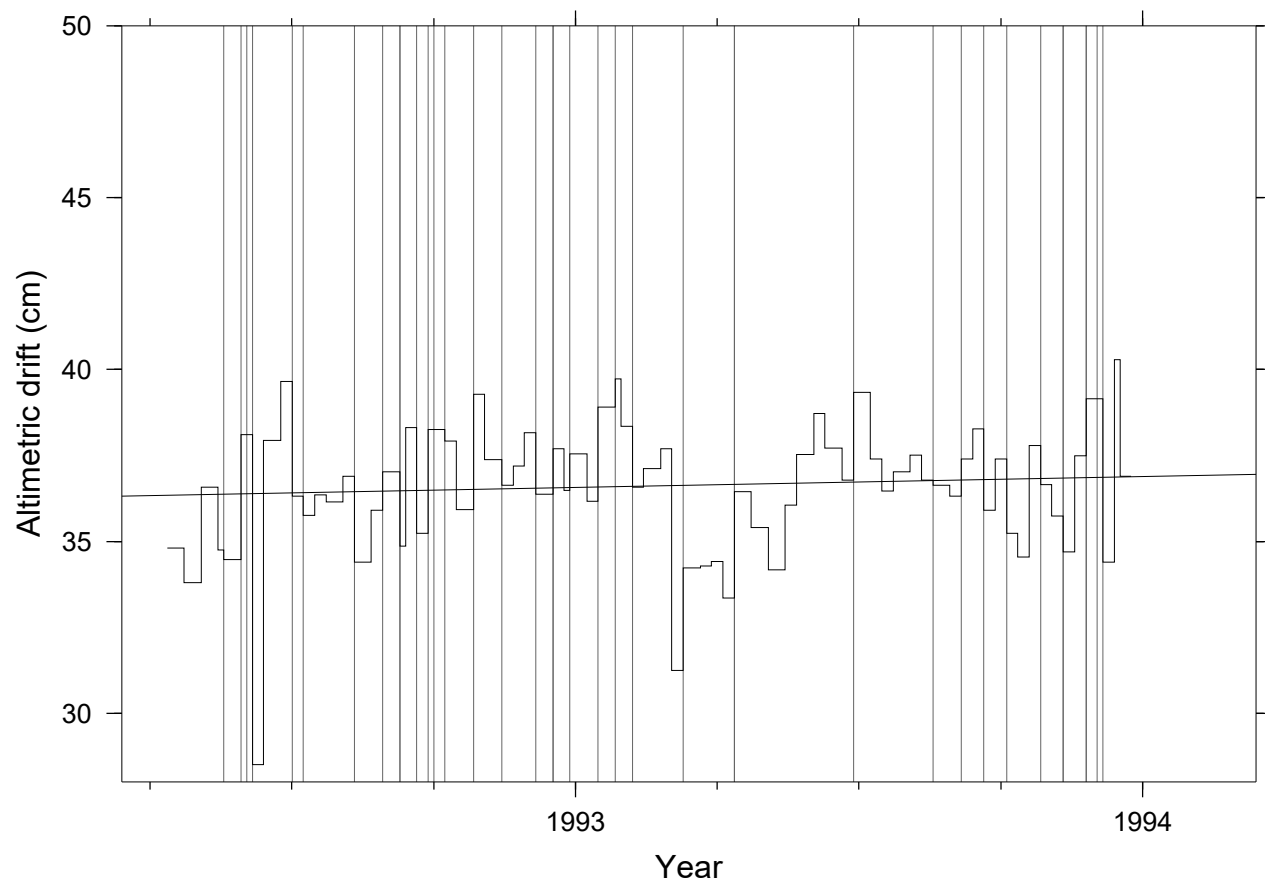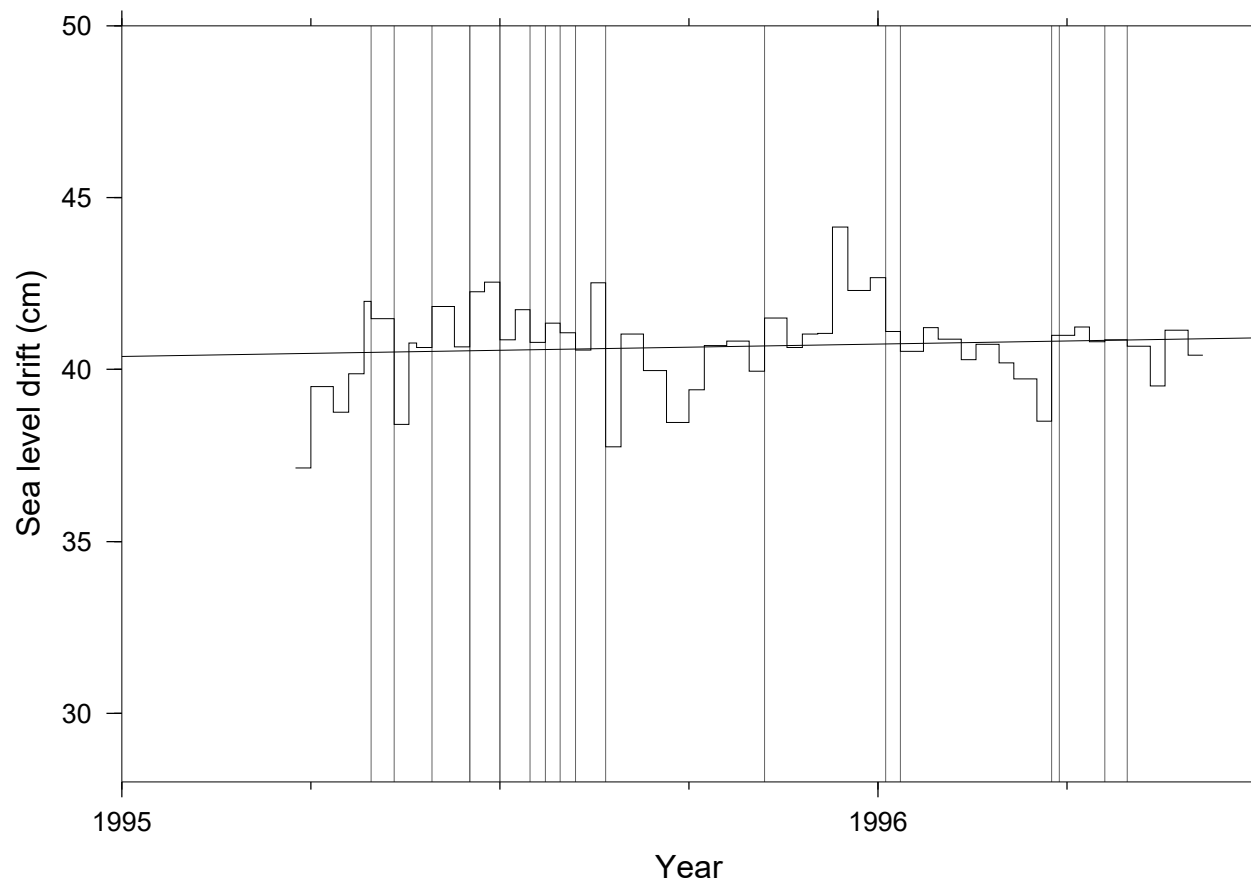
Figure 8.6: The estimated altimetric drift of the second multi-disciplinary phase of ERS 1 as derived from the inter-altimeter calibration. The continuous line shows the best t regression and the light vertical lines indicate the safe-hold events.

On inspection, the solution for TOPEX appears to exhibit a distinct drift corresponding to an increase in range bias over time. A drift of this magnitude is not apparent in the ERS 1 series. However there is an anomaly in the rst multi-disciplinary phase. The parameter centred on 11 June 1992 suggests that the altimetric sea surface deviates by about 8 cm from the mean for that phase. This is unlikely to have instrumental origin, especially since this segment does not coincide with expected bias jumps. This low parameter is one of three which occur between two safe-hold events. The other two parameters are actually higher than the average, suggesting that this is not an instrumental e ect. The principal suspect for causing this is a man uvre associated with orbit maintenance. However it was found that no man uvre was recorded to coincided with this parameter, or indeed occured within 10 days of it. The origin of the anomaly remains unknown and since the parameter corresponds to only eight days it is excluded from the following analyses.

The mean altimetric sea surfaces were calculated from the values in Figure 8.3 and found to be -2.38 1.13 cm, 36.62 1.68 cm and 40.67 1.27 for TOPEX, and for the rst and second multi-disciplinary phases of ERS 1 respectively. The uncertainties shown are one standard error. The derived average relative bias between TOPEX and ERS 1 is therefore +39.00 2.02 cm and +43.05 2.89 cm for the rst and second multi-disciplinary phases respectively. The relative bias is expressed here in the sense of the range bias of ERS 1 subtracted from that of TOPEX. The relative bias between the rst and the second multi-disciplinary phases of ERS 1 is thus estimated to be +4.05 4.44 cm in the sense that the range bias for the rst phase is less negative than that for the second.

Figure 8.4 shows the detail of the drift in TOPEX along with a linear regression of the solution. The observed slope is -0.42 0.06 cm/yr although exclusion of the rst 20 cycles will approximately halve the slope. Recall that the TOPEX altimetry has been corrected for the internal calibration so this drift cannot be attributed to that source. This result suggests that the altimeter is observing a spurious drop in sea level.

Detail of the drift solution for the rst multi-disciplinary phase of ERS 1 is given in Figure 8.5 with vertical lines marking the times of the safe-hold events. It is hoped that the most dramatic changes in the bias will coincide with the safe-hold events and that the variation for multiple parameters between two such events is minimal, showing a trend rather than erratic behaviour. This is born out by the results only to a limited extent. The two long segments during the summer of 1993 do not exhibit such ideal behaviour and the extensive movement in the drift is probably attributable to noise. However there is a segment in the late summer of 1992 with four parameters in good agreement showing a

gradual increase. At the time of the safe-hold event the drift drops by over 1.5 cm. Note that the model contains no mechanism to constrain the parameters between consecutive safe-hold events. Other examples can be found in this phase and the second multi-disciplinary phase of similar significant jumps coinciding to anticipated bias jumps, suggesting that the safe-hold events are indeed significant. This can be crudely quantified by calculating the mean magnitude of bias jump at times of safe-hold events, and the corresponding mean of jumps at other times. This was carried out using the solution from both phases and it was found that the mean magnitude of bias jump was 1.7 cm and 1.3 cm for safe-hold events and all other times respectively. This again suggests that the safe-hold events have a significant impact on altimetric drift.

If the anomalous parameter in June 1992 is excluded, regression suggests that the altimeter has a drift indistinguishable from zero at 0.32   0.40 cm/yr.

Detail of the drift in the second multi-disciplinary phase is given in Figure 8.6. In this case a slight drift of 0.35   0.51 cm is detected, again indistinguishable from zero. There appears to be less erratic behaviour here than in the case of the first multi-disciplinary phase, a factor which may be linked to the lower density of safe-hold events.

8.6   Discussion of the drift solution

This work has yielded estimates of the altimetric drift functions for the two altimeters. It is difficult to validate these results however, since the whole method is dependent upon the reliability of the tide gauges. A recent study by Mitchum (1997b) of TOPEX in isolation, also utilises the WOCE tide gauges and concludes that the altimetric drift function of TOPEX has a slope of -0.28 cm/yr after correction for the internal calibration. He identifies the principal suspect of the source of the drift to be the radiometer although it is unlikely to explain the whole drift. Although the drift derived by Mitchum (1997b) and the inter-altimeter calibration described in this chapter agree within 1.5 mm/yr, this difference is significant in terms of the standard errors, but the reason for the difference is unknown. One candidate is the concentration of high altimetric drift values at the start of the TOPEX mission. Up to mid-1993 the drift parameters exhibit behaviour out of character with the later parts of the mission. This is certainly having a dramatic effect of the regression of the function. If only parameters after the apparent discontinuity at cycle 32 are included in the regression the trend is found to be only -0.23   0.08 cm/yr. The method is therefore very sensitive to anomalies at the extremes.

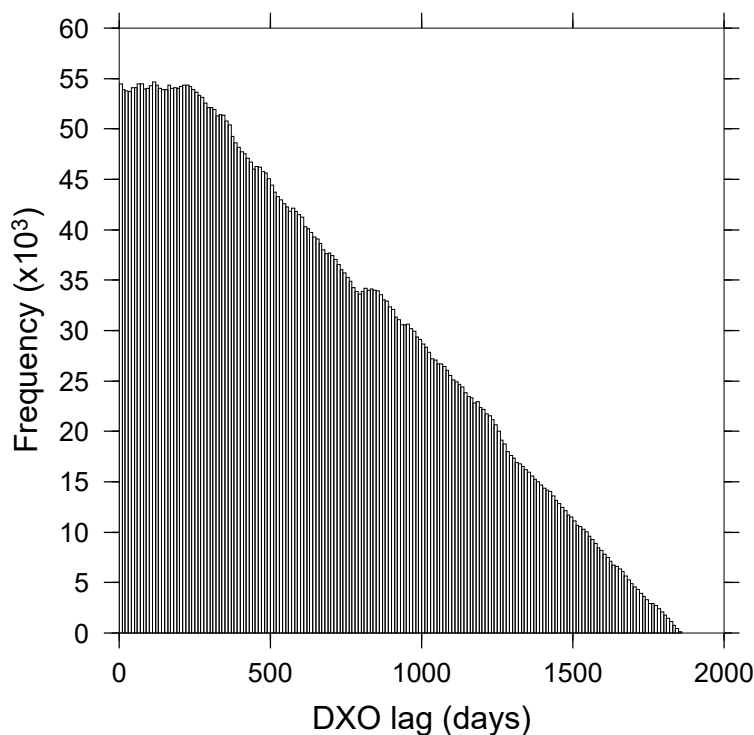The relative biases derived here may be compared with those derived from

Figure 8.7: Histogram showing the distribution of time lags of observations which contribute to DXOs in the solution.

the absolute calibration in Chapter 4. The relative bias between the two multi-disciplinary phases of ERS 1 as derived from the absolute calibration is +1.8 10.3 cm. This has the same sign as the di erence measured here but di ers dramatically in magnitude, although strictly there is agreement within the standard errors. There may be valid reasons for this di erence since, for instance, the DUT orbits have been used in this later calibration.

In the case of TOPEX however, the relative biases with the rst and second multi-disciplinary phases are +37.3 cm and +39.0 cm respectively when calculated from the absolute biases in Chapter 4. Although again these agree with the later work to within the error bars, the disagreement is disappointing and may have its origin in inherent di erences between the two versions of GDR used in the two experiments.

If di erent altimeters are to be linked reliably using this method then the DXO observations are a central issue. The use of gauge-augmented RP observations has been successful at resolving the USO drift in TOPEX and there seems no reason to doubt the reliability of the extension to gauge-augmented crossovers. Figure 8.7 shows the distribution of time lags between the two observation comprising each DXO in the solution. The heavy reliance on crossovers with a lag of the order of several years is signi cant in that altimeter missions with no overlap may in principle be calibrated with a similar method.
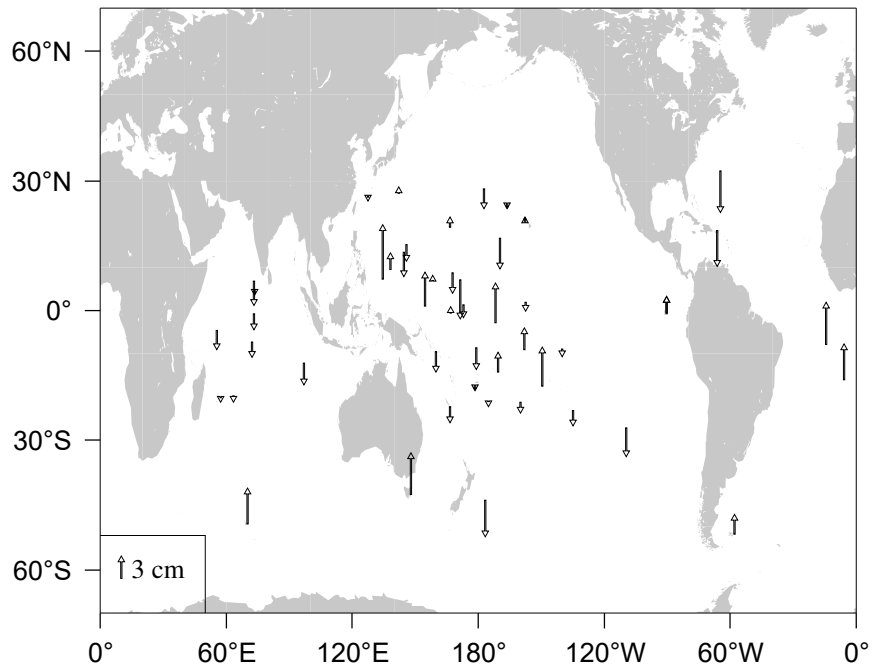
Figure 8.8: The estimated variable portion of the radial orbit error of ERS 1.

8.6.1 Radial orbit error revisited

The issue of radial orbit error is critical to the inter-calibration of altimeters. Despite the high quality of the orbits generated at DUT, there is still significant residual orbit error. The variable part of this which is part of the drift solution above is shown in Figure 8.8. Unfortunately no independent assessment of the radial error in multi-disciplinary orbit of ERS with respect to the DGM 4 gravity model is available. However this result may be assessed using the knowledge that this quantity typically has a long spatial wavelength. The values should therefore be reasonably correlated for gauges in similar geographical locations. Although the values in the Western Pacific to the East of the Philippines seem to be in transgression of this behaviour, the rest of the gauges are better behaved. In particular the values in the Indian Ocean exhibit remarkable conformity. Although the sample is smaller, the four gauges of the Atlantic Ocean are geographically-correlated. As would be expected, the derived values of radial orbit error are found to be identical at the two gauges on the Galapagos Islands (3 at Baltra and 30 at Santa Cruz), which are 35 km apart and rely on the same passes of both satellites.

Unfortunately this is not the end of the story as far as radial orbit error is concerned. This work has only concerned the part of this error which varies between the ascending and descending pass at a given location. The mean part is not resolvable with this method since it cannot be separated from the relative bias in the DXOs at each gauge. The effect of this is that the relative bias

will contain the xed radial orbit error averaged over all gauges. It would be convenient to assume that this average over all 50 gauges in the solution will be zero. The gauges are certainly not uniformly distributed but the coverage is fairly reasonable within the lower latitudes. Although there is no reason to assume that the average xed radial orbit error is zero, if the situation arose where a gap existed between two altimetric missions then this is probably the best method available to link them.

8.6.2   Geosat Follow-On

The problem of geographically-correlated radial orbit error does not arise when two satellites with the same ground-track pattern are compared. This is precisely the situation which will exist when Geosat Follow-On is launched. Since it will describe the same ground-track of the Exact Repeat Mission of the original Geosat, gauge-augmented repeat pass heights may be used to inter-calibrate the platforms without the uncertainty arising from the correlated orbit error. This is an exciting prospect since the altimetric series may be extended back over the gap between the failure of Geosat and the launch of ERS 1, adding several more years of data to the merged altimetric set.

Chapter 9

Conclusions

Modern climate models are sought to explain more accurately the mechanism of the prevailing rise in sea level, along with the origin of the acceleration in the rate experienced over the last couple of centuries. The bene t to these models of more extensive and precise observational data has been demonstrated. The objective is a set of re ned models able to describe the interactions between the various components of the global climate and weather systems, along with the response to forcing of anthropogenic origin or otherwise. There is a compelling body of evidence to suggest that there will be adverse climate change as a result of industrialisation. However, as long as doubts exist, it is hard to design rational responses to future threat scenarios.

Global sea level change is one facet of climate which is used to ne-tune, and may be predicted by, models of climate dynamics. The importance of sea level response to forcing by climate change cannot be overstated. It is the author s opinion that the continued monitoring of sea level to a high resolution and accuracy should be a high priority. This is an area in which satellite altimetry may be usefully employed. With the length of altimetric record growing continuously, more accurate estimates of sea level dynamics become a reality. Along with this opportunity comes a caution. It has been clear from the work detailed here that there exist various hurdles to the optimum exploitation of the full altimetric dataset. If these are overcome then altimetry may have an unprecedented impact in the eld of climate studies. This forms the motivation which lies behind the work presented in this thesis.

9.1   Review of main results

The absolute range bias of each altimeter has been shown to be one major hurdle which prevents immediate blending of altimetry from distinct altimeters. In Chapter 4 a technique which utilises existing instrumentation to measure this bias

has been successfully applied to several altimeters. This technique is based on independent estimates of the sea surface height which are derived initially using data from the tide gauge at Newhaven. These are corrected for sea surface topography differences between the tide gauge and the sub-satellite point by using models for the geoid, ocean tide and, where appropriate, storm surge. By comparison of this independent sea surface height with the same quantity as observed by the altimeter, the range bias is inferred. The effect of radial orbit error in the resulting bias estimates is reduced by using tracking data from the satellite laser ranger at Herstmonceux. This method has been applied successfully to TOPEX, where the range bias for the altimetry in the version 2 GDRs was estimated to be -14.7 cm. The bias of Poseidon was estimated to be 2.2 cm. In the case of ERS 1 a value of -39.3 cm for the bias of the first multi-disciplinary phase was recovered. During the post-launch calibration of ERS 2, the bias of this new satellite was estimated to be -37.9 cm while ERS 1 during the same period exhibited a bias of -41.0 cm. These results have generally been in good agreement with the values as derived using other methods. This in-situ calibration method has the potential to be applied as an independent check of the calibrations carried out using more established specialised techniques, at a fraction of the cost.

Apart from the absolute value of the range bias, the stability of this characteristic has been shown to be another hurdle to the accurate monitoring of sea level rise. The importance of monitoring any such instability has been clearly demonstrated and to that end, a theory of gauge-augmented satellite altimeter measurements has been developed in Chapter 5. This essentially provides the tools required for all types of altimeter measurement and altimeter difference measurement to be combined with tide gauge measurements. In this way, any altimeter measurements in the vicinity of a tide gauge may be corrected for long-term sea surface variability errors. Once corrected, any signal remaining in the altimeter measurements can be assumed to have altimetric origin.

The theory of gauge-augmented satellite measurements has particular application to the calibration for altimetric drift. This creates a demand for a set of tide gauges with time series which are representative of the variability in the surrounding ocean. Such a set has been derived in Chapter 6 by assessing the tide gauges of the WOCE. Of the 53 island WOCE gauges away from continental land mass which have been considered here, it is concluded that those at Rabaul and Juan Fernandez are unsuitable for altimetric calibration owing to significant vertical instability. Further, the gauges at Chichijima, Midway Island, Wake Island, Naha and San Felix have been shown to be unreliable in some circumstances.

The reliable tide gauges have been used to derive a set of gauge-augmented altimeter measurements for TOPEX in Chapter 7. The tools developed in Chapter

5 have been applied to these measurements allowing an estimate for the drift in the altimeter to be recovered. Analysis of this drift has revealed that the method is sensitive enough to detect the drift in the range bias of TOPEX arising from an error in the algorithm used to correct for instability in the ultra stable oscillator. In addition to standing as a proof of the concept of gauge-augmented altimeter measurements, this is testament to the importance of monitoring stability of altimeters and to the suitability of tide gauges in achieving this. Re-analysis of the observations after removal of the effect of the algorithm error indicates that the instrument underestimates the true extent of sea level rise by about 2 mm/yr if the internal calibration corrections are applied.

Finally, the principle of gauge-augmented altimeter observations have been applied in the development of a method of inter-altimeter calibration. This has been tested by application to the TOPEX and ERS 1 altimeters. This time gauge-augmented dual satellite crossovers allow the recovery of the relative offset between the altimetric sea surfaces of each altimeter while repeat pass measurements resolve the altimetric drift within each altimeter. The conclusion reached is that the characteristics of ERS 1 change between the version 3.0 ocean products of the first multi-disciplinary phase and the version 6.0 ocean products of the second multi-disciplinary phase. The sense of this change is such that the altimeter observes a significant spurious rise in sea level between the two phases. However no significant altimetric drift is detected within either of the phases. It is also concluded that altimetry from the reprocessed version 3.0 GDRs of TOPEX is again measuring a spurious sea level drop. This time the estimated rate is around 4 mm/yr, although the slope is reduced to about 2 mm/yr later in the mission.

9.2 Final remarks regarding the conclusions

If nothing else, the work presented here has shown that the development of satellite altimetry should not be at the expense of tide gauges. The drift caused by mis-handling of the instability in the ultra stable oscillator is significant and may have had serious consequences if left undetected. Tide gauges therefore have a crucial role to play in allowing such drift to be detected. The means to achieve this are provided by the theory of gauge-augmented altimeter measurements as developed here. In addition to allowing the drift in TOPEX to be recovered, the role of tide gauges extends to the estimation of the systematic differences between multiple altimeters. Indeed, a long and unbroken altimetric record may not be realised, but tide gauges have the potential to mitigate the detrimental effects of any break in coverage which does occur. Optimum exploitation of the full dataset may then be achieved, with important implications for climate science.

9.3   Proposals and future work

It is suggested that the absolute calibration scheme in the English Channel be extended and applied to the full TOPEX version 3.0 GDR dataset. With the greater number of cycles now available it will be possible to derive an estimate of the absolute bias of the instrument in which more con dence may be placed. With nearly three years of data from ERS 2 now available, the absolute bias of this altimeter may now be calculated with more certainty. To these ends the excellent work of the sta at the Royal Greenwich Observatory station at Herstmonceux who tirelessly produce satellite tracking data should be continued.

It is hoped that the monitoring of stability in satellite altimeters using tide gauges will become routine. If properly applied this precaution will insure against the risk of deriving misleading sea level rates, as it has been achieved in the case of TOPEX. This may be extended and improved by the inclusion of other tide gauges. In particular the Tropical Ocean-Global Atmosphere campaign supports many more tide gauges than the WOCE, some of which may well be suitable for altimetric calibration. This will reduce uncertainties associated with smaller sets of tide gauges.

When the Geosat Follow-On satellite is launched, it is recommended that this altimeter is linked to the Exact Repeat Mission phase of the original Geosat altimeter using gauge-augmented repeat passes. This will allow Geosat-observed sea level rates to be referenced to the rate measured by the current set of altimeters, thus bridging the gap between Geosat s failure and the launch of ERS 1. The fact that these satellites share the same ground-track means that this is a unique opportunity to compare the old and new altimeters with gauge-augmented repeat passes without, the uncertainties associated with di erences in the geographically-correlated orbit error. If successful, the full potential of the Geosat mission will nally be unlocked and consistent altimetric coverage will be extended back by over six years.

These opportunities cannot be exploited unless tide gauges are adequately supported. Every e ort should be put into maintaining the tide gauge series at as many sites as possible. To this end, monitoring of the vertical stability of these installations is strongly encouraged. The Global Positioning System for instance is ideal for this application if the work is carried out to the standards set out in the Carter Reports.

The opportunities for climate science presented by this new era of Earth observation are unprecedented. These opportunities should be exploited to the fullest extent with the aid of altimeters in conjunction with tide gauges.

Bibliography

Archiving, Validation and Interpretation of Satellite Data in Oceanography (AVISO) (1992). AVISO user handbook: Merged TOPEX/POSEIDON products. Technical Report AVI-NT-02-101-CN, Centre National d Etudes Spatiales, Toulous, France. ed. 2.1.

Ashkenazi, V. R., Bingley, M., Whitmore, G. M., and Baker, T. F. (1993). Monitoring changes in mean-sea-level to millimeters using GPS. *Geophysical Research Letters*, vol.20, no.18, pp.1951 1954.

Bloom eld, P. (1976). *Fourier Analysis of Time Series: An Introduction.*, pages 129 137. John Wiley and Sons., New York.

Born, G. H., Parke, M. E., Axelrad, P., Gold, K. L., Johnson, J., Key, K. W., and Kubitschek, D. G. (1994). Calibration of the TOPEX altimeter using a GPS buoy. *Journal of Geophysical Research*, vol.99, no.C12, pp.24517 24526.

Carnochan, S. (1996). *Orbit and altimetric corrections for the ERS satellites through analysis of single and dual satellite crossovers.* PhD thesis, The University of Aston in Birmingham, Birmingham, England.

Carter, W. E. (1994). Report of the Surrey Workshop of the IAPSO tide gauge bench mark xing committee. Technical Report NOSOES0006, NOAA, Geoscience Laboratory, National Ocean Service, 1305 East-West Highway, Silver Spring, MD 20910, USA.

Carter, W. E., Aubrey, D. G., Baker, T., Boucher, C., LeProvost, C., Pugh, D., Peltier, W. R., Zumberge, M., Rapp, R. H., Schutz, R. E., Emery, K. O., and En eld, D. B. (1989). Geodetic xing of tide gauge bench marks. Technical Report WHOI-89-31, Woods Hole Oceanographic Institution, Woods Hole, Massachusetts 02543, USA.

CERSAT (1993). Altimeter products, user manual. Technical Report C1-EX-MUT-A21-01-CN, Center ERS d Archivage et de Traitment (CERSAT), Brest, France.

Christensen, E. J., Haines, B. J., Keihm, S. J., Morris, C. S., Norman, R. A., Purcell, G. H., Williams, B. G., Wilson, B. D., Born, G. H., Parke, M. E., Gill, S. K., Shum, C. K., Tapley, B. D., Kolenkiewicz, R., and Nerem, R. S. (1994). Calibration of TOPEX/POSEIDON at platform Harvest. *Journal of Geophysical Research*, vol.99, no.C12, pp.24465 24485.

Colonna, M., Casanova, J., Dullo, W.-C., and Camoin, G. (1996). Sea-level changes and ^{18} record for the past 34,000 yr from Mayotte Reef, Indian Ocean. *Quaternery Research*, vol.46, pp.335 339.

Cotton, D. and Challenor, P. (1996). Calibration and validation of ERS-2 OPR wind/wave measurements. In *Minutes of RA and MWR 2 CWG (#10)*. ESA-ESRIN.

Douglas, B. C. (1995). Global sea-level change: determination and interpretation. *Reviews of Geophysics*, vol.33, no.Pt2 SS, pp.1425 1432.

Ehlers, S. (1993). *Various techniques and procedures for re ning ERS 1 orbits.* PhD thesis, The University of Aston in Birmingham, Birmingham, England.

Featherstone, W. E. (1992). *A GPS controlled gravimetric determination of the geoid of the British Isles.* PhD thesis, Oxford University, England.

Flather, R. A., Proctor, R., and Wolf, J. (1991). Oceanographic forecast models. In Farmer, D. G. and Rycroft, M. J. (eds.), *Computer Modelling in the Environmental Sciences*, pages 15 30. Clarendon, Oxford, England.

Francis, C. R. (1992). The calibration of the ERS-1 radar altimeter. Report ER-RP-ESA-RA-0257, ESA/ESTEC, Noordwijk, The Netherlands. Issue 1.0.

Francis, C. R. (1993). The height calibration of the ERS-1 radar altimeter. In *Proceedings of the First ERS-1 Symposium: Space at the Service of our Environment, ESA SP-359*, pages 381 393, Cannes, France.

Gaspar, P., Ogor, P. F., Le Traon, P. Y., and Zanife, O. Z. (1994). Estimating the sea state bias of the TOPEX/POSEIDON altimeters from crossover di erences. *Journal of Geophysical Research*, vol.99, no.C12, pp.24981 24994.

Haggart, B. A. (1987). Relative sea-level changes in the Moray Firth area, Scotland. In Tooley, M. J. and Shennan, I. (eds.), *Sea-level changes*, Institute of British Geographers, Special Publication Series. Blackwell, Oxford, England.

Hancock, III, D. W. and Hayne, G. S. (1994). Note on use of NASA radar altimeter data from the rst 8 data cycles. Unpublished manuscript.

Hancock, III, D. W. and Hayne, G. S. (1996). Error in TOPEX oscillator drift correction. Unpublished manuscript.

Hayne, G. S., Hancock III, D. W., and Purdy, C. L. (1994). TOPEX altimeter range stability from calibration mode data. *TOPEX/POSEIDON research news*, vol.3, pp.18 22.

Hofmann-Wellenhof, B., Lichtenegger, H., and Collins, J. (1994). *Global positioning system, theory and practice.* Novographic, Ing. Wolfgang Schmid, A-1230 Wien, Austria, third edition.

Houghton, J. T. (1977). *The physics of atmospheres.* Cambridge University Press, England.

Houghton, J. T., Filho, L. G. M., Callander, B. A., Harris, N., Kattenberg, A., and Maskell, K. (eds.) (1996). *Climate change 1995: The science of climate change. Contribution of working group 1 to the second assessment report of the Intergovernmental Panel on Climate Change.* Cambridge University Press, England.

Ireland, S. (1987). The halocene sedimentary history of the coastal lagoons of Rio de Janeiro State, Brazil. In Tooley, M. J. and Shennan, I. (eds.), *Sea-level changes*, Institute of British Geographers, Special Publication Series. Blackwell, Oxford, England.

Irvine, D. E. (1985). Waves across the sea. *Johns Hopkins APL Technical Digest*, vol.6, no.4,.

Klokocn k, J., Kostelecky, J., and Karasova, D. (1994). Satellite altimetry and its use in geoscience. Class Text 40(12), Research Institute of Geodesy, Topography and Cartography (VUGTK). ISBN 8085881004.

Lam, C. W. (1994). *Application of ERS 1 and TOPEX/POSEIDON altimetry using precise orbits.* PhD thesis, The University of Aston in Birmingham, Birmingham, England.

Lam, C. W., Moore, P., and Woodworth, P. L. (1993). Calibration of ERS-1 altimetry over the north sea. In *Proceedings of the First ERS-1 Symposium: Space at the Service of our Environment, ESA SP-359*, pages 85 90, Cannes, France. European Space Agency.

Lisitzin, E. (1974). *Sea level changes*, volume 8 of *Elsevier Oceanography Series*. Elsevier Scienti c Publishing Company, Amsterdam, The Netherlands.

Marshall, J. A., Zelensky, N. P., Klosko, S. M., Chinn, D. S., Luthcke, S. B., Rachlin, K. E., and Williamson, R. G. (1995). The temporal and spatial characteristics of TOPEX/POSEIDON radial orbit error. *Journal of Geophysical Research*, vol.100, no.C12, pp.25331 25352.

Martin, C. F. and Butler, M. L. (1977). Calibration results for the GEOS-3 altimeter. Report CR-141430, NASA.

Mathers, E. L. (1996). Meteorological forcings of sea level changes worldwide. First year report, Proudman Oceanographic Laboratory, Bidston Observatory, Birkenhead, Merseyside, L43 7RA, UK.

Menard, Y., Jeansou, E., and Vincent, P. (1994). Calibration of the TOPEX/POSEIDON altimeters at Lampedusa: Additional results at Harvest. *Journal of Geophysical Research*, vol.99, no.C12, pp.24487 24504.

Mitchum, G. T. (1994). Comparison of TOPEX sea surface heights and tide gauge sea levels. *Journal of Geophysical Research*, vol.99, no.C12, pp.24541 24553.

Mitchum, G. T. (1997a). Monitoring the stability of satellite altimeters using tide gauges. Submitted to J. Atmospheric and Oceanic Technology.

Mitchum, G. T. (1997b). The range stability in the TOPEX altimeter. Poster presentation at the TOPEX/POSEIDON Sceince Working Team held in Biarritz.

Moore, P., Carnochan, S., and Murphy, C. M. (1996a). Absolute and relative range bias estimation of the ERS radar altimeter using OPR-2 data. Report, Aston University, Birmingham, UK.

Moore, P., Ehlers, S., and Carnochan, S. (1996b). Accuracy assessment and re nement of the JGM-2 and JGM-3 gravity elds for radial positioning of ERS-1. Submitted to Journal of Geodesy (in press).

Morner, N.-A. (1987). Models of global sea-level changes. In Tooley, M. J. and Shennan, I. (eds.), *Sea-level changes*, Institute of British Geographers Special Publication Series, chapter 11, pages 332 355. Blackwell, Oxford, England.

Neumann, G. and Pierson, Jr., W. J. (1966). *Principles of physical oceanography.* Prentice-Hall Inc., Englewood Cli s, NJ.

Peltier, W. R. and Jian, X. H. (1996). Mantle viscosity from the simultaneous inversion of multiple data sets pertaining to postglacial rebound. *Geophysical Research Letters*, vol.23, no.5, pp.503 506.

Pugh, D. T. (1987). *Tides, surges and mean sea-level.* John Wiley and Sons Ltd.

Rapp, R. H., Wang, Y. M., and Pavlis, N. K. (1991). The Ohio state 1991 Geopotential and sea surface topography harmonic coe cient models. Report Rep 410, Department of Geodetic Science and Surveying, Ohio State University, Columbus, Ohio.

Rapp, R. H. and Zhang, C. (1996). Sea level changes estimated from the analysis of TOPEX cycles 9 to 142. Submitted to Marine Geodesy.

Robinson, I. S. (1985). *Satellite oceanography: an introduction for oceanographers and remote-sensing scientists.* Ellis Horwood Limited, Chichester, England.

Roca, M. and Francis, R. (1996). Identi cation and origin of on-board bias jumps. In *Minutes of RA and MWR 2 CWG (#9)*. ESA-ESRIN.

Rodrigues, E. and Martin, J. M. (1994). Estimation of the electromagnetic bias from retracked TOPEX data. *Journal of Geophysical Research*, vol.99, no.C12, pp.24,971 24,979.

Scharroo, R., Wakker, K. F., and Mets, G. J. (1994). The orbit determination accuracy of the ERS-1 mission. In *Proceedings of the Second ERS-1 Symposium: Space at the Service of our Environment, ESA SP-361*, pages 735 740, Hamburg, Germany.

Shennan, I. (1987). Halocene sea-level changes in the North Sea region. In Tooley, M. J. and Shennan, I. (eds.), *Sea-level changes*, Institute of British Geographers Special Publication Series. Blackwell, Oxford, England.

Smith, J. A. (1994). The operational storm surge model data archive. Report 34 1994, Proudman Oceanographic Laboratory, Bidston Observatory, Birkenhead, Merseyside, England.

Spencer, N. E. and Woodworth, P. L. (1991). Data holdings of the permanent service for the mean sea level. Technical report, Permanent Service for the Mean Sea Level, Bidston Observatory, Birkenhead, Merseyside, L43 7RA, UK.

Stum, J. (1996). Status of OPR 2 calibration: Existing di erences in OPR range. In *Minutes of RA and MWR 2 CWG (#9)*. ESA-ESRIN.

Tapley, B. D., Ries, J. C., Davis, G. W., Eanes, R. J., Schutz, B. E., Shum, C. K., Watkins, M. M., Marshall, J. A., Nerem, R. S., Putney, B. H., Klosko, S. M., Luthcke, S. B., Pavlis, D., Williamson, R. G., and Zelensky, N. P. (1994). Precision orbit determination for TOPEX/POSEIDON. *Journal of Geophysical Research*, vol.99, no.C12, pp.24,383 24,404.

Tapley, B. D. and Rosborough, G. W. (1985). Geographically correlated orbit error and its e ect on satellite altimetry missions. *Journal of Geophysical Research*, vol.90, no.C6, pp.11817 11831.

Trupin, A. and Wahr, J. (1990). Spectroscopic analysis of global tide-gauge sea-level data. *Geophys. J. Int.*, vol.100, no.3, pp.441 453.

Walsh, E. J., Jackson, F. C., Hines, D. E., Piazza, C., Hevizi, L. G., Mclaughlin, D. J., Mcintosh, R. E., Swift, R. N., Scott, J. F., Yungel, J. K., and Frederick, E. B. (1991). Frequency-dependence of electromagnetic bias in radar altimeter sea-surface range measurements. *Journal of Geophysical Research*, vol.96, no.NC11, pp.20,571 20,583.

Warrick, R. and Oerlemans, J. (1990). Sea level rise. In Houghton, J. T., Jenkins, G. J., and Ephraums, J. J. (eds.), *Climate change, the IPCC scienti c assessment*, chapter 9. Cambridge University Press, Cambridge, England. Published for the Intergovernmental Panel on Climate Change.

WOCE (1995). Woce data handbook. Report 135/95, WOCE Data Information Unit, WOCE International Project O ce.

Yaplee, B. S., Shapiro, A., Hammond, D. L., Au, B. D., and Uliana, E. A. (1971). Nanosecond radar observations of the ocean surface from a stable platform. *IEEE Transactions of Geoscience Electronics*, vol.GE, no.9, pp.171 174.

Yulsman, T. (1996). The sea oor laid bare. *Earth magazine*, vol.5, no.3, pp.42 51.

Zandbergen, R. C. A. (1991). *Satellite altimeter data processing: From theory to practice*. PhD thesis, Faculty of Aerospace Engineering, Delft University of Technology, Delft, The Netherlands.